



NTNU – Trondheim
Norwegian University of
Science and Technology

Anti-Sway Control and Wave Following System for Offshore Lattice Crane

Oddvar Gjelstenli

Master of Science in Engineering Cybernetics [2]

Submission date: August 2012

Supervisor: Tor Engebret Onshus, ITK

Co-supervisor: Stig Hornang, National Oilwell Varco

Norwegian University of Science and Technology
Department of Engineering Cybernetics

Anti-Sway Control and Wave Following System for Offshore Lattice Crane

Oddvar Gjelstenli

2012-08-07



MSC THESIS DESCRIPTION SHEET

Name: ODDVAR GJELSTENLI

Department: Engineering Cybernetics

Thesis Title (Norwegian):
Antisleng og bølge kompensering for offshore fagverks kran

Thesis Title (English):
Anti-sway Control and Wave Following System for Offshore Lattice Crane

Thesis description: The purpose of this thesis is to develop and implement mathematical model of a rotary crane with control systems for anti-sway, boom tip positioning and a wave following system.

Scope of work:

- Mathematical modelling:
 - Modelling of a trolley with pendant load
 - Modelling of a rotary crane with spherical pendulum
- Control design:
 - Design a controller to reduce the angular deflection of the wire on a rotary crane.
 - Design a controller to control the boom tip position to a desired set point.
 - Design a controller for the crane hoist winch system which purpose is to make the hook follow the oscillatory motion of the vessel below the oilrig, by use of real-time stereo video camera measurement.
- Simulation:
 - Make Simulink models to simulate both the trolley with pendant load and the rotary crane.
- Visualization:
 - Make 3D Visualization of the trolley and rotary crane.
- Instrumentation:
 - Investigate different methods to measure the angular deflection of the wire.
- Filter the sensor measurements and remove bias from the camera measurement.

Start date: 27. Februar 2012

Due date: 07. August 2012

Thesis performed at: Department of Engineering Cybernetics, NTNU

Supervisor: Professor Tor Onshus, NTNU
Co-supervisor: Håvard Knappskog, National Oilwell Varco

Abstract

Offshore crane operation is a complex task that demands the operator to control the position of the load, predict vessel motion and compensate for load sway, all at the same time. In this thesis an anti-sway, boom tip positioning and a wave following system is presented which purpose is to facilitate not automate the crane operation. Introducing such systems the operator has an extra set of tools to reduce risk of cargo damage and personnel injuries during operation. This is done by suppressing the sway angles and positioning the boom tip to a desired position with the anti-sway and boom tip positioning system, and be able to make the hook follow the heave motion of the vessel by using the wave following system.

This thesis contains modeling, visualization, simulation and control of a rotary crane with spherical pendulum. Also models for a trolley with pendant load, vessel motion, and angular deflection of the wire and a wind model is presented. Lagrangian describes the dynamics of the crane models and the equation of motion is derived with Euler-Lagrange equations.

The effect of measurement noise in the sensor signals has been reduced through the implementation of an adaptive Kalman-filter. Parameter estimation has been used to find unknown model parameters such as damping, frequency and bias in vessel heave motion model. Several suggestions of sensors to measure the swing angles of the hoist winch wire is presented. The 3D visualization is developed using the V-Realm 3D editor included in Simulink 3D Animation toolbox.

Results of the closed loop system shows that it is possible to control the load swing angles and boom tip position and still let the crane operator have the superior control of the crane. In case of stability it can be seen that since all friction terms is neglected in the mathematical model there is no dissipation of energy in the pendulum dynamics, meaning that the anti-sway controller causes any observed damping in the sway dynamics.

Preface

This thesis finalizes a Master's degree in Engineering Cybernetics at the Department of Engineering Cybernetics at the Norwegian University of Science and Technology in Trondheim, Norway. During the last two years as student at the University in Trondheim, I have been introduced to a lot of really interesting and challenging subjects.

Working on this thesis has been a great challenge, but has lead to a much greater understanding of modelling, simulation, control of physical systems and use of 3D visualization. Also it has been interesting to see the possibilities there is with online parameter estimation and filtering for sensor measurement purpose.

Thanks to all my fellow co-students for all the good teamwork and discussions during the last two years. It has been two intense years in form of the variety of subjects been covered, but it has been a steep increase in case of learning.

Thanks to my main supervisor Professor Tor Onshus and my co-supervisor Håvard Knappskog at National Oilwell Varco for valuable help. And finally I would also like to thank Stig Hornang and Bernt Sandøy at National Oilwell Varco, who initially allowed me to work on this project.

Oddvar Gjelstenli

Contents

List of figures	x
List of tables	xi
1 Introduction	1
1.1 Motivation	1
1.2 Theory Basis and Advised Literature	2
1.3 Outline	3
1.4 Previous work	4
1.5 Abbreviations / Glossary	5
2 Mathematical modelling	7
2.1 3DOF trolley with pendant load in wire	7
2.1.1 Payload position	8
2.1.2 Lagrangian	8
2.1.3 Equation of motion	8
2.2 Rotary Crane with Spherical Pendulum	9
2.2.1 Boom tip position, velocity and acceleration	9
2.2.2 Pendulum dynamics	10
2.2.3 Equation of motion for the load	12
2.2.4 Crane fixed frame	14
2.2.5 Equation of motion in the crane-fixed coordinate system	15
2.2.6 Model reduction	16
2.3 Linearized Crane Model	17
2.4 Vessel Heave Motion	19
2.4.1 State space representation	19
2.4.2 Discrete state space	19
2.5 Angular Deflection of the Hoist Winch Wire	20
2.5.1 State space representation	20
2.5.2 Discrete state space	20
2.6 Wind Model	21
2.6.1 Wind Forces	21
3 Filtering and Parameter Estimation	23
3.1 Estimation of Vessel Model Parameters	23
3.1.1 Heave measurement	23
3.1.2 Parametric model of the vessel heave motion	24
3.1.3 Normalized estimation error	24
3.1.4 Least-squares with covariance resetting	25

3.1.5	Least-squares with forgetting factor	25
3.2	Kalman Filtering of Sensor Measurement	25
3.2.1	Kalman filter with variable Kalman gain	26
3.2.2	Comparison between the two parameter estimation algorithm	26
3.2.3	Prediction	27
4	Control Design	29
4.1	Anti-sway control and boom tip positioning control for rotary crane . .	29
4.1.1	Actuator dynamics	29
4.1.2	Anti-sway control	30
4.1.3	Boom tip positioning control	30
4.1.4	Cascade Control with Operator in-the-loop	31
4.2	Wave following control system	32
5	Visualization	35
5.1	3DOF Trolley with pendant load	35
5.2	Rotary crane with spherical pendulum	36
5.2.1	Visualization of rotary crane with box shaped boom	36
5.2.2	Visualization of rotary crane with inventor drawings	37
5.2.3	Visualization of rotary crane with graphs	38
6	Simulation	41
6.1	Rotary crane with spherical pendulum	41
6.1.1	Introduction	41
6.1.2	Scenarios	42
6.2	Simulation of Wave Following System	56
7	Instrumentation	59
7.1	Off lead/Side lead	59
7.1.1	Off lead/Side lead description	59
7.1.2	Angle measurement of whip line by use of potentiometers .	60
7.1.3	Position measurement of whip line by use of ultrasound and inclinometer	60
7.1.4	Experiment	62
7.1.5	Measure the position of the whip line and main hoist line by use of real-time stereo video measurements	64
8	Conclusion	65
9	Further work	69
A	Contents of the digital attachment	73
A.1	Literature	73
A.2	Matlab	73
A.3	Data sheets	74
A.4	VRML	74

B	Mathematical modeling of trolley	75
B.1	3DOF trolley with pendant load in wire	75
B.1.1	Position	76
B.1.2	Velocity	76
B.1.3	Lagrangian	77
B.1.4	Equation of motion	79
B.1.5	Equation of motion on matrix form	81
C	Mathematical model of spherical pendulum	83
C.1	Position and velocity of the load	83
C.1.1	Equation of motion for the load	85
C.2	Model problems	87
C.2.1	$\ddot{\phi} \rightarrow \infty$	87
D	Derivation of the Equations of Motion for a Pendulum	89
D.1	Crane-Fixed Coordinate System	89
E	Plots	93
E.1	Parameter estimation and Kalman filtering	94
F	Simulink models	95
F.1	Rotary Crane Model Overview	96
G	Matlab files	97
G.1	Initialization file for Rotary Crane Model	97
	Bibliography	103

List of Figures

1.1	Sketch of test rig for camera system made by Hornang 2010	5
2.1	Sketch of trolley with pendant load in wire	7
2.2	Sketch of rotary offshore crane	9
2.3	Spherical pendulum notation	11
2.4	Crane-fixed coordinate system c and swing angle notation	14
2.5	Schematic view of the crane geometry	17
3.1	Sketch of real-time stereo video camera measurement system	23
3.2	Detail view of Kalman filter with two different parameter estimation algorithm as input	27
4.1	Example of set-point trajectory $T(k)$. $T_s = 1/15$, $T_{ref} = 5$	33
4.2	Simulink diagram of the PI regulator with anti windup	33
4.3	Speed profile of 1 fall configuration hoist winch	34
5.1	Visualisation of 3DOF trolley with pendant load	36
5.2	Visualisation of rotary crane with spherical pendulum	37
5.3	Visualisation of rotary crane made from inventor drawing	38
5.4	3D visualization with graphs	38
5.5	3D visualization with graphs - mask parameters	39
6.1	Plot of the test signal used for slew q_1 and boom motion q_2	41
6.2	Plot of the test signal used for l_w and \dot{l}_w	42
6.3	Plot of scenario 1 of the rotary crane simulation	44
6.4	Plot of scenario 2 of the rotary crane simulation	45
6.5	Plot of scenario 3 of the rotary crane simulation	46
6.6	Plot of scenario 4 of the rotary crane simulation	47
6.7	Plot of scenario 5 of the rotary crane simulation	48
6.8	Plot of scenario 6 of the rotary crane simulation	49
6.9	Plot of scenario 7 of the rotary crane simulation	50
6.10	Plot of scenario 8 of the rotary crane simulation	51
6.11	Plot of scenario 9 of the rotary crane simulation	52
6.12	Plot of scenario 10 of the rotary crane simulation	53
6.13	Plot of scenario 11 of the rotary crane simulation	54
6.14	Plot of scenario 12 of the rotary crane simulation	55
6.15	Simulation with Kalman predicted set point from camera measurement, 5t hook load, 2.2m/s max velocity	56

6.16	Simulation with Kalman predicted set point from camera measurement, 10ton hook load, 1.57m/s max velocity	57
7.1	Hook position relative to crane boomtip [19]	59
7.2	Sway measurement of whipline by use of potentiometers [28]	60
7.3	Sketch of sensor for measurement of off lead/side lead angle for whip line	61
7.4	Suggestion of Ultrasonic sensor installation	62
7.5	Lab test	62
7.6	Ultrasound resolution and measurement area	63
B.1	Sketch of trolley with pendant load in wire	75
C.1	Sketch of spherical pendulum	83
D.1	Mathematica output of the EOM for $c_{\alpha_v} l_w \ddot{\beta}_v$	90
D.2	Mathematica output of the EOM for $2l_w \ddot{\alpha}_v$	91
E.1	Comparison between two parameter estimation algorithms as input to the Kalman filter	94
F.1	Rotary Crane Simulink Model Overview	96

List of Tables

2.1	Notation for 3DOF trolley with pendant load in wire	8
2.2	Boom tip coordinate system	10
3.1	Notation of variables for figure 3.2	26
4.1	Crane actuator velocity limitations	29
5.1	3D visualization with graphs - object description	39
6.1	Simulation scenario overview	43
7.1	Limit values for off lead and side lead [19]	59
7.2	List of equipment used in ultrasound proximity switch test	63
7.3	Test of Ultrasound Distance Sensor, showing measured(M), actual(A) and deviation(D) distance in [cm]	64
B.1	Notation for 3DOF trolley with pendant load in wire	76
C.1	Hook coordinate system	84

Chapter 1

Introduction

1.1 Motivation

Crane operation offshore is a complex task which demands full concentration from the crane operator. During a normal crane operation, the operator has to compensate for load sway, determine the distance to the platform deck or the deck of the vessel and also positioning the crane at the desired position, simultaneous.

By introduction an anti-sway system and a boom tip positioning system the crane operator has an extra set of tools which can be used to reduce the risk of damaging cargo, and it might also reduce the risk of personnel injuries since the operator can activate the control system and suppress the load sway prior to landing cargo.

1.2 Theory Basis and Advised Literature

Writing a thesis about cranes and crane control system require some insight in several different topics. This thesis covers topics like mathematical modelling, control engineering, filtering, parameter estimation, instrumentation among others. It is therefore convenient to know where to look for information. During the pre thesis autumn semester 2011 and this master thesis a lot of sources of information and similar projects has been located and used for inspiration.

Regarding mathematical modelling and rigid body dynamics and kinematics useful references is [23], [8] and [20]. Topics such as friction and actuator limitations is also covers in [23].

Linear control theory with subjects as pole placement, feed-forward, feedback controllers and linearisation is covered in [3], while non-linear control theory is found in [4]. A good reference to information about Kalman filtering is [9], while subject of parameter estimation is covered in [14].

1.3 Outline

A short description of the chapters contained in this thesis is given:

Chapter 2 - Mathematical modelling

In this chapter the following mathematical models is derived

- Section 2.1 - Trolley with pendant load.
- Section 2.2 - Rotary crane with spherical pendulum.
- Section 2.3 - Linear crane model
- Section 2.4 - Vessel heave motion.
- Section 2.5 - Angular deflection of the hoist winch wire.
- Section 2.6 - Simple Wind Model

Chapter 3 - Filtering and Parameter Estimation

This chapter presents the use of online parameter estimation in section 3.1, and the use of Kalman filter in section 3.2.

Chapter 4 - Control Design

In section 4.1 a cascade control system with a anti sway controller which purpose is to minimize the sway angles β_v and α_v , and a boom tip positioning controller for the crane is presented. In section 4.2 an wave following system (WFS) is presented.

Chapter 5 - Visualization

3D Visualizations of the mathematical models made by use of Simulink 3D animation toolbox is presented here, in addition to an figure with 3D visualization with graphs made with an S-function.

Chapter 6 - Simulation

In section 6.1 simulations of both the open and closed loop system of the rotary crane is presented and discussed. And in section 6.2 the simulation of the WFS using the linear crane model described in 2.3 is presented.

Chapter 7 - Instrumentation

In this chapter several suggestions on how to use instrumentation to measure the sway angles β and α described in section 2.2 is presented.

Chapter 8 - Conclusion

Conclusion drawn based on the results in this thesis is presented in this chapter.

Chapter 9 - Further work

Suggested topics and issues for further work is presented in this chapter.

1.4 Previous work

Significant wave height H_s

The significant wave height H_s is defined by the mean wave height of the one-third highest waves during the last 20 minutes. Significant wave height is often denoted as $H^{1/3}$.

The company Shore Connections has recently introduced a system that transfer data from vessel to rig via wireless connection. The special thing with this system that it has a algorithm that calculates the significant wave height based on Real-time data from the vessel which are approved for use. This means that the significant wave height is corrected continuously which again means that the crane operation can be approved more often then if the significant wave height calculations is based on weather forecast, which may not be updated so often. [7]

Anti-sway system

Anti-sway system is a system which purpose is to minimize or remove any angular deflection on the hoist winch wire, such system is implemented in wide scale on container cranes and in industrial gantry cranes. This system allows an operator to control the crane in a safe manner to minimize the risk of damage on equipment, cargo or human. When it comes to offshore rotary cranes, there is much less literature about this subject, but a good reference is [20] who discuss anti-sway systems for both rotary crane and rotary leaning cranes. In section 2.2 the work of [20] has been used as motivation.

Crane dynamics

National Oilwell Varco has developed a linear crane model based on first principles method, where the dynamics of the structure of the crane is implemented. This model was used in [2] to investigate the forces during pick up off load from a offshore vessel, and in [25] as model of the hoist dynamics when deriving the wave following system, and is presented in this thesis in 2.3.

Camera measurement system

In 2010, Stig Hornang investigated the possibility to determine the positions of a sea going vessel based on Real-Time Stereo Video Measurements. [5], A scaled test rig was developed and time series were produced. This time series of the vessels heave motion was used in [25] to test the wave following system.

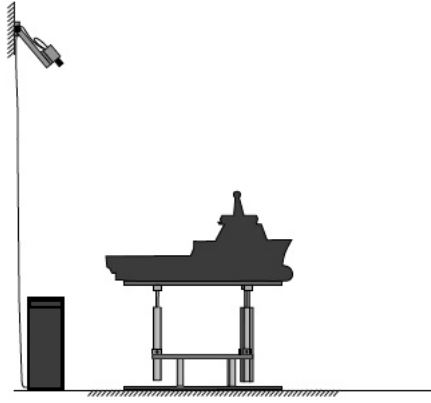


Figure 1.1: Sketch of test rig for camera system made by Hornang 2010

Wave following system

During autumn 2011 the author of this thesis derived an suggestion of an wave following system for offshore rig crane [25] by use of real-time stereo video measurement described in [5] and an linear crane model [2]. The suggested controller is included in this thesis in section 4.2, while the simulation results of the wave following system is presented in 6.2.

1.5 Abbreviations / Glossary

CT	-	Constant Tension.
FPSO	-	Floating production, storage and offloading unit
WFS	-	Wave following system
AHC	-	Active heave compensation
MRU	-	Motion reference unit
DOF	-	Degree of freedom
MOP	-	Manual Overload Protection
AOP	-	Automatic Overload Protection
GOP	-	Gross Overload Protection
SWL	-	Safe Working Load
HMI	-	Human Machine Interface
EOM	-	Equation of motion
COG	-	Center of gravity
OSV	-	Offshore Special Vessel
DP	-	Dynamic Positioning
Splash zone	-	The point when a load hanging in a wire is entering the water.

Chapter 2

Mathematical modelling

2.1 3DOF trolley with pendant load in wire

In this section a mathematical model is derived for the trolley with pendant load using Euler-Lagrange, this model is found in [16]. This model was chosen to be tested in Simulink since the model derived in appendix B contains errors. This model is used for implementation purpose in Simulink, testing of joystick interface and to experiment with the 3D Visualization. Therefore there is no controller algorithm derived for this model in chapter 4.

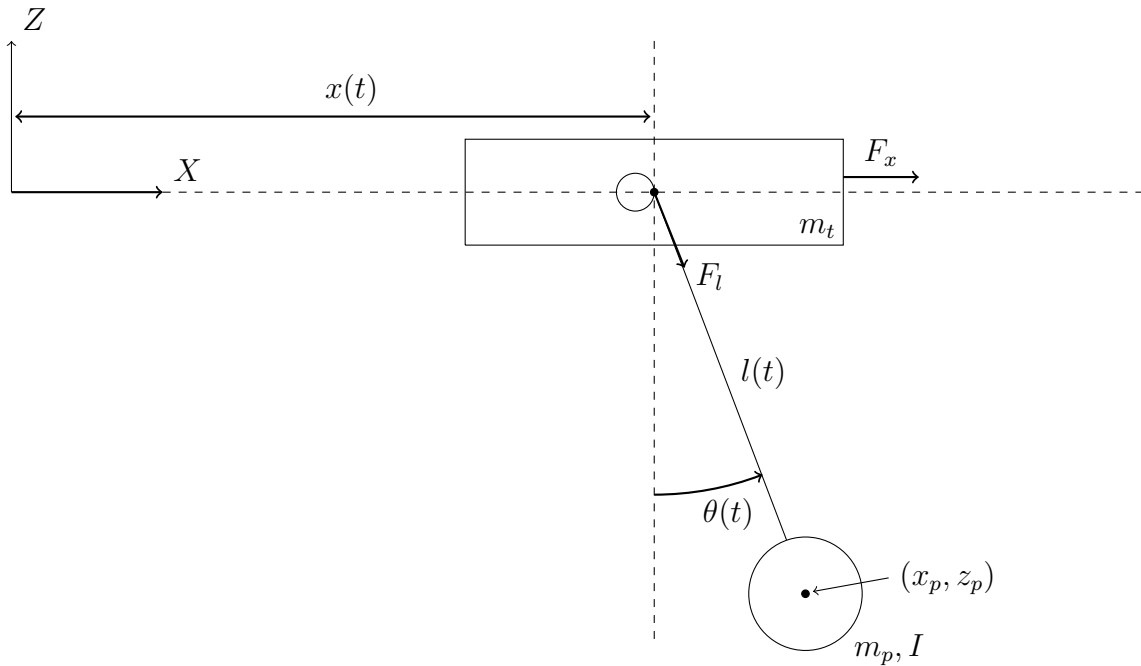


Figure 2.1: Sketch of trolley with pendant load in wire

The following assumptions is taken:

- The payload and trolley is connected by a massless rigid rod.
- The trolley mass and the position of the trolley is known.
- All frictional elements in the trolley and hoist motions can be neglected.

Notation	Description
θ	Load sway angle
x	Position of the trolley relative to the fixed X-axis
l	Length of wire between the trolley and load (varies with time)
m_p	Payload mass [kg]
m_t	Trolley mass [kg]
m_l	Wire mass [kg]
I	Mass moment of inertia of the payload
F_x	Control force applied to the trolley in X-direction
F_l	Control force applied to the wire in l-direction

Table 2.1: Notation for 3DOF trolley with pendant load in wire

- The rod elongation is negligible.

This assumption give a three degree of freedom crane model, with the generalized coordinate vector $q(t) \in R^3$.

$$q(t) = [x(t) \quad l(t) \quad \theta(t)]^T \quad (2.1)$$

2.1.1 Payload position

From figure 2.1 it can be seen that the position of the load can be described as

$$x_p = x + l \sin \theta \quad (2.2)$$

$$z_p = -l \cos \theta \quad (2.3)$$

2.1.2 Lagrangian

By using (2.2),(2.3) the kinetic energy T and potential energy U is given as

$$L = T - U \quad (2.4)$$

$$T = \frac{1}{2}(m_t + m_p) \dot{x}^2 + \frac{1}{2}(m_p + m_l) \dot{l}^2 + \frac{1}{2}m_p (l\dot{\theta}^2) + m_p \dot{x} (l \cos \theta \dot{\theta} + \sin \theta \dot{l}) + \frac{1}{2}I\dot{\theta}^2 \quad (2.5)$$

$$U = -m_p g l \cos \theta \quad (2.6)$$

2.1.3 Equation of motion

The Euler-Lagrange equations of motion is defined as

$$\frac{d}{dt} \frac{\partial L}{\partial \dot{q}} - \frac{\partial L}{\partial q} = \tau \quad (2.7)$$

where q is defined in (2.1), and the Lagrangian L is defined in (2.4). Then using (2.7) the equations of motion yields.

$$(m_t + m_p)\ddot{x} + m_p \sin \theta \ddot{l} + m_p l \cos \theta \ddot{\theta} + 2m_p \cos \theta \dot{l} \dot{\theta} - m_p l \sin \theta \dot{\theta}^2 = F_x \quad (2.8)$$

$$m_p \sin \theta \ddot{x} + (m_p + m_l) \ddot{l} - m_p l \dot{\theta}^2 - m_p g \cos \theta = F_l \quad (2.9)$$

$$m_p \cos \theta \ddot{x} + (m_p l^2 + I) \ddot{\theta} + 2m_p l \dot{l} \dot{\theta} + m_p g l \sin \theta = 0 \quad (2.10)$$

2.2 Rotary Crane with Spherical Pendulum

In the following section an model for an rotary crane and spherical pendulum is derived with the following assumptions:

- A.1 The rotary crane is defined as a rigid body.
- A.2 The crane is modelled as a stiff model, meaning that the dynamic influence of the load on the crane is neglected.
- A.3 The wire is a massless.
- A.4 Any wire deflection is neglected, under the assumption that the mass of the payload m_p is much greater than the mass of the wire m_w .
- A.5 Assume that the payload is a point mass.
- A.6 Assume that the rotary angle of the crane q_1 and the angle of the boom q_2 is perfectly measured.
- A.7 Assuming that the angular deflection of the wire β_v and α_v is available through measurement.

2.2.1 Boom tip position, velocity and acceleration

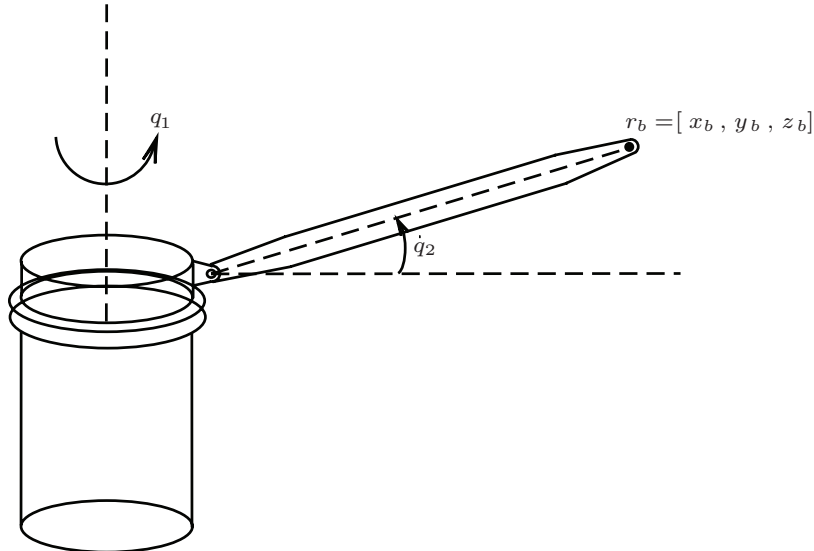


Figure 2.2: Sketch of rotary offshore crane

The position of the boom tip is described relative to the earth fixed coordinate system.

Notation	Description	Value
r_p	Radius from center of pedestal to boom hinge	1.75m
l_b	Length of boom from center boom hinge to whip hoist wire	56m
l_p	Length of pedestal	10m
q_1	Slew angle	0-359.9 degrees
q_2	Luffing angle	14-84.2 degrees
\dot{l}_w	hoist wire velocity	± 2.2 [m/s]

Table 2.2: Boom tip coordinate system

The position of the boom tip is found with using equation (2.11), and the measurement of q_1 and q_2 shown in figure 2.2.

$$r_b = \begin{bmatrix} -(r_p + l_b \cos q_2) \sin q_1 \\ (r_p + l_b \cos q_2) \cos q_1 \\ l_p + l_b \sin q_2 \end{bmatrix} \quad (2.11)$$

The differentiate of equation (2.11) with respect to time, describes the velocities of the boom tip.

$$\dot{r}_b = \begin{bmatrix} -(r_p + l_b \cos q_2) \cos q_1 \dot{q}_1 + l_b \sin q_1 \sin q_2 \dot{q}_2 \\ -(r_p + l_b \cos q_2) \sin q_1 \dot{q}_1 - l_b \cos q_1 \sin q_2 \dot{q}_2 \\ l_b \cos q_2 \dot{q}_2 \end{bmatrix} \quad (2.12)$$

Differentiate equation (2.12) with respect to time to describe the acceleration of the boom tip. The following notation is used; $c_1 : \cos q_1$, $s_1 : \sin q_1$, $c_2 : \cos q_2$ and $s_2 : \sin q_2$.

$$\ddot{r}_b = \begin{bmatrix} (r_p + l_b c_2) s_1 \dot{q}_1^2 + 2l_b s_2 c_1 \dot{q}_1 \dot{q}_2 - (r_p + l_b c_2) c_1 \ddot{q}_1 + l_b s_1 c_2 \dot{q}_2^2 + l_b s_1 s_2 \ddot{q}_2 \\ -r_p c_1 \dot{q}_1^2 - r_p s_1 \ddot{q}_1 + 2l_b s_1 s_2 \dot{q}_1 \dot{q}_2 - l_b c_1 c_2 \dot{q}_1^2 - l_b s_1 c_2 \ddot{q}_1 - l_b c_1 c_2 \dot{q}_2^2 - l_b c_1 c_2 \ddot{q}_2 \\ -l_b s_2 \dot{q}_2^2 + l_b c_2 \ddot{q}_2 \end{bmatrix} \quad (2.13)$$

2.2.2 Pendulum dynamics

In the following subsection the pendulum dynamics will be derived. This representation is based on the selection of Euler angles done in the doctoral thesis of Thomas Gustafsson,1993 [20].

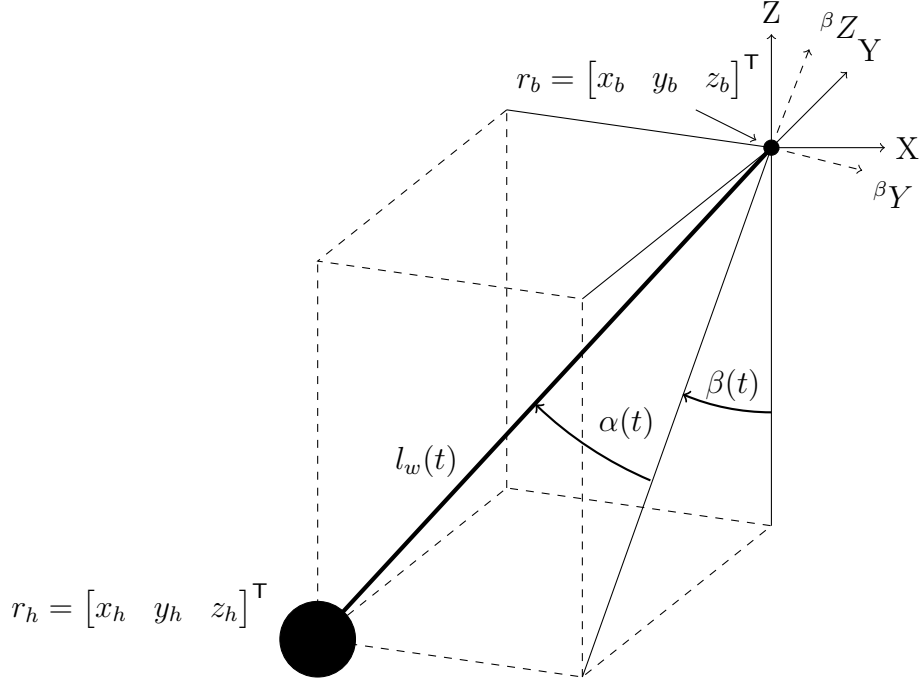


Figure 2.3: Spherical pendulum notation

In figure (2.3) the swing angles β, α and the wire length l_w is defined. β is defined as a positive rotation around the X -axis and α as a positive rotation around the ${}^\beta Y$ -axis. The notation is used to emphasize that the second rotation, as illustrated in figure (2.3), is in the new frame define by the first rotation. Such set of rotation angles is called Euler angles [8] and gives the following expression for the coordinate of the load, where $r_h = [x_h \ y_h \ z_h]^\top$.

$$r_h = r_b + l_w \begin{bmatrix} -\sin \alpha \\ \cos \alpha \sin \beta \\ -\cos \alpha \cos \beta \end{bmatrix} \triangleq r_b + l_w \Omega \quad (2.14)$$

This parametrization is valid for $-\pi < \alpha \leq \pi$, and $-\frac{\pi}{2} \leq \beta \leq \frac{\pi}{2}$, and can be used for simulation purposes unlike the model derived in Appendix C which had singularity issues in $\ddot{\phi}$ when $\phi \rightarrow 0$. The velocity of the payload with respect to time is described as.

$$\dot{r}_h = \dot{r}_b + \dot{l}_w \Omega + l_w \dot{\Omega} \quad (2.15)$$

$$\dot{r}_h = \begin{bmatrix} \dot{x}_b + \dot{l}_w (-s_\alpha) + l_w (-c_\alpha \dot{\alpha}) \\ \dot{y}_b + \dot{l}_w (c_\alpha s_\beta) + l_w (-s_\alpha s_\beta \dot{\alpha} + c_\alpha c_\beta \dot{\beta}) \\ \dot{z}_b + \dot{l}_w (-c_\alpha c_\beta) + l_w (s_\alpha c_\beta \dot{\alpha} + c_\alpha s_\beta \dot{\beta}) \end{bmatrix} \quad (2.16)$$

By the assumption that the hook is a concentrated mass connected to the end of a massless rod the Lagrangian is defined as

$$L_p = T_p - U_p \quad (2.17)$$

where

$$T_p = \frac{1}{2}m_p \|\dot{r}_h\|^2 \quad (2.18)$$

$$U_p = m_p g z_h \quad (2.19)$$

where L_p is the kinetic energy and U_p is the potential energy caused by gravity and z_h is potential above the resting point of the "pendulum".

$$\begin{aligned} T_p = & \frac{1}{2}m_p \left[\dot{x}_b^2 + \dot{y}_b^2 + \dot{z}_b^2 + \dot{l}_w^2 + l_w^2 \dot{\alpha}^2 + l_w^2 c_\alpha^2 \dot{\beta}^2 \right. \\ & - 2\dot{x}_b \left(\dot{l}_w s_\alpha + l_w c_\alpha \dot{\alpha} \right) + 2 \left(\dot{l}_w s_\alpha l_w c_\alpha \dot{\alpha} \right) \\ & + \dot{y}_b^2 + \dot{l}_w^2 c_\alpha^2 s_\beta^2 + l_w^2 s_\alpha^2 s_\beta^2 \dot{\alpha}^2 + l_w^2 c_\alpha^2 c_\beta^2 \dot{\beta}^2 \\ & + 2\dot{y}_b \left(\dot{l}_w c_\alpha s_\beta - l_w s_\alpha s_\beta \dot{\alpha} + l_w c_\alpha c_\beta \dot{\beta} \right) \\ & + 2\dot{l}_w c_\alpha s_\beta \left(-l_w s_\alpha s_\beta \dot{\alpha} + l_w c_\alpha c_\beta \dot{\beta} \right) \\ & + 2 \left(-l_w s_\alpha s_\beta \dot{\alpha} \right) \left(l_w c_\alpha c_\beta \dot{\beta} \right) \\ & + \dot{z}_b^2 + \dot{l}_w^2 c_\alpha^2 c_\beta^2 + l_w^2 s_\alpha^2 c_\beta^2 \dot{\alpha}^2 + l_w^2 c_\alpha^2 s_\beta^2 \dot{\beta}^2 \\ & + 2\dot{z}_b \left(-\dot{l}_w c_\alpha c_\beta + l_w s_\alpha c_\beta \dot{\alpha} + l_w c_\alpha s_\beta \dot{\beta} \right) \\ & + 2 \left(-\dot{l}_w c_\alpha c_\beta \right) \left(l_w s_\alpha c_\beta \dot{\alpha} + l_w c_\alpha s_\beta \dot{\beta} \right) \\ & \left. + 2 \left(l_w s_\alpha c_\beta \dot{\alpha} \right) \left(l_w c_\alpha s_\beta \dot{\beta} \right) \right] \quad (2.20) \end{aligned}$$

The potential energy for the load is then simply

$$U_p = m_p g (z_b - l_w c_\alpha c_\beta) \quad (2.21)$$

giving the total Lagrangian for the load described in (2.17) as

$$\begin{aligned} L_p = & \frac{1}{2}m_p \left[\dot{x}_b^2 + \dot{y}_b^2 + \dot{z}_b^2 + \dot{l}_w^2 + l_w^2 \dot{\alpha}^2 + l_w^2 c_\alpha^2 \dot{\beta}^2 \right. \\ & - 2\dot{x}_b \left(\dot{l}_w s_\alpha + l_w c_\alpha \dot{\alpha} \right) + 2 \left(\dot{l}_w s_\alpha l_w c_\alpha \dot{\alpha} \right) + 2\dot{y}_b \left(\dot{l}_w c_\alpha s_\beta - l_w s_\alpha s_\beta \dot{\alpha} + l_w c_\alpha c_\beta \dot{\beta} \right) \\ & \left. + 2\dot{z}_b \left(-\dot{l}_w c_\alpha c_\beta + l_w s_\alpha c_\beta \dot{\alpha} + l_w c_\alpha s_\beta \dot{\beta} \right) \right] - m_p g (z_b - l_w c_\alpha c_\beta) \quad (2.22) \end{aligned}$$

2.2.3 Equation of motion for the load

The equation of motion of the pendulum is given by

$$\frac{d}{dt} \frac{\partial L}{\partial \dot{q}} - \frac{\partial L}{\partial q} = \tau \quad (2.23)$$

where L is the total Lagrangian, q is the degrees of freedom here represented by $q = \{\beta, \alpha\}^\top$ and $\tau = \{0, 0\}^\top$.

$$\frac{\partial L_p}{\partial \beta} = m_p \left[\dot{y}_b \left(\dot{l}_w c_\alpha c_\beta - l_w s_\alpha c_\beta \dot{\alpha} - l_w c_\alpha s_\beta \dot{\beta} \right) \right]$$

$$+ \dot{z}_b \left(\dot{l}_w c_\alpha s_\beta - l_w s_\alpha s_\beta \dot{\alpha} + l_w c_\alpha c_\beta \dot{\beta} \right) - g l_w c_\alpha s_\beta \Big] \quad (2.24)$$

$$\frac{\partial L_p}{\partial \dot{\beta}} = m_p \left[l_w^2 c_\alpha^2 \dot{\beta} + \dot{y}_b l_w c_\alpha c_\beta + \dot{z}_b l_w c_\alpha s_\beta \right] \quad (2.25)$$

$$\begin{aligned} \frac{d}{dt} \frac{\partial L_p}{\partial \dot{\beta}} &= m_p \left[2l_w \dot{l}_w c_\alpha^2 \dot{\beta} - 2l_w^2 s_\alpha c_\alpha \dot{\alpha} \dot{\beta} + l_w^2 c_\alpha^2 \ddot{\beta} \right. \\ &\quad + \ddot{y}_b l_w c_\alpha c_\beta + \dot{y}_b \left(\dot{l}_w c_\alpha c_\beta - l_w s_\alpha c_\beta \dot{\alpha} - l_w c_\alpha s_\beta \dot{\beta} \right) \\ &\quad \left. + \ddot{z}_b l_w c_\alpha s_\beta + \dot{z}_b \left(\dot{l}_w c_\alpha s_\beta - l_w s_\alpha s_\beta \dot{\alpha} + l_w c_\alpha c_\beta \dot{\beta} \right) \right] \end{aligned} \quad (2.26)$$

$$\begin{aligned} \frac{d}{dt} \frac{\partial L_p}{\partial \dot{\beta}} - \frac{\partial L_p}{\partial \beta} &= m_p \left[2l_w \dot{l}_w c_\alpha^2 \dot{\beta} - 2l_w^2 s_\alpha c_\alpha \dot{\alpha} \dot{\beta} + l_w^2 c_\alpha^2 \ddot{\beta} \right. \\ &\quad \left. + \ddot{y}_b l_w c_\alpha c_\beta + \ddot{z}_b l_w c_\alpha s_\beta + g l_w c_\alpha s_\beta \right] \end{aligned} \quad (2.27)$$

$$\begin{aligned} \frac{\partial L_p}{\partial \alpha} &= m_p \left[-l_w^2 s_\alpha c_\alpha \dot{\beta}^2 + \dot{x}_b \left(\dot{l}_w c_\alpha - l_w s_\alpha \dot{\alpha} \right) + l_w \dot{l}_w \left(c_\alpha^2 - s_\alpha^2 \right) \dot{\alpha} \right. \\ &\quad - \dot{y}_b \left(\dot{l}_w s_\alpha s_\beta + l_w c_\alpha s_\beta \dot{\alpha} + l_w s_\alpha c_\beta \dot{\beta} \right) \\ &\quad \left. + \dot{z}_b \left(\dot{l}_w s_\alpha c_\beta + l_w c_\alpha \dot{\alpha} - l_w s_\alpha s_\beta \dot{\beta} \right) \right] - m_p g l_w s_\alpha c_\beta \end{aligned} \quad (2.28)$$

$$\frac{\partial L_p}{\partial \dot{\alpha}} = m_p \left[l_w^2 \dot{\alpha} - \dot{x}_b l_w c_\alpha + \dot{l}_w l_w s_\alpha c_\alpha - \dot{y}_b l_w s_\alpha s_\beta + \dot{z}_b l_w s_\alpha c_\beta \right] \quad (2.29)$$

$$\begin{aligned} \frac{d}{dt} \frac{\partial L_p}{\partial \dot{\alpha}} &= m_p \left[2l_w \dot{l}_w \dot{\alpha} + l_w^2 \ddot{\alpha} - \ddot{x}_b l_w c_\alpha - \dot{x}_b \left(\dot{l}_w c_\alpha - l_w s_\alpha \dot{\alpha} \right) + \ddot{l}_w l_w s_\alpha c_\alpha \right. \\ &\quad + \dot{l}_w^2 s_\alpha c_\alpha + l_w \dot{l}_w \left(c_\alpha^2 - s_\alpha^2 \right) \dot{\alpha} - \ddot{y}_b l_w s_\alpha s_\beta \\ &\quad - \dot{y}_b \left(\dot{l}_w s_\alpha s_\beta + l_w c_\alpha s_\beta + l_w s_\alpha c_\beta \right) + \ddot{z}_b l_w s_\alpha c_\beta \\ &\quad \left. + \dot{z}_b \left(\dot{l}_w s_\alpha c_\beta + l_w c_\alpha \dot{\alpha} - l_w s_\alpha s_\beta \dot{\beta} \right) \right] \end{aligned} \quad (2.30)$$

$$\begin{aligned} \frac{d}{dt} \frac{\partial L_p}{\partial \dot{\alpha}} - \frac{\partial L_p}{\partial \alpha} &= m_p \left[l_w^2 s_\alpha c_\alpha \dot{\beta}^2 + 2l_w \dot{l}_w \dot{\alpha} + l_w^2 \ddot{\alpha} - \ddot{x}_b l_w c_\alpha + \ddot{l}_w l_w s_\alpha c_\alpha + \dot{l}_w^2 s_\alpha c_\alpha \right. \\ &\quad \left. - \ddot{y}_b l_w s_\alpha s_\beta + \ddot{z}_b l_w s_\alpha c_\beta + g l_w s_\alpha c_\beta \right] \end{aligned} \quad (2.31)$$

Solving equation (2.27) and (2.31) with respect to $\ddot{\beta}$ and $\ddot{\alpha}$ yields the coupled pair of differential equation for the dynamics of the pendulum .

$$\ddot{\beta} = \frac{1}{l_w^2 c_\alpha^2} \left(-l_w c_\alpha c_\beta \ddot{y}_b - l_w c_\alpha s_\beta \ddot{z}_b + 2l_w \left(l_w s_\alpha c_\alpha \dot{\alpha} - \dot{l}_w c_\alpha^2 \right) \dot{\beta} - g l_w c_\alpha s_\beta \right) \quad (2.32)$$

$$\begin{aligned} \ddot{\alpha} &= \frac{1}{l_w^2} \left(l_w c_\alpha \ddot{x}_b + l_w s_\alpha s_\beta \ddot{y}_b - l_w s_\alpha c_\beta \ddot{z}_b - l_w s_\alpha c_\alpha \ddot{l}_w - l_w^2 s_\alpha c_\alpha \dot{\beta}^2 - s_\alpha c_\alpha \dot{l}_w^2 \right. \\ &\quad \left. - 2l_w \dot{l}_w \dot{\alpha} - g l_w s_\alpha c_\beta \right) \end{aligned} \quad (2.33)$$

According to [20] the choice of load swing angles made in (2.14) gives a compact, if not the most compact, equation of motion.

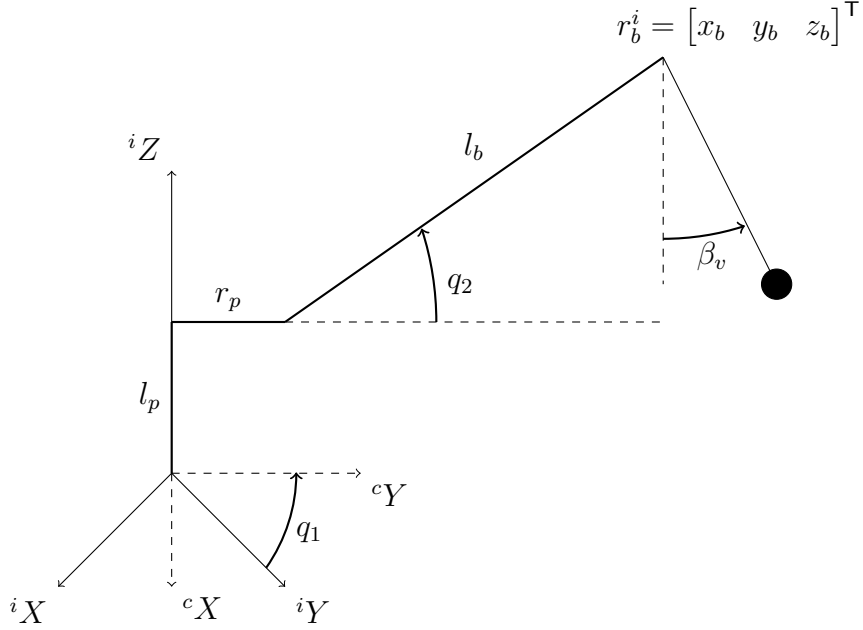


Figure 2.4: Crane-fixed coordinate system c and swing angle notation

2.2.4 Crane fixed frame

In equation (2.32) and (2.33) the swing angles is defined in the inertial frame. This is not ideal since the measurement of the swing angles will be measured in a crane-fixed coordinate system. Also it looks like the system has four inputs and two outputs with very strong connection, which makes it difficult to design a controller for a strongly coupled system. In order to achieve decoupling we define a crane-fixed frame c . The relation between a point in the inertial frame i and the crane-fixed frame c is then given by a rotation q_1 about the z-axis of the inertial frame i .

$$r^i = \begin{bmatrix} c_{q_1} & -s_{q_1} & 0 \\ s_{q_1} & c_{q_1} & 0 \\ 0 & 0 & 1 \end{bmatrix} r^c \triangleq R_c^i r^c \quad (2.34)$$

Defining a new set of Euler angles β_v and α_v , in the crane-fixed coordinate system giving the coordinates of the load r_h^c as

$$r_h^c = r_b^c + l_w \begin{bmatrix} -s_{\alpha_v} \\ c_{\alpha_v} s_{\beta_v} \\ -c_{\alpha_v} c_{\beta_v} \end{bmatrix} \triangleq r_b^c + l_w \Omega_v \quad (2.35)$$

Using the definition of the hook position (2.14) in the inertial frame and in the crane-fixed frame (2.35) with the rotation matrix defined in (2.34) to show the relation between the coordinates in the inertial frame i and the crane-fixed frame c .

$$r_b^i + l_w \Omega = R_c^i (r_b^c + l_w \Omega_v) = r_b^i + l_w R_c^i \Omega_v \quad (2.36)$$

which yields the transformation of the Euler angles from the inertial to the crane-fixed coordinate system.

$$\Omega = R_c^i \Omega_v \quad (2.37)$$

2.2.5 Equation of motion in the crane-fixed coordinate system

By using $r_h^i = r_b + l_w R_c^i \Omega_v$ when deriving the Euler-Lagrange equation (2.23) with the terms of x_b, y_b and z_b from equation (2.11), yields the equation of motion for the pendulum represented by the crane-fixed load swing angles β_v and α_v , the crane slew angle q_1 and the boom angle q_2 .

$$r_h^i = \begin{bmatrix} -(r_p + l_b c_{q_2}) s_{q_1} \\ (r_p + l_b c_{q_2}) c_{q_1} \\ l_p + l_b s_{q_2} \end{bmatrix} + l_w \begin{bmatrix} c_{q_1} & -s_{q_1} & 0 \\ s_{q_1} & c_{q_1} & 0 \\ 0 & 0 & 1 \end{bmatrix} \begin{bmatrix} -s_{\alpha_v} \\ c_{\alpha_v} s_{\beta_v} \\ -c_{\alpha_v} c_{\beta_v} \end{bmatrix} \quad (2.38)$$

$$\dot{r}_h^i = \begin{bmatrix} -r_p s_{q_1} - l_b c_{q_2} s_{q_1} - l_w c_{q_1} s_{\alpha_v} - l_w s_{q_1} c_{\alpha_v} s_{\beta_v} \\ r_p c_{q_1} + l_b c_{q_2} c_{q_1} - l_w s_{q_1} s_{\alpha_v} + l_w c_{q_1} c_{\alpha_v} s_{\beta_v} \\ l_p + l_b s_{q_2} - l_w c_{\alpha_v} c_{\beta_v} \end{bmatrix} \quad (2.39)$$

Differentiate equation (2.39) with respect to time to describe the velocity of the load in the inertial frame, where $\dot{r}_h^i = [\dot{x}_h^i \quad \dot{y}_h^i \quad \dot{z}_h^i]^T$.

$$\begin{aligned} \dot{x}_h^i &= -r_p c_{q_1} \dot{q}_1 - l_b (-s_{q_2} s_{q_1} \dot{q}_2 + c_{q_2} c_{q_1} \dot{q}_1) - \dot{l}_w c_{q_1} s_{\alpha_v} - l_w (-s_{q_1} s_{\alpha_v} \dot{q}_1 + c_{q_1} c_{\alpha_v} \dot{\alpha}_v) \\ &\quad - \dot{l}_w s_{q_1} c_{\alpha_v} s_{\beta_v} + l_w (c_{q_1} c_{\alpha_v} s_{\beta_v} \dot{q}_1 - s_{q_1} s_{\alpha_v} s_{\beta_v} \dot{\alpha}_v + s_{q_1} c_{\alpha_v} c_{\beta_v} \dot{\beta}_v) \end{aligned} \quad (2.40)$$

$$\begin{aligned} \dot{y}_h^i &= -r_p s_{q_1} \dot{q}_1 - l_b s_{q_2} c_{q_1} \dot{q}_2 - l_b c_{q_2} s_{q_1} \dot{q}_1 - \dot{l}_w s_{q_1} s_{\alpha_v} - l_w (c_{q_1} s_{\alpha_v} \dot{q}_1 - s_{q_1} c_{\alpha_v} \dot{\alpha}_v) \\ &\quad + \dot{l}_w c_{q_1} c_{\alpha_v} s_{\beta_v} + l_w (-s_{q_1} c_{\alpha_v} s_{\beta_v} \dot{q}_1 - c_{q_1} s_{\alpha_v} s_{\beta_v} \dot{\alpha}_v + l_w c_{q_1} c_{\alpha_v} c_{\beta_v} \dot{\beta}_v) \end{aligned} \quad (2.41)$$

$$\dot{z}_h^i = l_b c_{q_2} \dot{q}_2 - \dot{l}_w c_{\alpha_v} c_{\beta_v} + l_w (s_{\alpha_v} c_{\beta_v} \dot{\alpha}_v + c_{\alpha_v} s_{\beta_v} \dot{\beta}_v) \quad (2.42)$$

Recall that the Lagrangian is defined as

$$L_p = T_p - U_p \quad (2.43)$$

where

$$T_p = \frac{1}{2} m_p \|\dot{r}_h^i\|^2 \quad (2.44)$$

$$U_p = m_p g z_h^i \quad (2.45)$$

then the equation of motions for the pendulum yields

$$\begin{aligned} \ddot{\beta}_v &= \frac{1}{c_{\alpha_v} l_w} \left[-g s_{\beta_v} - 2c_{\alpha_v} \dot{\beta}_v \dot{l}_w + 2c_{\beta_v} s_{\alpha_v} \dot{l}_w \dot{q}_1 + r_p c_{\beta_v} \dot{q}_1^2 + l_b c_{\beta_v} c_{q_2} (\dot{q}_1^2 + \dot{q}_2^2) \right. \\ &\quad \left. + l_b s_{\beta_v} s_{q_2} \dot{q}_2^2 + l_w \left(2\dot{\alpha}_v (s_{\alpha_v} \dot{\beta}_v + c_{\alpha_v} c_{\beta_v} \dot{q}_1) + c_{\beta_v} (c_{\alpha_v} s_{\beta_v} \dot{q}_1^2 + s_{\alpha_v} \ddot{q}_1) \right) \right. \\ &\quad \left. - l_b c_{q_2} s_{\beta_v} \ddot{q}_2 + l_b c_{\beta_v} s_{q_2} \ddot{q}_2 \right] \end{aligned} \quad (2.46)$$

$$\begin{aligned} \ddot{\alpha}_v &= \frac{1}{2l_w} \left[-l_w \left(s_{2\alpha_v} \dot{\beta}_v^2 + 4c_{\alpha_v}^2 c_{\beta_v} \dot{\beta}_v \dot{q}_1 - c_{\beta_v}^2 s_{2\alpha_v} \dot{q}_1^2 + 2s_{\beta_v} \ddot{q}_1 \right) \right. \\ &\quad - 2 \left(g c_{\beta_v} s_{\alpha_v} + 2\dot{\alpha}_v \dot{l}_w + 2s_{\beta_v} \dot{l}_w \dot{q}_1 + r_p s_{\alpha_v} s_{\beta_v} \dot{q}_1^2 + l_b c_{q_2} s_{\alpha_v} s_{\beta_v} \dot{q}_1^2 \right. \\ &\quad \left. - 2l_b c_{\alpha_v} s_{q_2} \dot{q}_1 \dot{q}_2 + l_b c_{q_2} s_{\alpha_v} s_{\beta_v} \dot{q}_2^2 - l_b c_{\beta_v} s_{\alpha_v} s_{q_2} \dot{q}_2^2 + r_p c_{\alpha_v} \ddot{q}_1 + l_b c_{\alpha_v} c_{q_2} \ddot{q}_1 \right. \\ &\quad \left. + l_b c_{\beta_v} c_{q_2} s_{\alpha_v} \ddot{q}_2 + l_b s_{\alpha_v} s_{\beta_v} s_{q_2} \ddot{q}_2 \right) \end{aligned} \quad (2.47)$$

The above derivation of the equation of motion is done using Mathematica [24]. And the code is shown in appendix .

2.2.6 Model reduction

Despite the fact that the non-linear model of the pendulum motion in equation (2.46) and (2.47) may be accurate it is of interest to reduce the complexity of the model to be able to use the model for control design. The following assumption is made

B.1 The swing angles β_v and α_v is small

Assumption B.1 seems to be a fair, since it the oscillation of the load swing angles seldom is above 10° during normal operation. This assumption results in an elimination of all the sinus and cosines in equation (2.46)-(2.47), by stating that $s_{q_i} = q_i$ and $c_{q_i} = 1$, where $q_i = \{\beta_v, \alpha_v\}$ the model equations then reduces to

$$\begin{aligned} \ddot{\beta}_v = & \frac{1}{l_w} \left[-g\beta_v - 2\dot{\beta}_v\dot{l}_w + 2\alpha_v\dot{l}_w\dot{q}_1 + r_p\dot{q}_1^2 + l_b c_{q_2} (\dot{q}_1^2 + \dot{q}_2^2) \right. \\ & + l_b \beta_v s_{q_2} \dot{q}_2^2 + l_w \left(2\dot{\alpha}_v (\alpha_v \dot{\beta}_v + \dot{q}_1) + \beta_v \dot{q}_1^2 + \alpha_v \ddot{q}_1 \right) \\ & \left. - l_b c_{q_2} \beta_v \ddot{q}_2 + l_b s_{q_2} \ddot{q}_2 \right] \end{aligned} \quad (2.48)$$

$$\begin{aligned} \ddot{\alpha}_v = & \frac{1}{l_w} \left[-l_w (\alpha_v \dot{\beta}_v^2 + 2\dot{\beta}_v \dot{q}_1 - \alpha_v \dot{q}_1^2 + \beta_v \ddot{q}_1) \right. \\ & - \left(g\alpha_v + 2\dot{\alpha}_v \dot{l}_w + 2\beta_v \dot{l}_w \dot{q}_1 + r_p \alpha_v \beta_v \dot{q}_1^2 + l_b c_{q_2} \alpha_v \beta_v \dot{q}_1^2 \right. \\ & \left. - 2l_b s_{q_2} \dot{q}_1 \dot{q}_2 + l_b c_{q_2} \alpha_v \beta_v \dot{q}_2^2 - l_b \alpha_v s_{q_2} \dot{q}_2^2 + r_p \ddot{q}_1 + l_b c_{q_2} \ddot{q}_1 \right. \\ & \left. + l_b c_{q_2} \alpha_v \ddot{q}_2 + l_b \alpha_v \beta_v s_{q_2} \ddot{q}_2 \right) \end{aligned} \quad (2.49)$$

An attempt to reduce the model equations further, (2.48) and (2.49) is rewritten as follow [20].

$$\ddot{\beta}_v = -\omega_{\beta_v}^2 \beta_v + L_{\beta_v} \ddot{q}_2 - L_{\alpha_v} \dot{q}_1^2 + L_2 \dot{q}_1 + L_3 \dot{q}_2^2 - 2 \frac{\dot{l}_w \dot{\beta}_v}{l_w} + \left(2\dot{\alpha}_v \dot{\beta}_v + \ddot{q}_1 \right) \alpha_v \quad (2.50)$$

$$\ddot{\alpha}_v = -\omega_{\alpha_v}^2 \alpha_v - L_1 \dot{q}_1 - L_{\alpha_v} \ddot{q}_1 - \frac{2\dot{l}_w \dot{\alpha}_v}{l_w} + \beta_v \ddot{q}_1 \quad (2.51)$$

where

$$\omega_{\beta_v}^2 = \omega^2 - \frac{l_b s_{q_2}}{l_w} \dot{q}_2^2 + \frac{l_b c_{q_2}}{l_w} \ddot{q}_2 - \dot{q}_1^2 \approx \omega^2 \quad (2.52)$$

$$\begin{aligned} \omega_{\alpha_v}^2 = & \omega^2 + \dot{\beta}_v^2 - \frac{l_b (s_{q_2} - \beta_v c_{q_2})}{l_w} \dot{q}_2^2 - \dot{q}_1^2 \\ & + \frac{r_p + l_b c_{q_2} + \beta_v \dot{q}_1^2}{l_w} + \frac{l_b (c_{q_2} + \beta_v s_{q_2})}{l_w} \ddot{q}_2 \approx \omega^2 \end{aligned} \quad (2.53)$$

$$L_1 = \frac{2\dot{l}_w}{l_w} \beta_v + 2\dot{\beta}_v - \frac{2l_b \dot{q}_2 s_{q_2}}{l_w} \quad (2.54)$$

$$L_2 = 2\dot{\alpha}_v + 2 \frac{\dot{l}_w}{l_w} \alpha_v \quad (2.55)$$

$$L_3 = \frac{l_b c_{q_2}}{l_w} \quad (2.56)$$

$$L_{\beta_v} = \frac{l_b s_{q_2}}{l_w} \quad (2.57)$$

$$L_{\alpha_v} = \frac{r_p + l_b c_{q_2}}{l_w} \quad (2.58)$$

$$\omega^2 = \frac{g}{l_w} \quad (2.59)$$

By using the approximation that $\omega_{\beta_v} = \omega_{\alpha_v} \approx \omega$ [20] equation (2.50) and (2.51) can be written

$$\ddot{\beta}_v = -\omega^2 \beta_v + L_{\beta_v} \ddot{q}_2 - L_{\alpha_v} \dot{q}_1^2 + L_2 \dot{q}_1 + L_3 \dot{q}_2^2 - 2 \frac{\dot{l}_w \dot{\beta}_v}{l_w} + (2 \dot{\alpha}_v \dot{\beta}_v + \ddot{q}_1) \alpha_v \quad (2.60)$$

$$\ddot{\alpha}_v = -\omega^2 \alpha_v - L_1 \dot{q}_1 - L_{\alpha_v} \ddot{q}_1 - \frac{2 \dot{l}_w \dot{\alpha}_v}{l_w} + \beta_v \ddot{q}_1 \quad (2.61)$$

2.3 Linearized Crane Model

In this section a linearized crane model derived by [2] is presented. The same model was also used in [25]. This model is used to test the dynamics of the hoist winch in the WFS described in 4.2.

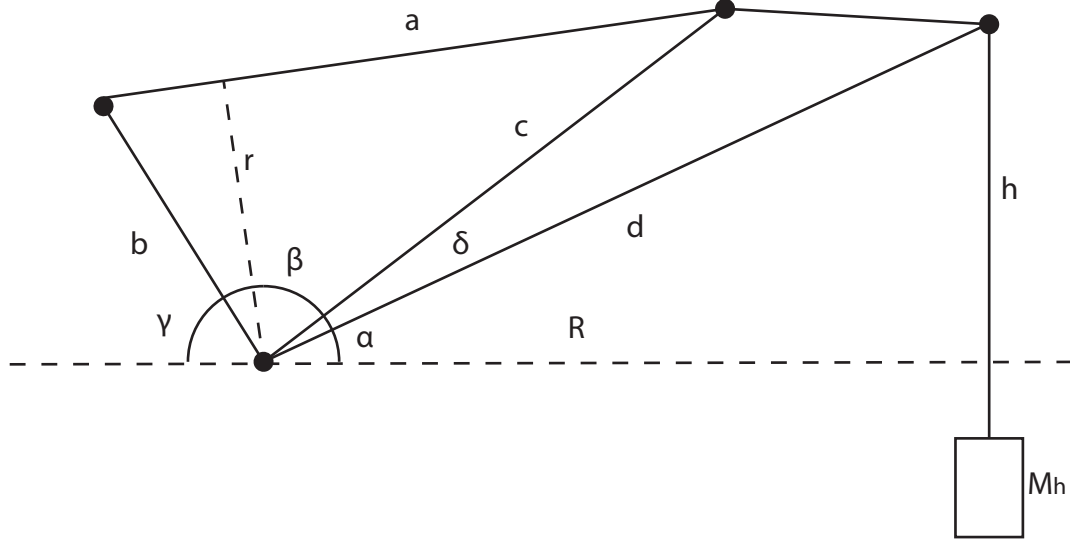


Figure 2.5: Schematic view of the crane geometry

In figure 2.5 the geometry aspect of the crane are shown. The following parameters are considered to be fixed on this model: b, c, d, δ . The other parameters will vary as the load varies or during winch motor operations.

Equations of motion

In order to derive the equations of motions some assumptions are made:

- The angular motions of the crane are small, so that the equation of motion can be linearized.
- The inertia of the pedestal is low and can be neglected in comparison with the boom inertia.

- The hinge is fixed.
- The centre of gravity of the boom is at half the distance between the hinge and the hoist crown sheaves.

The first assumption means that the varying radii $R = d \cos \alpha$ and $r = bc \sin \beta / a$ are treated as constants during simulations. Note that $R = d \cos \alpha$ is the cantilever radius and not the load radius, which refers to the rotation axis of the crane itself.

The equation of angular motion for the boom is

$$J_b \ddot{\alpha} = F_a r - F_h R - G_b R \quad (2.62)$$

where J_b is the moment of inertia, $G_b = M_b g / 2$ is half the weight of the boom, F_a is the (total) tension force in the luffing wire ropes, F_h is the (total) tension force in the hoist wire ropes. It is convenient to define an equivalent (vertical) boom tip force $F_b = F_a r / R$ giving the same force moment as the first term in (2.62). It is also convenient to transform the above equation to an equivalent motion of a linearly moving mass. By introducing the vertical boom tip motion by $y = (\alpha - \alpha_0) R$ and an effective boom tip mass $M_b = J_b / R^2$ the equation can be written as

$$M_b \ddot{y} = F_b - F_h - G_b \quad (2.63)$$

The equation of vertical motion for the external load is simply

$$M_h \ddot{z} = F_h - G_h \quad (2.64)$$

Where z is the vertical motion of the load, defined to be positive upwards. The hook load tension force can be expressed by

$$F_h = S_h (\zeta + y - z) \quad (2.65)$$

Where S_h is the stiffness or spring rate of the hoist line, ζ is the motor based shortening of the hoist line. The tension force of the luffing lines can similarly be expressed as a result of the elastic stretch of the luffing lines and the bending of the pedestal. Denoting the angular compliance of the pedestal by $C_\gamma = (\gamma - \gamma_0) / (F_b R)$ and the longitudinal luffing line compliance by C_a we can define an effective boom tip stiffness by

$$S_b = \frac{R^2}{C_\gamma + r^2 C_a} \quad (2.66)$$

The boom tip tension force can now be expressed by

$$F_b = S_b (\eta - y) \quad (2.67)$$

Where η is the motor based vertical motion of the boom tip.

By combining equation (2.63), (2.64), (2.65) and (2.67) the equation of motion can be written on matrix form as

$$\begin{bmatrix} M_b & 0 \\ 0 & M_h \end{bmatrix} \begin{bmatrix} \ddot{y} \\ \ddot{z} \end{bmatrix} + \begin{bmatrix} S_b + S_h & -S_h \\ -S_h & S_h \end{bmatrix} \begin{bmatrix} y \\ z \end{bmatrix} = \begin{bmatrix} S_b & 0 \\ 0 & S_h \end{bmatrix} \begin{bmatrix} \eta \\ \zeta \end{bmatrix} + \begin{bmatrix} G_b \\ G_h \end{bmatrix} \quad (2.68)$$

2.4 Vessel Heave Motion

In order to predict any future behaviour of the vessels heave motion it is necessary to have a mathematical model that describes the heave motion of the vessel. The following model is found in [8].

$$G(s) = \frac{K\omega_0 s}{s^2 + 2\lambda\omega_0 s + \omega_0^2} w_3 + d_3 \quad (2.69)$$

where d_3 is modeled as slowly varying bias term

$$\dot{d}_3 = w_6 \quad (2.70)$$

and w_3, w_6 is Gaussian white noise processes.

2.4.1 State space representation

A linear state space representation obtained from (2.69) by transforming the transfer function to time domain with $\dot{y}(0) = y(0) = 0$.

$$\dot{\mathbf{x}} = \mathbf{A}\mathbf{x} + e w_3 \quad (2.71)$$

$$y = \mathbf{c}^T \mathbf{x} \quad (2.72)$$

By choosing $x_1 = z$, $x_2 = \dot{z}$ and $x_3 = w$, where z is measured heave motion from the camera system, \dot{z} is heave velocity and w is bias, the linear state space can be written on matrix form as

$$\begin{bmatrix} \dot{x}_1 \\ \dot{x}_2 \\ \dot{x}_3 \end{bmatrix} = \begin{bmatrix} 0 & 1 & 0 \\ -\omega_0(t)^2 & 2\lambda\omega_0(t) & \omega_0(t)^2 \\ 0 & 0 & 0 \end{bmatrix} \begin{bmatrix} x_1 \\ x_2 \\ x_3 \end{bmatrix} \quad (2.73)$$

where the system matrices $\mathbf{A}(t)$ and \mathbf{C} is

$$\mathbf{A}(t) = \begin{bmatrix} 0 & 1 & 0 \\ -\omega_0(t)^2 & 2\lambda\omega_0(t) & \omega_0(t)^2 \\ 0 & 0 & 0 \end{bmatrix} \quad (2.74)$$

$$\mathbf{C} = [1 \ 0 \ 0] \quad (2.75)$$

where λ and ω_0 and w is all unknown variables needed to be estimated.

2.4.2 Discrete state space

The state space is discretized using an first-order approximation (Euler discretization). See [8] Appendix B.

$$\mathbf{A}_d[k] = \mathbf{I} + \mathbf{A}(t)\Delta t \approx e^{\mathbf{A}T} \quad (2.76)$$

$$\mathbf{C}_d = \mathbf{C} \quad (2.77)$$

2.5 Angular Deflection of the Hoist Winch Wire

In order to use a Kalman filter to remove the influence of measurement noise from the sensors measuring the angular deflection β_v , α_v of the wire on the rotary crane a mathematical model is necessary. The model described in equation (2.78) is obtained from [8], and is used to describe the oscillation of the angular deflection of the hoist winch wire relative to the crane fixed coordinate system.

$$G(s) = \frac{K\omega_0 s}{s^2 + 2\lambda\omega_0 s + \omega_0^2} w_3 + d_3 \quad (2.78)$$

where d_3 is modeled as slowly varying bias term

$$\dot{d}_3 = w_6 \quad (2.79)$$

2.5.1 State space representation

A linear state space representation obtained from (2.78) by transforming the transfer function to time domain with $\dot{y}(0) = y(0) = 0$.

$$\dot{\mathbf{x}} = \mathbf{A}\mathbf{x} + e w_3 \quad (2.80)$$

$$y = \mathbf{c}^\top \mathbf{x} \quad (2.81)$$

By choosing $x_1 = x_i$, $x_2 = \dot{x}_i$ and $x_3 = w$, where x_i is measured angular deflection from the sensors where $i = \{1, 2\}$ represents the two measured angles β_v and α_v . \dot{x}_i is angular velocity and w is bias, the linear state space can be written on matrix form as

$$\begin{bmatrix} \dot{x}_1 \\ \dot{x}_2 \\ \dot{x}_3 \end{bmatrix} = \begin{bmatrix} 0 & 1 & 0 \\ -\omega_0(t)^2 & 2\lambda\omega_0(t) & \omega_0(t)^2 \\ 0 & 0 & 0 \end{bmatrix} \begin{bmatrix} x_1 \\ x_2 \\ x_3 \end{bmatrix} \quad (2.82)$$

where the system matrices $\mathbf{A}(t)$ and \mathbf{C} is

$$\mathbf{A}(t) = \begin{bmatrix} 0 & 1 & 0 \\ -\omega_0(t)^2 & 2\lambda\omega_0(t) & \omega_0(t)^2 \\ 0 & 0 & 0 \end{bmatrix} \quad (2.83)$$

$$\mathbf{C} = [1 \ 0 \ 0] \quad (2.84)$$

where $\lambda = 0.1$ is chosen by experimental result, $\omega_0(t) = \sqrt{\frac{g}{l_w(t)}}$, $g = 9.81$ and $l_w(t)$ is the wire length at time t .

2.5.2 Discrete state space

An discrete model of the state space is found using an first-order approximation (Euler discretization). See [8] Appendix B.

$$\mathbf{A}_d[k] = \mathbf{I} + \mathbf{A}(t)\Delta t \approx e^{\mathbf{A}T} \quad (2.85)$$

$$\mathbf{C}_d = \mathbf{C} \quad (2.86)$$

2.6 Wind Model

In this section a simple wind model is described [29]

$$\ddot{\xi} = k_{\delta w} \delta(t) - 2\zeta \omega_0 - \zeta \omega_0^2 \quad (2.87)$$

$$w = \xi + \bar{w} \quad (2.88)$$

where w is the wind in $[m/s]$ along X axis in the inertial frame respectively, $\delta(t)$ is unity white noise, \bar{w} is wind middle value and $\omega_0, \zeta, k_{\delta w}$ is design parameters set to

$$k_{\delta w} = 3 \quad (2.89)$$

$$\omega_0 = \pi \quad (2.90)$$

$$\zeta = 0.3 \quad (2.91)$$

$$\bar{w} = 10 \quad (2.92)$$

2.6.1 Wind Forces

The wind forces are described as [8]

$$\tau_{wind} = \frac{1}{2} \rho_a w^2 c A \quad (2.93)$$

where $\rho_a = 1.293[kg/m^3]$ is the air density, w is the wind described in (2.88), $c = 0.47$ is the drag coefficient, and $A = \pi r^2 = 9[m^2]$ is the projected area of the sphere. In order to add the wind forces to the equation of motion of the pendulum the following assumptions are done

$$\tau_{wind\beta} = \tau_{wind} \cos(q_1) \quad (2.94)$$

$$\tau_{wind\alpha} = \tau_{wind} \sin(q_1) \quad (2.95)$$

The wind forces is then added to the equation of motion in (2.46),(2.47) as an additional term

$$\ddot{\beta}_{vwind} = \ddot{\beta}_v + \frac{1}{c_{\alpha_v} l_w} \left(\frac{\tau_{wind\beta}}{m} \right) \quad (2.96)$$

$$\ddot{\alpha}_{vwind} = \ddot{\alpha}_v + \frac{1}{2l_w} \left(\frac{\tau_{wind\alpha}}{m} \right) \quad (2.97)$$

where m is the mass of the load.

Chapter 3

Filtering and Parameter Estimation

3.1 Estimation of Vessel Model Parameters

3.1.1 Heave measurement

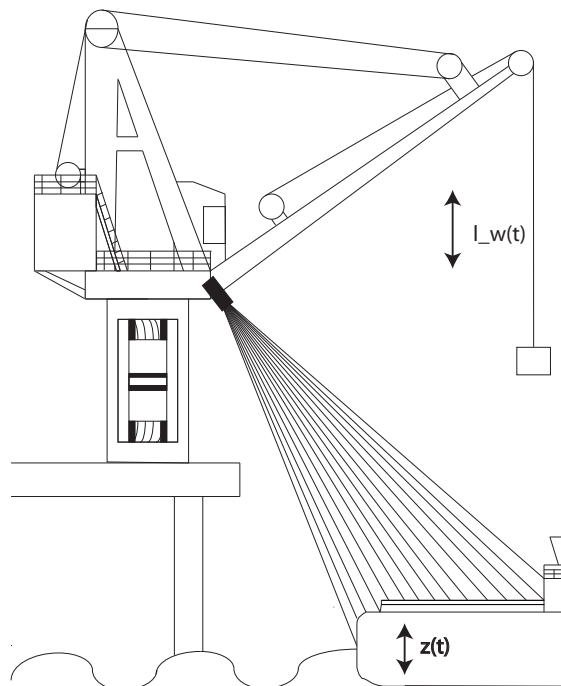


Figure 3.1: Sketch of real-time stereo video camera measurement system

The heave measurement z is measured using an real-time stereo video system derived by Hornang, S. in 2010 [5]. The details of the algorithm used in the stereo video camera systems will not be discussed in this thesis since the report is not public available until June 26, 2015. In this thesis it is assumed that the camera system output the heave signal to the wave synchronization system at 100Hz.

3.1.2 Parametric model of the vessel heave motion

The online parameter estimation algorithms presented in this section are intended to estimate the unknown vessel heave motion model parameters described in section 2.4.

Rewriting equation (2.73) with respect to \ddot{z} where $x_1 = z$, $x_2 = \dot{z}$, $x_3 = w$, and w is bias yields

$$\ddot{z} = \omega_0^2 z + 2\lambda\omega_0 \dot{z} + \omega_0^2 w \quad (3.1)$$

Rewrite equation (3.1) with respect to z to get it on parametric form

$$z = -\frac{1}{\omega_0^2} \ddot{z} + \frac{2\lambda}{\omega_0} \dot{z} + w \quad (3.2)$$

Defining $Y = \psi^\top \theta$, where

$$Y = z \quad (3.3)$$

$$\psi = [-\ddot{z} \quad \dot{z} \quad w]^\top \quad (3.4)$$

$$\theta = \left[\frac{1}{\omega_0^2} \quad \frac{2\lambda}{\omega_0} \quad w \right]^\top \quad (3.5)$$

As seen the ψ vector includes the derivatives of z . This is not optimal since the derivatives can contribute to noise and unboundedness. To avoid derivatives in the calculation both sides of equation (3.1) is filtered with a stable filter. Define

$$Z(s) = \phi(s)^\top \theta = \frac{1}{\Lambda(s)} Y(s) \quad (3.6)$$

$$\phi(s) = \frac{1}{\Lambda(s)} \psi(s) \quad (3.7)$$

$$\psi(s) = [-s^2 z \quad s z \quad 1]^\top \quad (3.8)$$

$$\Lambda(s) = s^2 + s + 1 \quad (3.9)$$

Two different parameter estimation algorithms are tested. The algorithms used are taken from [21].

3.1.3 Normalized estimation error

In order to measure the quality of the parameter estimates an estimation error variable ε is defined.

$$\varepsilon = \frac{z - \hat{z}}{m^2} \quad (3.10)$$

where z is the measurement (3.2), \hat{z} is the estimate and m^2 is a design variable.

$$z = \theta^{*\top} \phi \quad (3.11)$$

$$\hat{z} = \theta^\top \phi \quad (3.12)$$

$$m^2 = 1 + n_s^2 \quad (3.13)$$

where θ and ϕ is the vectors defined in (3.5),(3.7) and n_s is a design variable which definition is depended on choice of algorithm.

3.1.4 Least-squares with covariance resetting

The adaptive law for the parameter estimation is

$$\dot{\theta} = P\varepsilon\phi \quad (3.14)$$

the update of the covariance matrix P is

$$\dot{P} = -P\frac{\phi\phi^\top}{m^2}P, \quad P(t_r^+) = P_0 = \rho_0 I \quad (3.15)$$

where t_r is the time for which

$$\lambda_{min}(P) \leq \rho_1 \quad (3.16)$$

$\lambda_{min}(P)$ is the smallest eigenvalue of P , m^2 is defined in (3.13) and the design variables is defined as

$$\rho_0 > \rho_1 > 0 \quad (3.17)$$

$$n_s^2 = \alpha\phi^\top\phi \quad (3.18)$$

where $\alpha > 0$, such that $\frac{\phi}{m} \in \mathcal{L}_\infty$.

The choice of variables from experimental result is $\alpha = 10$, $\rho_0 = 10^2$ and $\rho_1 = 10$.

3.1.5 Least-squares with forgetting factor

The adaptive law $\dot{\theta}$ is the same as in (3.14), while covariance update \dot{P} is defined as

$$\dot{P} = \begin{cases} \beta P - \frac{P\phi\phi^\top P}{m^2}, & \text{if } \|P(t)\| \leq R_0 \\ 0 & \text{otherwise} \end{cases} \quad (3.19)$$

where m^2 is defined in (3.13), while the initial values and design variables is defined as

$$P(0) = P_0 \quad (3.20)$$

$$n_s^2 = \phi^\top P \phi \quad (3.21)$$

$$\beta > 0 \quad (3.22)$$

$$R_0 > 0 \quad (3.23)$$

$$P_0 = P_0^\top > 0 \quad (3.24)$$

$$\|P_0\| \leq R_0 \quad (3.25)$$

The choice of variables from experimental result is $\beta = 0.97$, $R_0 = 10^2$ and $P_0 = 10^3 \times \text{diag}([1 \ 1 \ 1])$.

3.2 Kalman Filtering of Sensor Measurement

By using a Kalman filter it is possible to minimize the effect of measurement noise from sensors without having problem with time delay between the input and the output from the filter. In this thesis Kalman filter is applied to the measurement of the angular deflection of the wire (β_v, α_v) , and also the heave measurement z from the camera system used in the WFS.

3.2.1 Kalman filter with variable Kalman gain

The adaptive Kalman gain \mathbf{K} is calculated for each timestep

$$\mathbf{P} = \mathbf{A}_d \mathbf{P} \mathbf{A}_d^T + \mathbf{Q} \quad (3.26)$$

$$S = \mathbf{C} \mathbf{P} \mathbf{C}^T + R \quad (3.27)$$

$$\mathbf{K} = \mathbf{P} \mathbf{C}^T S^{-1} \quad (3.28)$$

$$\mathbf{P} = (\mathbf{I} - \mathbf{K} \mathbf{C}) \mathbf{P} \quad (3.29)$$

The weight matrices for the Kalman filter are selected by parameter experimentation, and becomes

$$R = 1 \quad (3.30)$$

$$\mathbf{Q} = \begin{bmatrix} 0 & 0 & 0 \\ 0 & 0.1 & 0 \\ 0 & 0 & 0.5 \end{bmatrix} \quad (3.31)$$

And the update of the state estimate $\hat{\mathbf{x}}[k+1]$, the output from the Kalman filter $\hat{y}[k]$ and the error $e[k]$ is then calculated by

$$\hat{\mathbf{x}}[k] = \mathbf{A}_d \hat{\mathbf{x}} + \mathbf{K} e \quad (3.32)$$

$$\hat{y}[k] = \mathbf{C} \hat{\mathbf{x}} \quad (3.33)$$

$$e[k] = x - \hat{y} \quad (3.34)$$

where x is the angle measurement.

3.2.2 Comparison between the two parameter estimation algorithm

z	-	Heave measurement from the camera system
\hat{y}_1	-	\hat{y} from Kalman filter with least-squares with covariance resetting algorithm *
\hat{y}_2	-	\hat{y} from Kalman filter with least-squares with forgetting factor **
*	-	see equation (3.15)
**	-	see equation (3.19)

Table 3.1: Notation of variables for figure 3.2

Figure 3.2 represent a detail view of the plot where the two different parameter estimation algorithms described in equation (3.14),(3.15) and (3.14),(3.19) are tested as input to the Kalman filter and compared. In appendix E.1 a plot of the whole input signal is found.

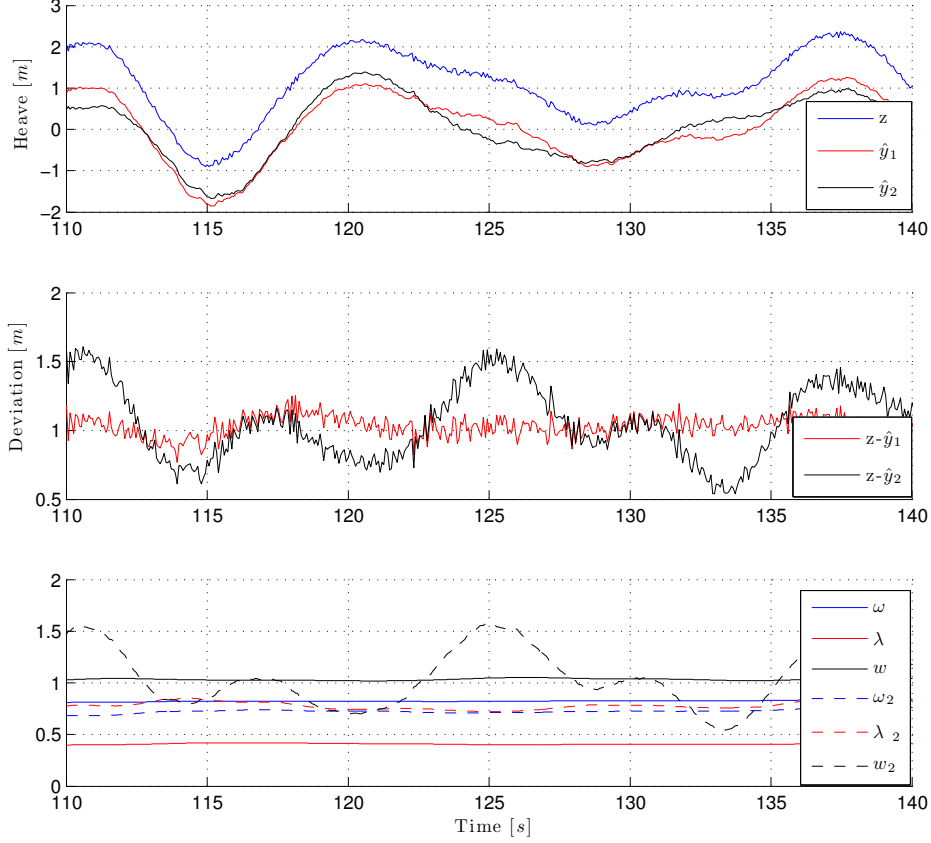


Figure 3.2: Detail view of Kalman filter with two different parameter estimation algorithm as input

As seen in figure 3.2, \hat{y}_1 gives the best representation of a filtered, unbiased version of the input signal z .

3.2.3 Prediction

To cancel the effect of time delays in both the crane control system, and in the camera measurement system it is necessary to predict future behaviour of the vessel. The prediction time is assumed to be static. This assumption is fair, since an real experiment on a full scale crane will show the time delays in the control systems, and a comparison between the camera measurement output and a MRU time series from the vessel will reveal the time delay in the camera system. The prediction is

$$\hat{x}(k+d) = A^D \hat{x}(k) \quad (3.35)$$

$$D = d + \varepsilon \quad (3.36)$$

$$\hat{y}(k+d) = \hat{x}(k+d) \quad (3.37)$$

where $k+d$ is the prediction of $\hat{x}(k)$ d steps in the future, and ε is a static tuning parameter.

Chapter 4

Control Design

The rotary crane with spherical pendulum is classified as a under actuated system since the model consists of five degrees of freedom $\{q_1, q_2, l_w, \beta_v, \alpha_v\}$, where only three are controllable, that is $\{q_1, q_2, l_w\}$. Stating the actuator velocity limitations as

Notation	Description	Limit
\dot{q}_1	Slew angle velocity	± 0.1 [rad/s]
\dot{q}_2	Boom angle velocity	± 0.02 [rad/s]
\dot{l}_w	hoist wire velocity	± 2.2 [m/s]

Table 4.1: Crane actuator velocity limitations

4.1 Anti-sway control and boom tip positioning control for rotary crane

Defining a vector representing the crane rotation angles and its derivative as

$$r_c = [q_1 \quad q_2]^T \quad (4.1)$$

$$\dot{r}_c = [\dot{q}_1 \quad \dot{q}_2]^T \quad (4.2)$$

where q_1, q_2 is slew angle and boom angle as described in figure 2.2.

4.1.1 Actuator dynamics

In this thesis the dynamics of the rotary crane is not modelled, since the boom and slew machinery of the crane is assumed to be stiff, see assumption A.2 in section 2.2. Although the crane is assumed to be stiff the slew and boom machinery has some dynamics in case of response time which needs to be implemented in order to get a somewhat realistic response of the control system and the crane operator input. To simulate this actuator dynamics a low pass filter is designed with the desired velocity $u(t)$ as input through a first order exponential filter.

The desired velocity input to the crane model is proportional to the filtered joystick

input multiplied by the actuator limitations. The exponential filter used in the crane model is defined as

$$\dot{r}_c(t) = \dot{r}_c(t-1) + (u(t) - \dot{r}_c(t-1)) \left(1 - e^{-\frac{T_s}{T}}\right) \quad (4.3)$$

where \dot{r}_c is the actual angle velocity of the actuators described in , $\dot{r}_c(t-1)$ is the velocity at previous output, $u(t)$ is the desired actuator velocity , T_s is the sample time and T is the desired time constant of the filter.

4.1.2 Anti-sway control

Starting by defining an error measurement ϵ for each of the angular deflections.

$$\epsilon_\beta = \beta_{des} - \hat{\beta}_v \quad (4.4)$$

$$\epsilon_\alpha = \alpha_{des} - \hat{\alpha}_v \quad (4.5)$$

where $\beta_{des} = \alpha_{des} = 0$ is the desired angular deflection of the wire and $\hat{\alpha}_v, \hat{\beta}_v$ is the filtered measurement of the angular deflection of the wire. Then defining the controller as

$$\tau_{sway} = \begin{bmatrix} \tau_\alpha \\ \tau_\beta \end{bmatrix} \quad (4.6)$$

$$\tau_\beta = K_\beta \epsilon_\beta \quad (4.7)$$

$$\tau_\alpha = K_\alpha \epsilon_\alpha \quad (4.8)$$

where $K_\beta = 20$ and $K_\alpha = -10$ is the proportional gains, chosen by experiment.

4.1.3 Boom tip positioning control

The object for the positioning controller is to control the crane angles to a desired value. The desired slew and boom angle r_{des} for the controller is stored when the operator activates the controller as described in the following algorithm.

Algorithm 1 Store the boom angle and slew angle when the controller is activated

```

if controller-active then
  if activated==0 then
     $q_{1_{des}} = q_1$ 
     $q_{2_{des}} = q_2$ 
    activated == 1
  end if
else if activated==1 && controller-active==0 then
  activated == 0
   $q_{1_{des}} = 0$ 
   $q_{2_{des}} = 0$ 
end if
if activated==1 && controller-active==1 then
   $r_{des} = \begin{bmatrix} q_{1_{des}} + \int \tau_{operator_{q1}} \\ q_{2_{des}} + \int \tau_{operator_{q2}} \end{bmatrix}$ 
else
   $r_{des} = \begin{bmatrix} q_{1_{des}} \\ q_{2_{des}} \end{bmatrix}$ 
end if

```

The error input ε to the controller is

$$\varepsilon_{pos} = r_{des} - r_c \quad (4.9)$$

$$r_c = \begin{bmatrix} q_1 \\ q_2 \end{bmatrix} \quad (4.10)$$

where q_1, q_2 is the crane slew and boom angle. The controller is chosen as a Proportional-Integral controller with anti windup [12] where the limited output τ_{pos} is

Algorithm 2 Boom tip position controller with saturation

```

 $\tau_{pos} = \left(k_p + \frac{k_i}{s}\right) \varepsilon$ 
if  $\tau_{pos} > 1$  then
   $\tau_{pos} = 1$ 
else if  $\tau_{pos} < -1$  then
   $\tau_{pos} = -1$ 
end if

```

where the controller gains $k_i = 60$ and $k_p = 120$ is chosen by experiment, and ε is described in (4.9).

4.1.4 Cascade Control with Operator in-the-loop

The two controllers described in 4.1.2 and 4.1.3 is connected in cascade with the operator input by the following algorithm

Algorithm 3 Cascade control of anti-sway, boom tip positioning and operator

```
if controller-active then
  if  $abs(\beta_v) > 0.05$  or  $abs(\alpha_v) > 0.05$  then
     $\tau_{controller} = 0.85 \times \tau_{sway} + 0.15 \times \tau_{pos}$ 
  else
     $\tau_{controller} = \tau_{pos}$ 
  end if
else
   $\tau_{controller} = \begin{bmatrix} 0 \\ 0 \end{bmatrix}$ 
end if
 $\tau_{tot} = \tau_{controller} + \tau_{operator}$ 
if  $\tau_{tot} > 1$  then
   $\tau_{tot} = 1$ 
else if  $\tau_{tot} < -1$  then
   $\tau_{tot} = -1$ 
end if
```

where $\tau_{operator}$ is the operator input through the joystick interface, $\tau_{operator} \in \{-1, 1\}$.

4.2 Wave following control system

This section is previously presented in [25].

The wave synchronization system is a system which purpose is to make the hook follow the oscillatory motion of the vessel $z(t)$, with same phase and amplitude by controlling the wire length $l_w(t)$.

Set point trajectory

At start up the distance between the crane hook and the vessel is set to 35m. To be able to simulate the crane operator and control the hook towards the vessel in a smooth way a set-point trajectory is derived.

$$T(k) = Z_{ref} (1 - e^{(-T_s k)/T_{ref}}) \quad (4.11)$$

where Z_{ref} is the desired motion of the crane, T_s is the sample time of the measurement (15Hz), T_{ref} is the time where 63% of the measurement is used as set-point, and k is the sample number.

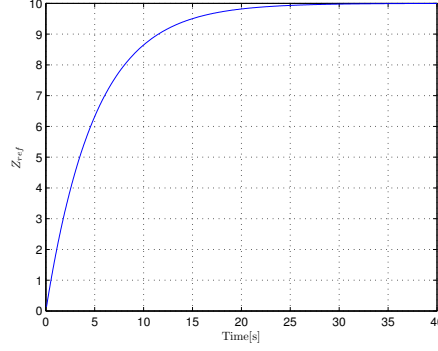


Figure 4.1: Example of set-point trajectory $T(k)$. $T_s = 1/15$, $T_{ref} = 5$

Controller error

The main objective is to control the hook load to follow the motion of the vessel, the controller error is therefore

$$e_1(k) = T(k) - Z_{load} \quad (4.12)$$

where Z_{load} is the measured position of the load, this position is available in the crane simulator, but is not available in the real control system. Therefore an alternative control error is defined.

$$e_2(k) = T(k) - Z_{hook} \quad (4.13)$$

where Z_{hook} is the measured position of the hook, based on the encoder mounted on the hoist winch. This measurement does not include the dynamics of the hoist wire nor the boom dynamics. This measurement is available in the crane control system.

Controller

The controller chosen for this test is a limited PI-controller with anti wind-up, where $P = 1.8$, $T_i = 15$ and $T_a = T_i$ are the controller parameters chosen by experiment.

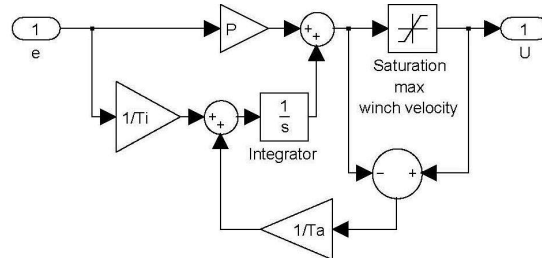


Figure 4.2: Simulink diagram of the PI regulator with anti windup

The saturation block in the regulator controls the upper and lower limit of the output. The limitation is chosen based on hook load, see figure (4.3).

Actuator limitations

The hoist winch has limitations on maximum speed depended on various loads. One one fall configuration on the hoist, the following figure shows the constraints of maximum speed as a function of hook load.

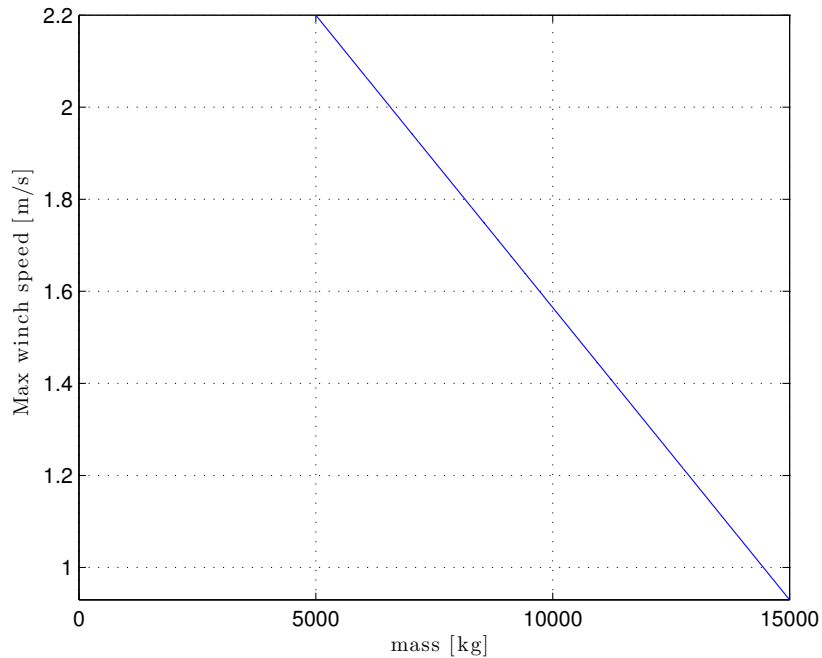


Figure 4.3: Speed profile of 1 fall configuration hoist winch

Prediction error

To be able to check the quality of the prediction the prediction error is defined as

$$\varepsilon(k) = \hat{y}_{pred}(k-d) - \hat{y}(k) \quad (4.14)$$

where $\hat{y}_{pred}(k-d)$ is the predicted signal d samples ago, and $\hat{y}(k)$ is the Kalman filtered measurement from the camera system.

Chapter 5

Visualization

In this chapter visualizations of both the 3DOF trolley with pendant load model presented in section 2.1, and the rotary crane with spherical pendulum presented in section 2.2. The visualization is made by use of the V-Realm Builder. This builder is a built-in editor in the 3D animation toolbox. The builder compiles the finished visualization as a VRML (*.wrl) file [22], and is implemented in Simulink by use of the "VR Sink" block in the Simulink 3D animation library. Using this sort of visualization gives the programmer an alternative tool to determine model errors during simulation, by looking at the modelled object in a "real" environment.

5.1 3DOF Trolley with pendant load

In this section the visualization of the 3DOF trolley with pendant load will be presented, which model is presented in section 2.1. The visualization is made by use of the 3D Animation Toolbox in Simulink. The following variables are implemented in the visualization.

- X-axis translation $x_t(t)$ of the trolley.
- Wire length $l_w(t)$.
- Pendulum angle $\theta(t)$

Figure 5.1 shows a screen shot from the visualization made by 3D animation studio in Simulink.

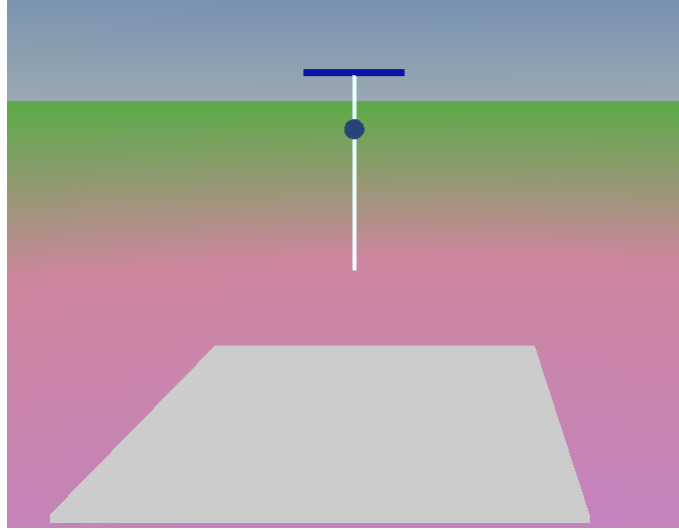


Figure 5.1: Visualisation of 3DOF trolley with pendant load

5.2 Rotary crane with spherical pendulum

In this section the visualization of the rotary crane with spherical pendulum is presented. In this visualization the following variables are implemented.

- Slew angle $q_1(t)$ [rad]
- Boom angle $q_2(t)$ [rad]
- Wire length $l_w(t)$ [m]
- Wire velocity $\dot{l}_w(t)$ [m/s]
- Pendulum angle $\alpha(t)$ [rad]
- Pendulum angle $\beta(t)$ [rad]
- Boom tip position vector r_b [m]
- Load position vector r_p [m]

5.2.1 Visualization of rotary crane with box shaped boom

Figure 5.2 shows a screen shot from the visualization made of the rotary crane. As seen the visualization has two text fields implemented in the visualization which updates the information about the hoisting velocity \dot{l}_w and the wire length l_w . Also the reflection of the boom tip on the ground (red) is implemented, along with the reflection of the load (blue). This is done by using the r_b, r_h vector where the z-axis values is chosen as a constant. Also the presentation of the load is chosen to be drawn by use of the x, y and z component of the r_h vector.

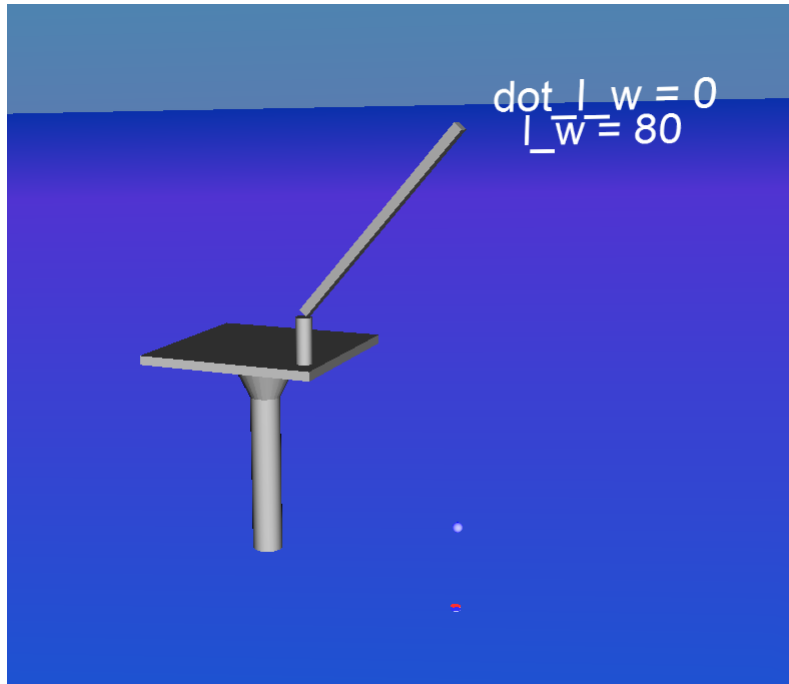


Figure 5.2: Visualisation of rotary crane with spherical pendulum

5.2.2 Visualization of rotary crane with inventor drawings

In figure 5.3 an different visualization of the rotary crane is presented. This visualization of the crane graphics has been made by transforming a stripped version of a Lattice Offshore Crane Inventor [26] assembly drawing from National Oilwell Varco, to a VRML [22] file using a trial version of the program PolyTrans [27].

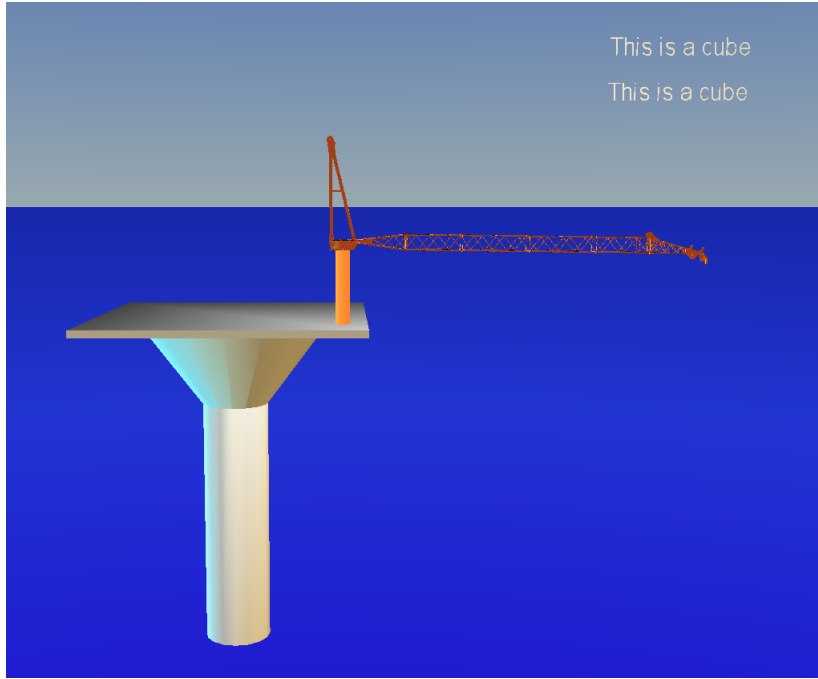


Figure 5.3: Visualisation of rotary crane made from inventor drawing

5.2.3 Visualization of rotary crane with graphs

Figure 5.4 shows an 3D visualization of the boxed shaped crane with graphs. This visualization was made by modifying an Matlab S-function found in the Simulink 3D Animation demo *vr_octavia_graphs*. In order to use this visualization it is necessary to run the same VRML file in the model using a VR Sink block.

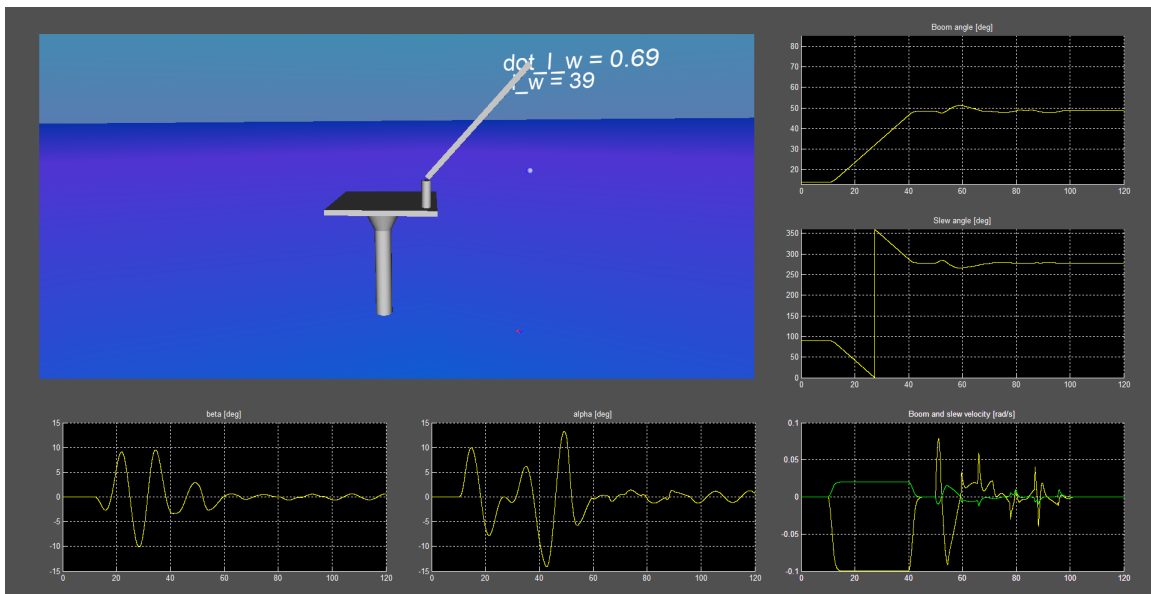


Figure 5.4: 3D visualization with graphs

This visualization consist of the following elements

Object position	Description
Top Left	3D Visualization of the VRML object.
Bottom Left	Plot of β_v [deg]
Bottom Center	Plot of α_v [deg]
Bottom Right	Plot of \dot{q}_1 and \dot{q}_2 [rad/s]
Center Right	Plot of q_1 [deg]
Top Right	Plot of q_2 [deg]

Table 5.1: 3D visualization with graphs - object description

The Y-axis limits for the plots and the VRML file used is defined by the function mask parameters as shown in figure 5.5. The X-axis limits for the plots are captured from the Simulink simulation stop time parameter.

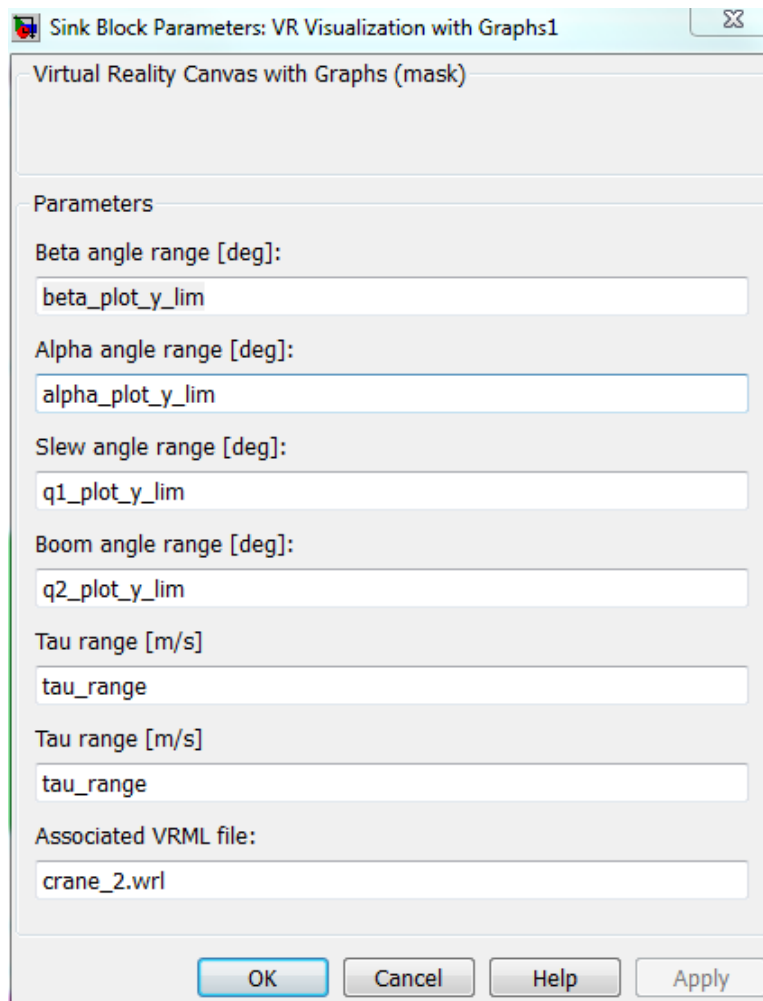


Figure 5.5: 3D visualization with graphs - mask parameters

Chapter 6

Simulation

6.1 Rotary crane with spherical pendulum

In this section the closed loop system of the rotary crane model with spherical pendulum presented in section 2.2.5 is simulated with the anti-sway controller and the boom tip positioning controller derived in 4.1. The results of the simulation is presented and discussed in 6.1.2.

6.1.1 Introduction

Every simulation start with $\beta_v = \alpha_v = \dot{\beta}_v = \dot{\alpha}_v = 0$. The test signal used is a ramp that starts at $t = 10s$ and stops at $t = 40s$, the regulators is activated at $t = 50s$, and deactivated at $t = 100s$. All scenarios stops at $t = 120s$. Figure 6.1 shows the test signal used to rotate the crane and hoist the boom. The crane angles starts at $q_1 = 90^\circ, q_2 = 14^\circ$, and stops at $q_1 \approx 279^\circ, q_2 \approx 48^\circ$.

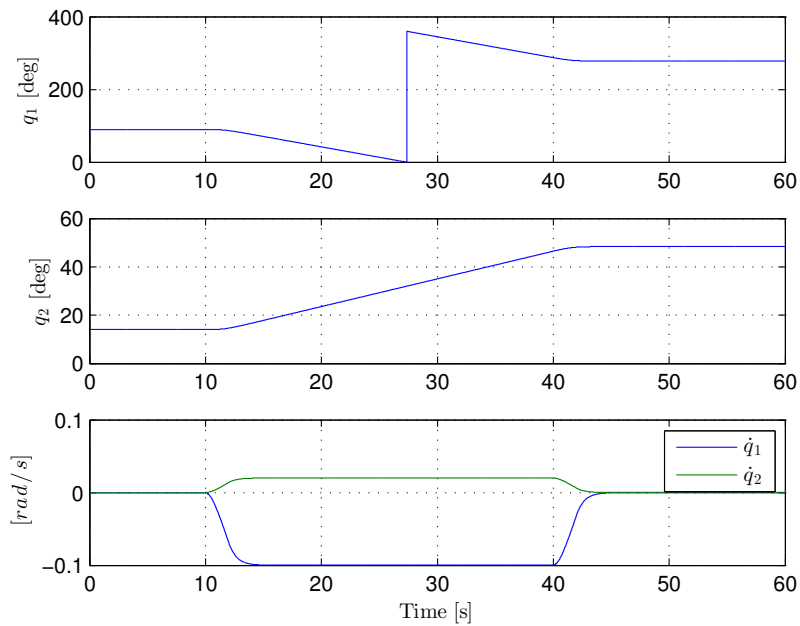


Figure 6.1: Plot of the test signal used for slew q_1 and boom motion q_2

Figure 6.2 presents a plot of the hoist winch test signal, which is used to evaluate which effect $\dot{l}_w \neq 0$ has on the pendulum dynamics. The test signal used is bounded within the winch actuator constraints of $\dot{l}_w \pm 2.2m/s$.

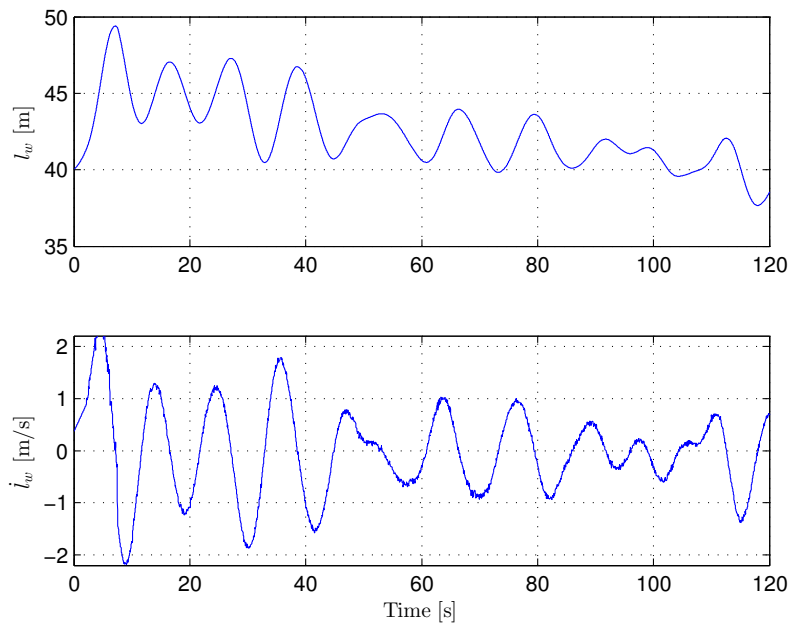


Figure 6.2: Plot of the test signal used for l_w and \dot{l}_w

6.1.2 Scenarios

A set of scenarios have been made to show the results of the controllers, when tested alone or in cascade and when the length of the wire l_w is either set to a static setpoint or tested with a time varying test signal. Also the system is tested both with "perfect" measurement r_p of the angular deflection of the wire β_v, α_v and with a simulated sensor signal \hat{r}_p as input to the controller. The simulated sensor signal \hat{r}_p is made by applying white noise to the perfect measurement r_p and then Kalman filter this signal using the Kalman filter described in 3.2.

Scenario number	Active controller		Hoist test signal	initial l_w	Measurement r_p or \hat{r}_p	Wind
	Sway	Position				
1	No	No	No	40	r_p	No
2	No	No	Yes	40	r_p	No
3	Yes	No	No	40	r_p	No
4	Yes	Yes	No	40	r_p	No
5	Yes	Yes	Yes	40	r_p	No
6	Yes	Yes	Yes	40	\hat{r}_p	No
7	No	No	No	80	\hat{r}_p	No
8	Yes	No	No	80	\hat{r}_p	No
9	Yes	Yes	No	80	\hat{r}_p	No
10	Yes	Yes	Yes	80	\hat{r}_p	No
11	Yes	Yes*	Yes	80	\hat{r}_p	No
12	Yes	Yes	Yes	80	\hat{r}_p	Yes

* - The joystick is operated which changes the setpoint of the position controller

Table 6.1: Simulation scenario overview

Scenario 1

This scenario is done to show the amplitude of the sway angles when no regulator is activated. In this test, the test signal for the boom and sway motion of the crane is activated at $t = 10s$, and deactivated at $t = 40s$. It can be seen that before the crane induced motion starts $t < 10s$, the sway angles is $\beta_v = \alpha_v = 0$. Then when the test signal starts the sway dynamics is affected by the crane induced motion and an oscillatory motion of the sway angles begins. Then at $t = 40s$ the test signal used on the slew and boom motion fades to zero, which leads to a damping of the magnitude of β_v , but an increase in the magnitude of α_v . Notice that since there is no damping of the sway angles after the crane induced motion stops, due to the fact that there is no friction terms in the mathematical model of the sway dynamics.

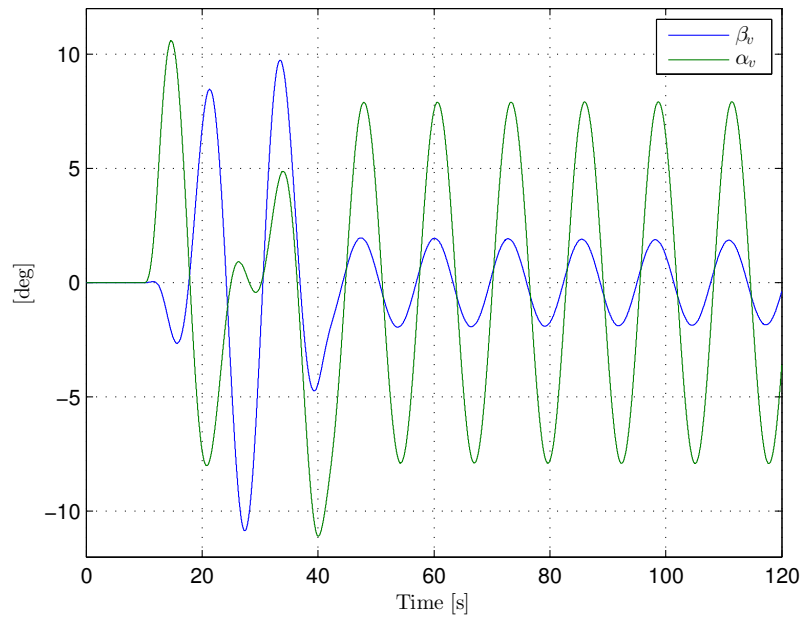


Figure 6.3: Plot of scenario 1 of the rotary crane simulation

Scenario 2

Scenario 2 shows which impact a time varying wire length has on the sway dynamics. The test signal for the boom and slew motion is the same as in scenario 1, but in addition the test signal for the hoist machinery is activated through the whole test. In figure 6.4 it can be seen that by operating the hoisting machinery, the dynamics of the pendulum is affected in way of higher amplitude. Also we recall that $\omega = \sqrt{\frac{g}{l}}$, which means that by increasing the wire length the period time of the pendulum increases.

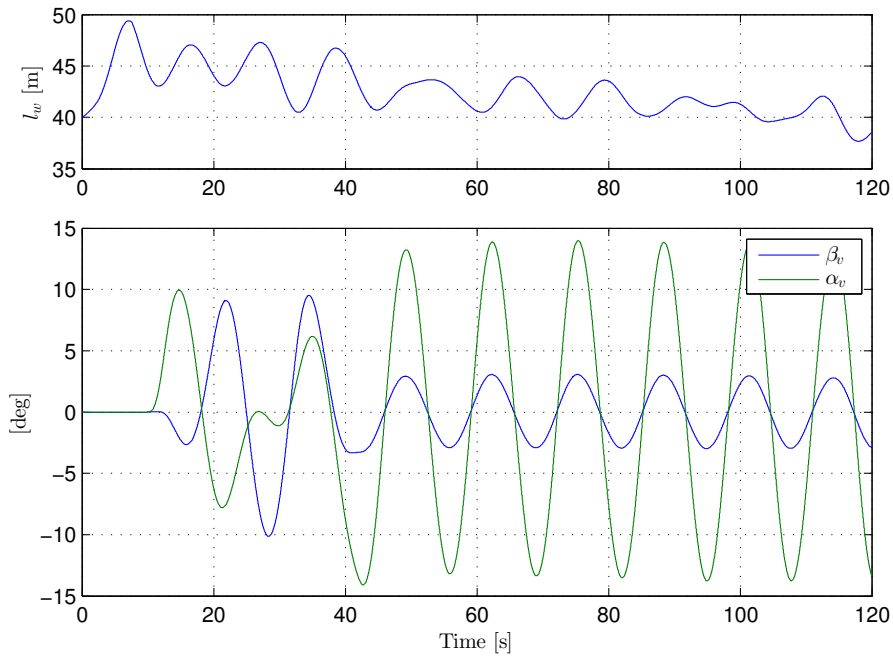


Figure 6.4: Plot of scenario 2 of the rotary crane simulation

Scenario 3

In scenario 3 the sway controller is activated at $t = 50$, and from the results in 6.5 it can be seen that the controller effectively reduces the sway angles. As seen the slew angle q_1 changes over 10 degrees in order to minimize the sway angle α , and the boom angle q_2 moves from $q_2 \approx 48^\circ$ to $q_2 \approx 50^\circ$ in order to suppress the sway angle β . Also it is worth to notice that the controller used to suppress the sway angle q_2 by controlling the boom angle is using almost 20seconds. This is due to actuator limitations since $\max(\dot{q}_2) = 0.02[\text{rad}/\text{s}]$, while $\max(\dot{q}_1) = 0.1[\text{rad}/\text{s}]$.

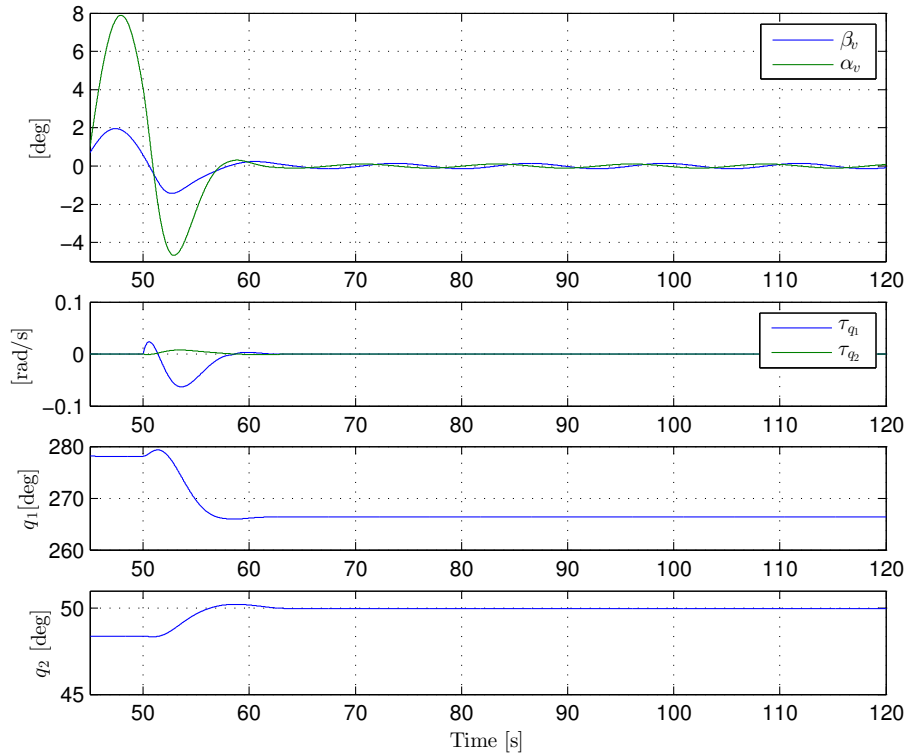


Figure 6.5: Plot of scenario 3 of the rotary crane simulation

Scenario 4

In scenario 4 both the sway and boom tip positioning controller are active, and it can be seen that the sway angles are reduced but not completely suppressed. The boom tip position controller is able to control the position towards the desired position in case of q_{1des}, q_{2des} but it does not converge to the desired set-point within the time the controller is activated.

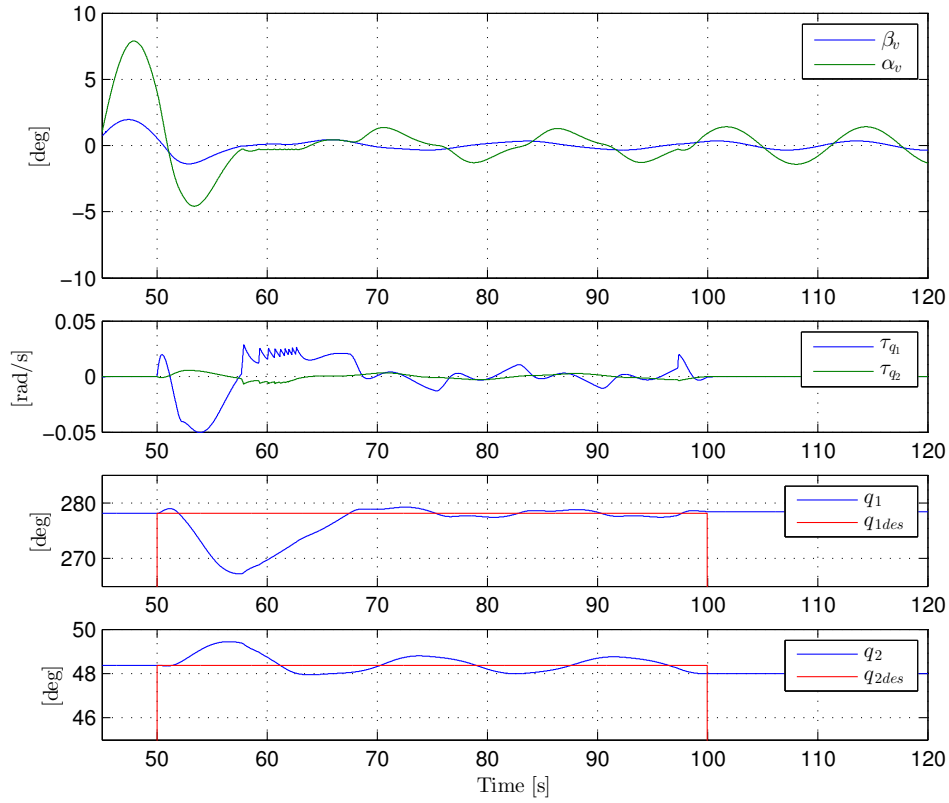


Figure 6.6: Plot of scenario 4 of the rotary crane simulation

Scenario 5

Scenario 5 simulates the model with the hoist winch test signal. From the plot of the sway angles in figure 6.7 it can be seen that the magnitude of the sway angles is higher around $t = 45s$ then in scenario 4. Also it can be seen that the controller is able to reduce the sway angle quite effective but as seen in the plots of q_1 and q_2 the controller uses more time and is more aggressive in this scenario.

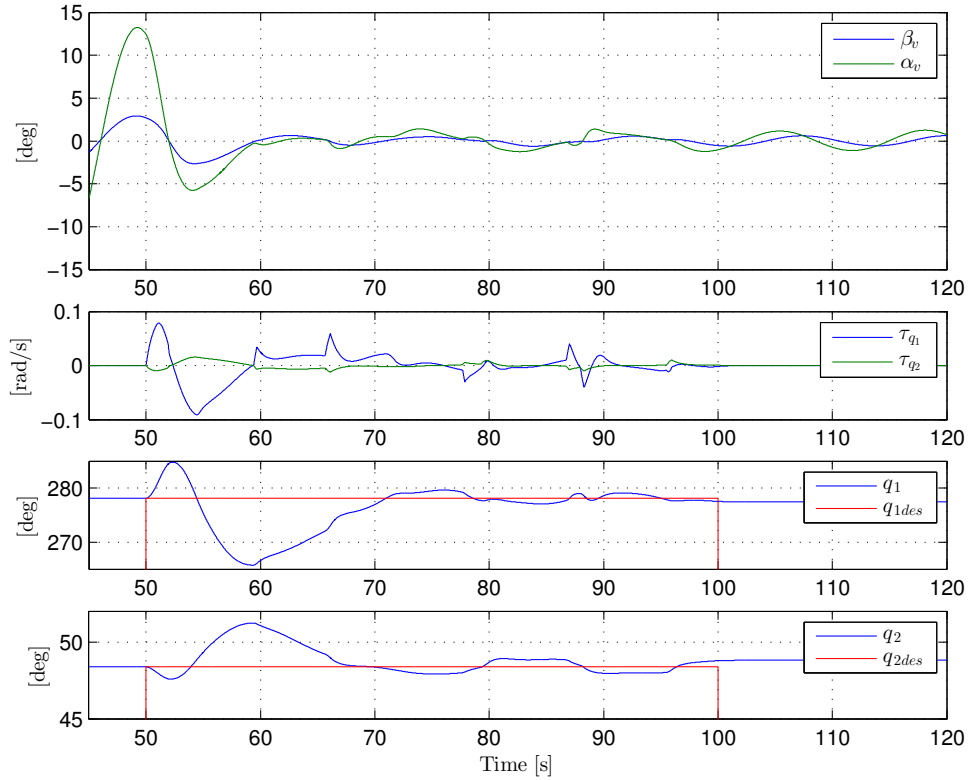


Figure 6.7: Plot of scenario 5 of the rotary crane simulation

Scenario 6

Scenario 6 uses the same test input as in scenario 5, but the sway angle measurement r_p has been replaced by the simulated sensor measurement \hat{r}_p . By comparing the results in figure 6.7 and figure 6.8 it can be seen that the results of the regulation is almost identical. This result shows that the Kalman filtered sway angle measurement \hat{r}_p is a measurement that is usable for regulation purpose.

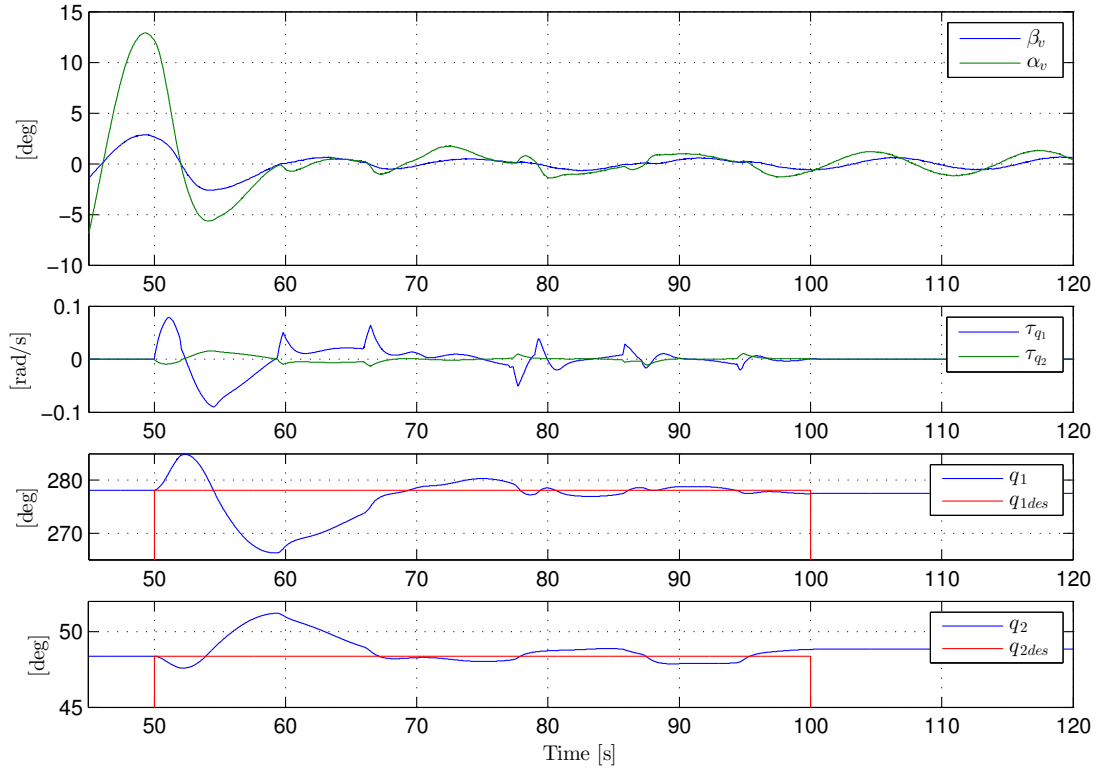


Figure 6.8: Plot of scenario 6 of the rotary crane simulation

Scenario 7

In scenario 7 the initial wire length is changed from $l_w = 40m$ to $l_w = 80m$. And the model is simulated with the test signal for the boom and slew motion. By comparing the plot in figure 6.3 and figure 6.9 it can be seen that the magnitude of the sway angles at $t > 60s$ is almost the same, but the period time of the oscillation is longer.

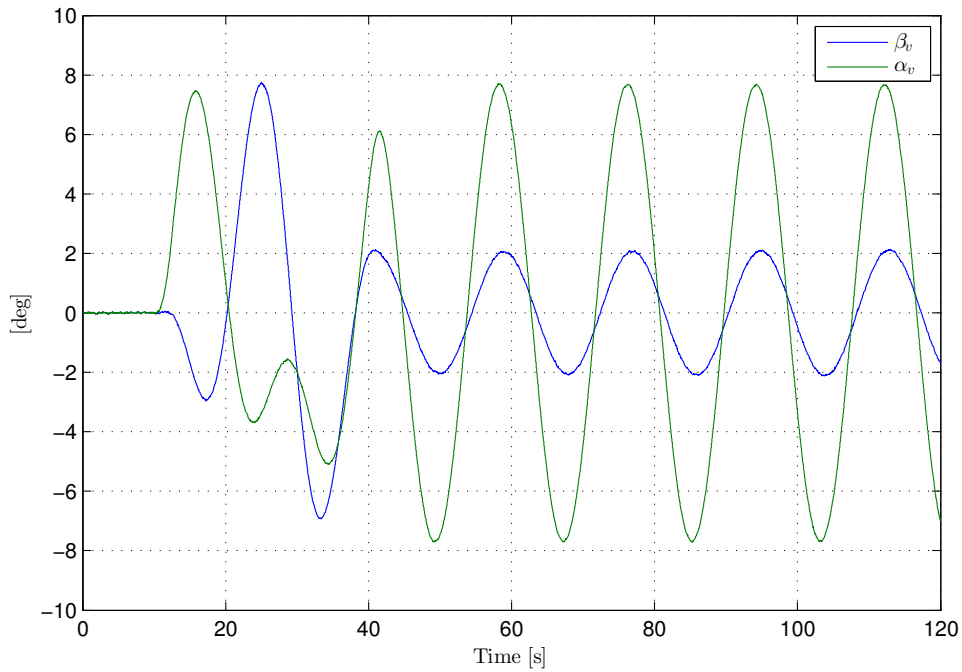


Figure 6.9: Plot of scenario 7 of the rotary crane simulation

Scenario 8

In scenario 8 the sway controller is activated, and the test signal is only boom and slew. As seen in figure 6.10 the sway controller is able to suppress the sway angles, but uses more time now as $l_w = 80m$, compared to scenario 3 (figure 6.5) where the wire length was $l_w = 40m$.

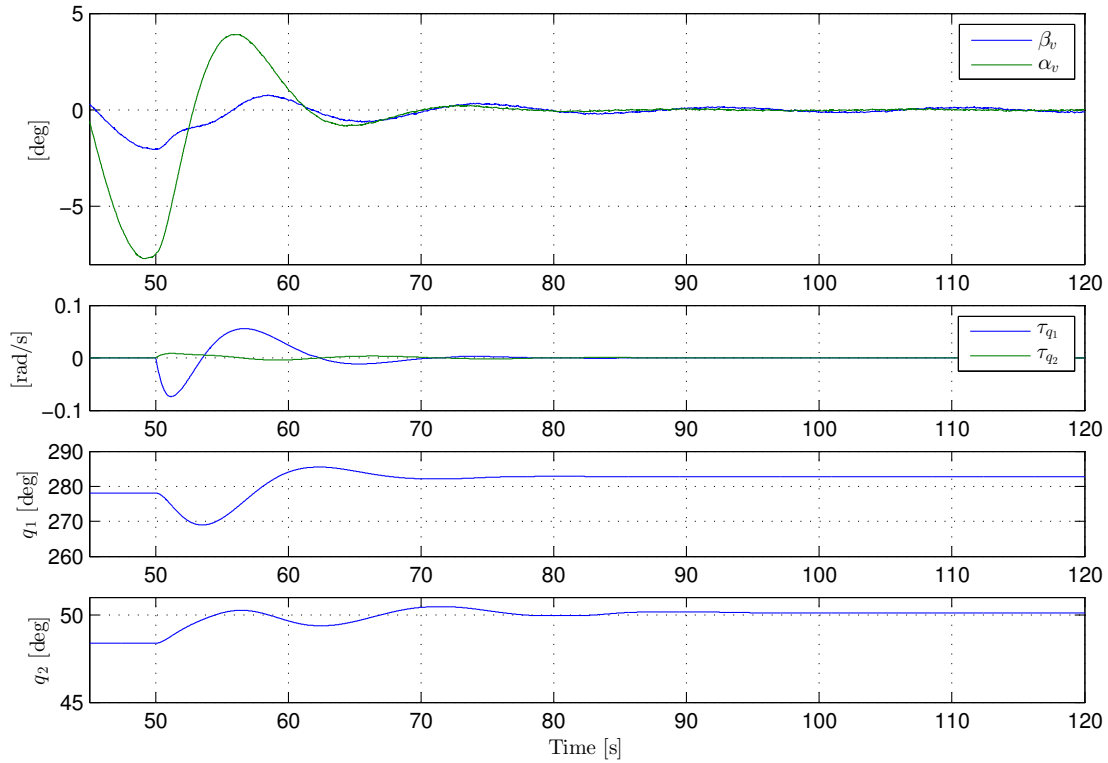


Figure 6.10: Plot of scenario 8 of the rotary crane simulation

Scenario 9

In scenario 9 both the sway and the positioning controller is activated while the test signal for hoist winch is not enabled. By comparing the results in figure 6.10 and 6.11 it can be seen that by activating the boom tip positioning controller, the sway controller is not able to reduce the sway angles as much as in scenario 8. But it can be seen in figure 6.11 that even though the sway controller is trying to suppress the sway angles all through the scenario, the boom tip position controller is almost able to position the boom tip according to q_{1des} , q_{2des} .

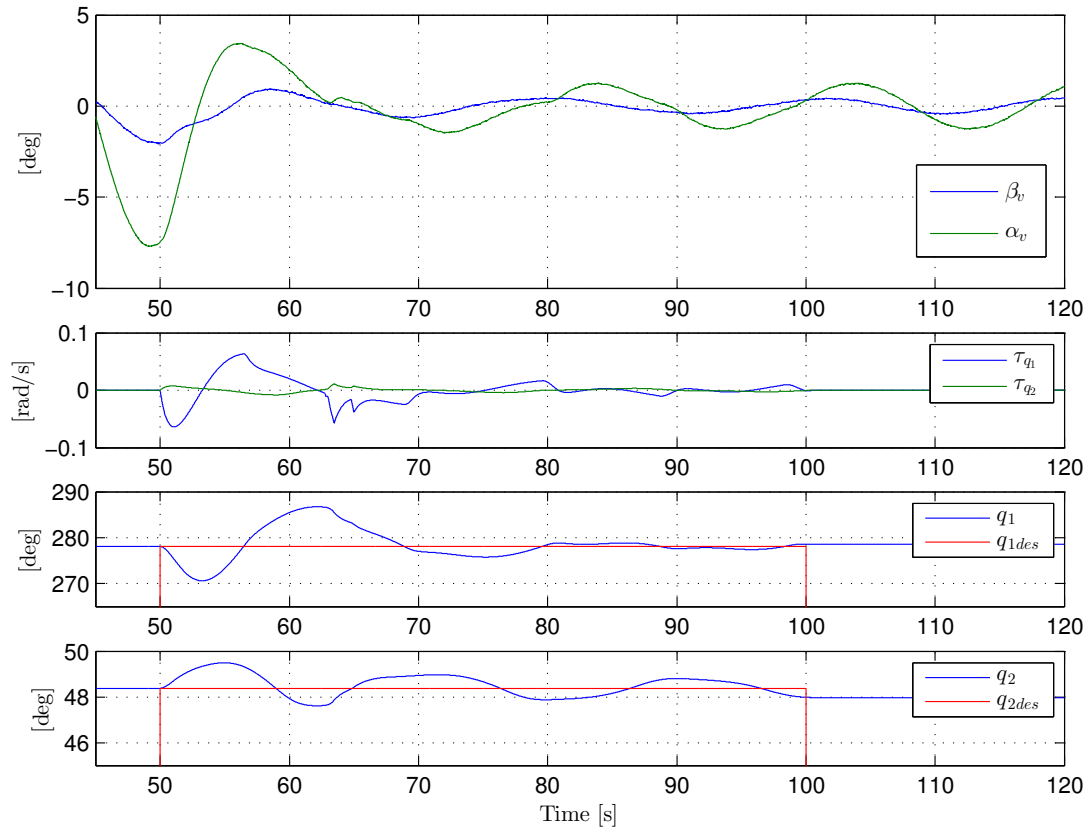


Figure 6.11: Plot of scenario 9 of the rotary crane simulation

Scenario 10

Scenario 10 the hoist winch test signal is activated, and both the anti-sway and boom tip positioning controller is active. In figure 6.12 that the controller output is quite aggressive compared to scenario 9. The controller is able to reduce the sway angles but not effectively. And the boom is oscillating quite much around the desired angle q_{2des} .

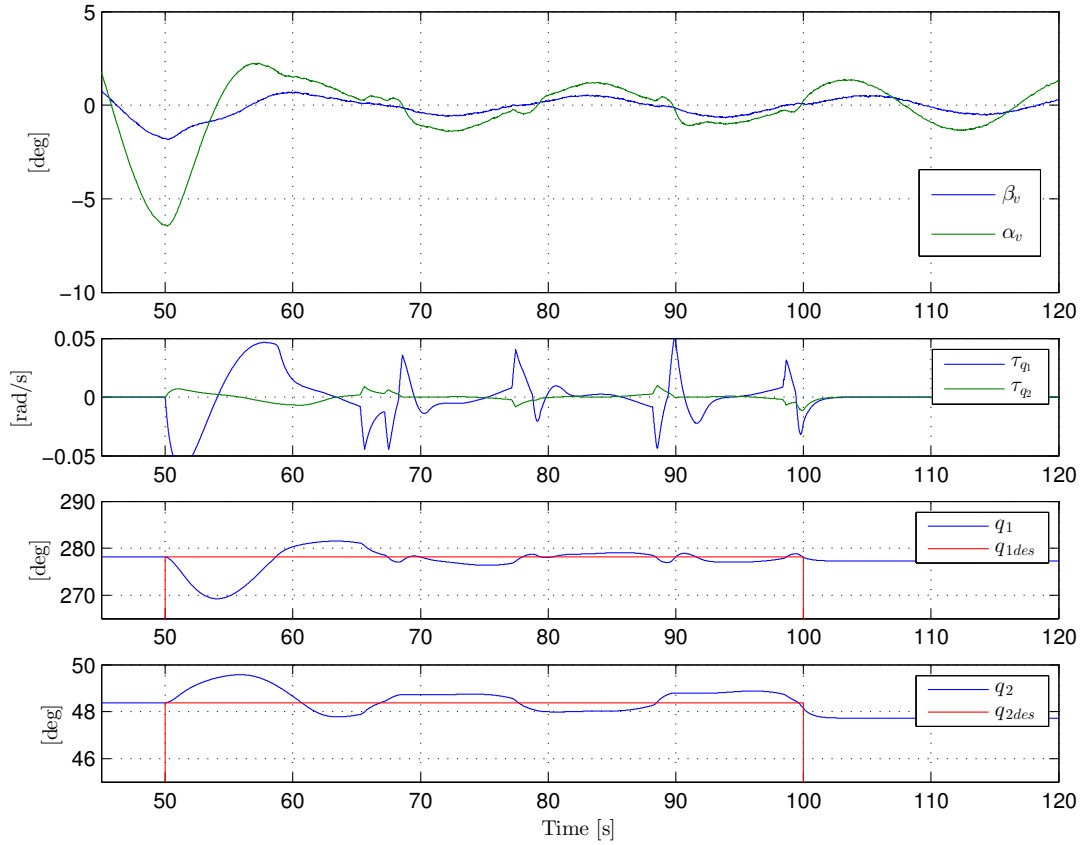


Figure 6.12: Plot of scenario 10 of the rotary crane simulation

Scenario 11

In scenario 11 the test signal is activated for both slew and boom. The varying hoist signal is activated, and at time $t \approx 58$ the operator uses the joystick to move the crane. It can be seen from figure 6.13 that the desired setpoint q_{1des}, q_{2des} changes when the joystick is operated, and the boom tip position system tracks the time varying reference quite effectively. By looking at the sway angles it can be seen that the change in desired boom tip position leads to a increase in the magnitude of α_v , but when the the new desired position is tracked, the magnitude of the sway angles is again reduced by the anti-sway controller.

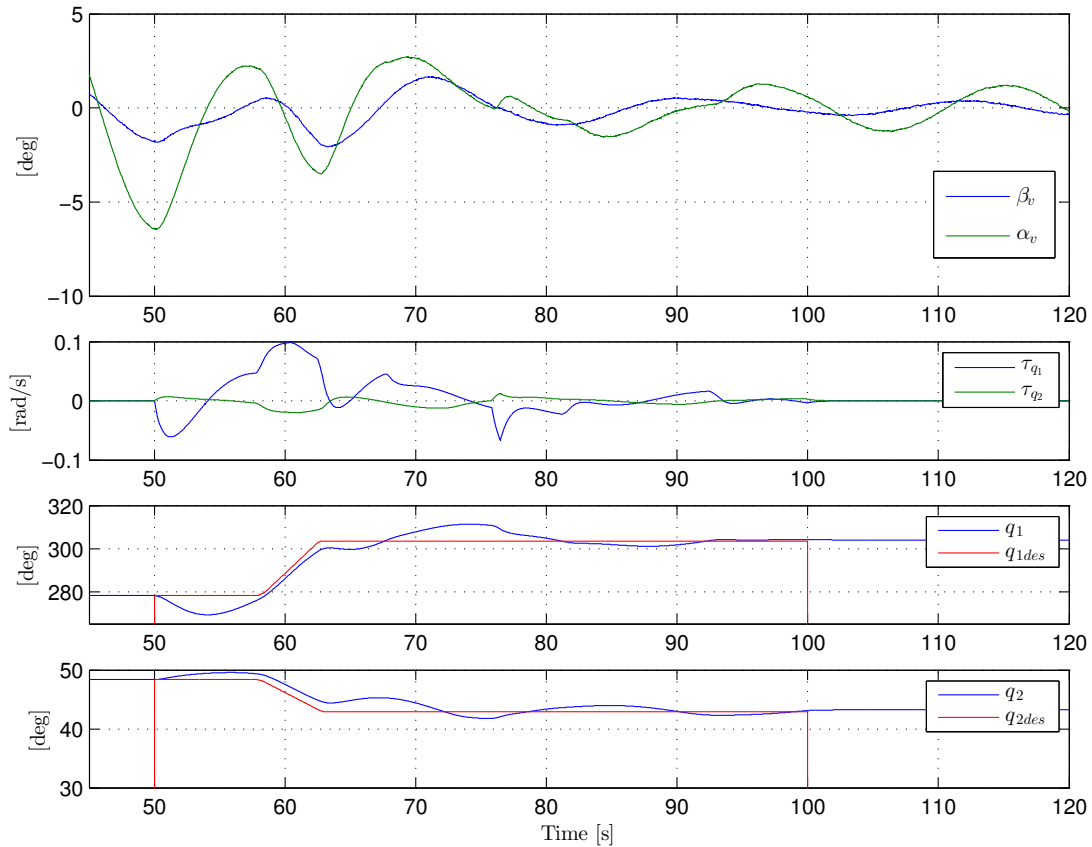


Figure 6.13: Plot of scenario 11 of the rotary crane simulation

Scenario 12

In this scenario the crane model is tested with time varying wire length using the camera measurement, and an additional wind force with $\bar{w} = 10m/s$ is added to the sway dynamics as described in section 2.6. As seen in figure 6.14 the anti-sway regulator is capable to reduce the magnitude of the sway. Due to the wind force, the measured angle β_v is biased and the anti-sway controller controlling the boom angle is constantly trying to remove this error. It can be said that this regulator is not robust in sense of environmental disturbances or sensor measurement errors.

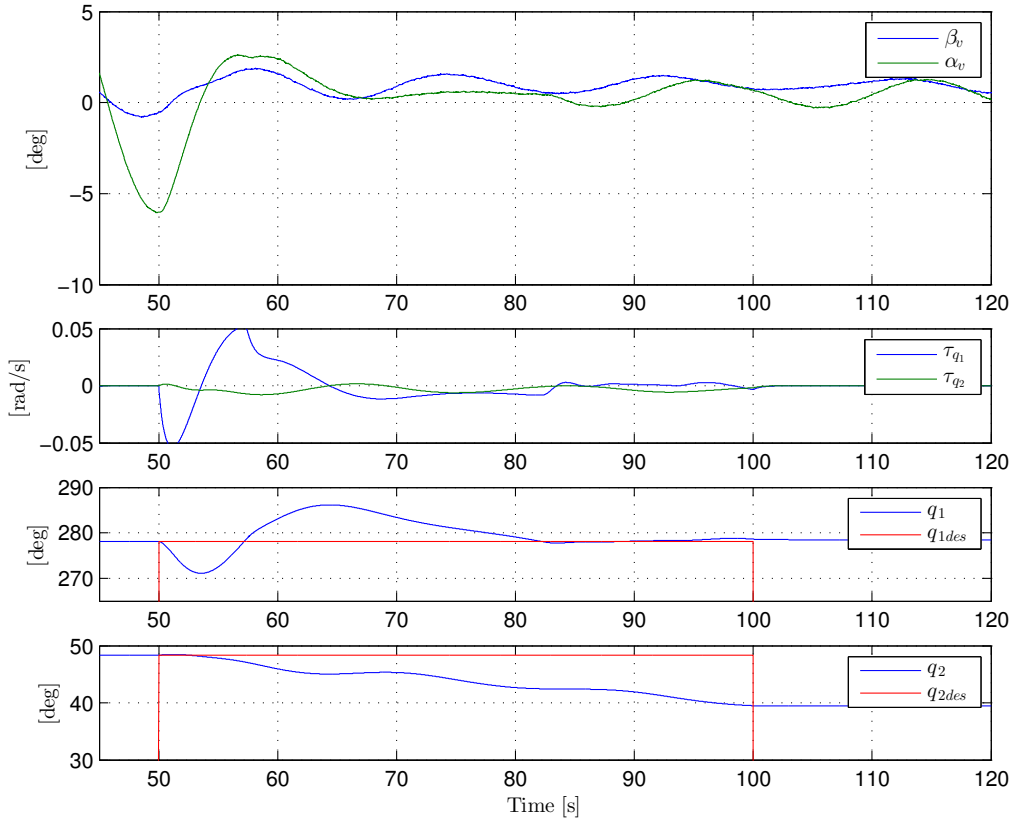


Figure 6.14: Plot of scenario 12 of the rotary crane simulation

6.2 Simulation of Wave Following System

This section is based on the work presented in [25]. In this section the linearised crane model presented in [2] is tested with the predicted camera measurement as input to the WFS controller described in 4.2. Under all simulations the boom winch will be fixed.

Camera measurement predicted reference, 5 ton hook load

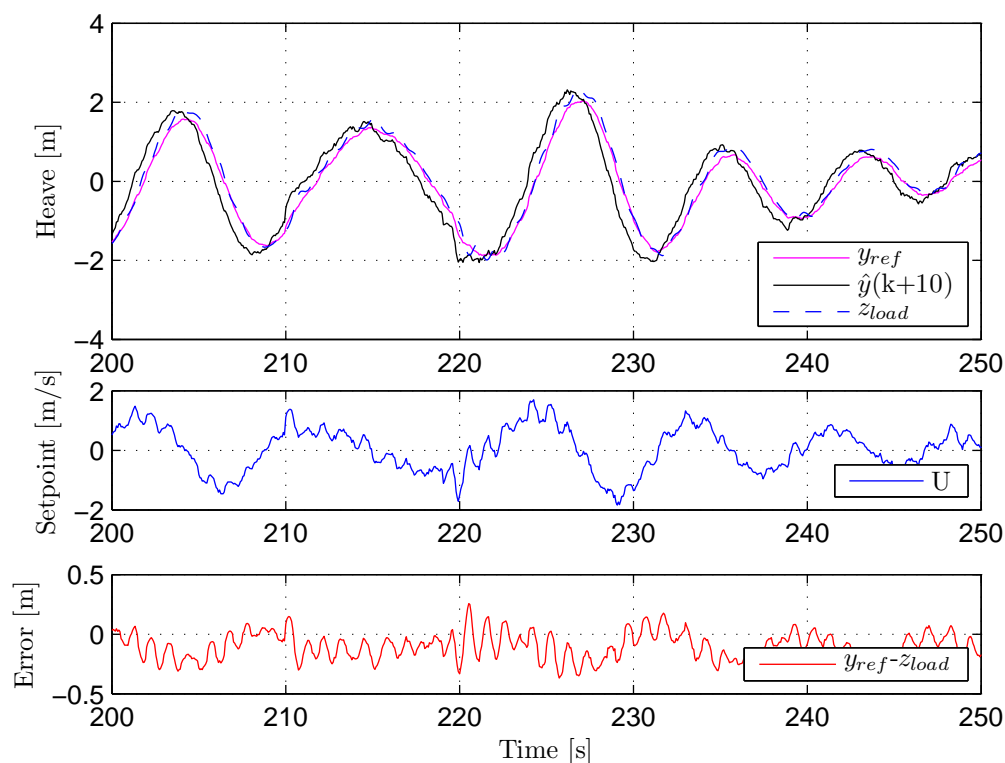


Figure 6.15: Simulation with Kalman predicted set point from camera measurement, 5t hook load, 2.2m/s max velocity

As seen in figure 6.15 the hook is able to follow the desired trajectory y_{ref} quite good, when applying the predicted input signal $\hat{y}(k+10)$ to the controller. By observing the error measurement it can be seen that the maximum deviation between y_{ref} and z_{load} are never more than $\pm 0.25m$. As seen at the plot of the controller output U the desired winch velocity never exceed the speed constraint of the hoist winch of $\pm 2.2m/s$.

Camera measurement predicted reference, 10ton hook load

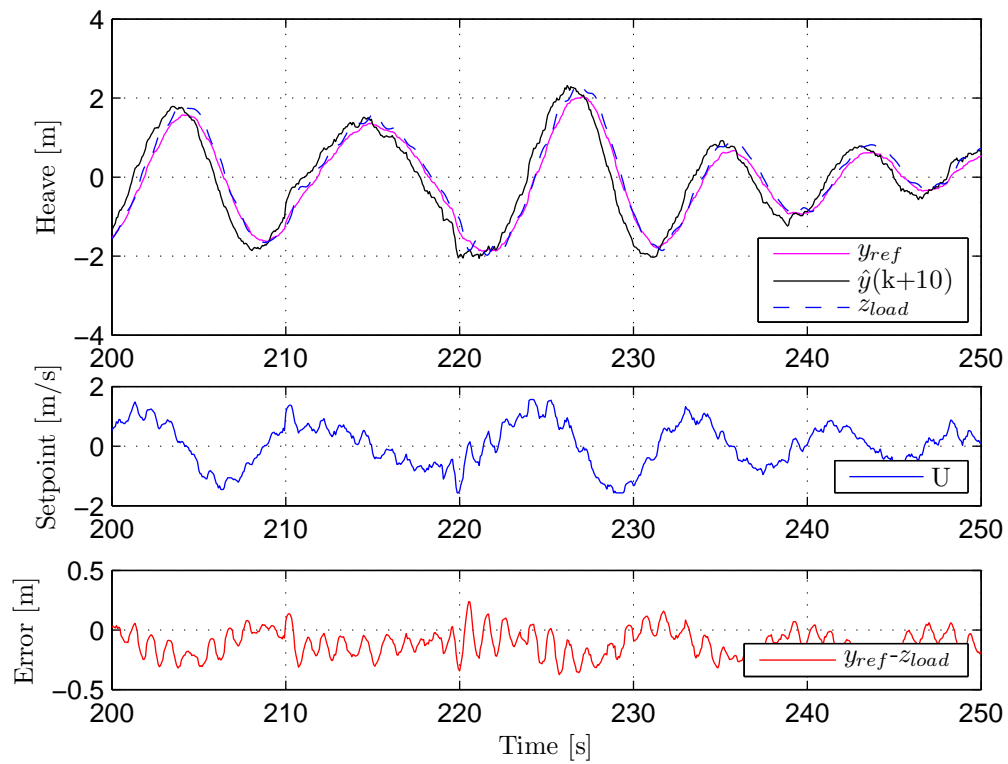


Figure 6.16: Simulation with Kalman predicted set point from camera measurement, 10ton hook load, 1.57m/s max velocity

In figure 6.16 it can be seen that with a hook load of 10ton the controller hits the maximum winch speed constraint of 1.57 around time 230s, which leads to a small variation in the result compared to the simulation where the hook load was 5t.

7.1.2 Angle measurement of whip line by use of potentiometers

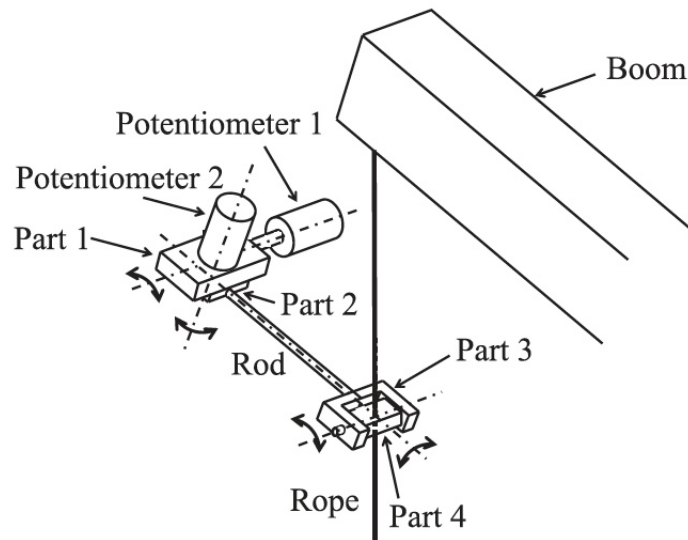


Figure 7.2: Sway measurement of whipline by use of potentiometers [28]

By using two potentiometers connected to a teflon ring as seen in figure (7.2) it would be possible to measure the angle of side lead and side lead from the load resting position. The details regarding this instrumentation can be found in [28].

Discussion

One disadvantage with this solution is that the teflon ring that surrounds the wire has to have a larger diameter than the maximum diameter of the wire, since the wire is not perfectly shaped the typical tolerance is 4% of $\varnothing 32\text{mm}$. This would lead to an imprecise measurement of the wire off lead/side lead angle around its resting point, where it would be crucial to have a precise measurement to obtain good anti sway control of the load.

7.1.3 Position measurement of whip line by use of ultrasound and inclinometer

An idea is to use ultrasound sensors to be able to track the wire in the horizontal plane. The concept is to use two sensors which are mounted in x-axis and y-axis respectively. In addition to the ultrasound sensors, a thought is to have a inclinometer to measure the deviation of the ring relative to the vertical plane.

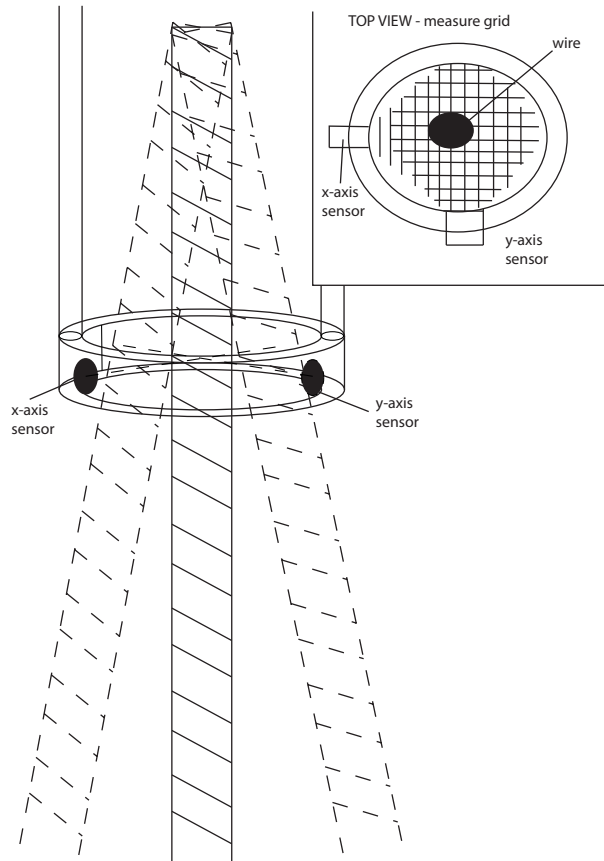


Figure 7.3: Sketch of sensor for measurement of off lead/side lead angle for whip line

As seen in (Figure 7.3) the idea is to install the two sensor within a cylinder shaped form which is to be installed around the whip line, below the boom tip of the offshore lattice crane. Since the boom tip is moving from both vibrations during operation, and when the change of radius is wanted the installation should be installed by the use of oil dampers, and the ring should have some added mass to ensure that it will be stay horizontal when the boom is stationary.

Discussion

Some possible disadvantages with this solution are installation and calibration of the instrumentation on semi submerged rigs, where the rig trim angles can be affected by the wave induced motion causing the wire to be out of range for the sensors. Also the robustness of the measurement and sensors must be tested in harsh enviroment such as rain,snow, wind and salt.

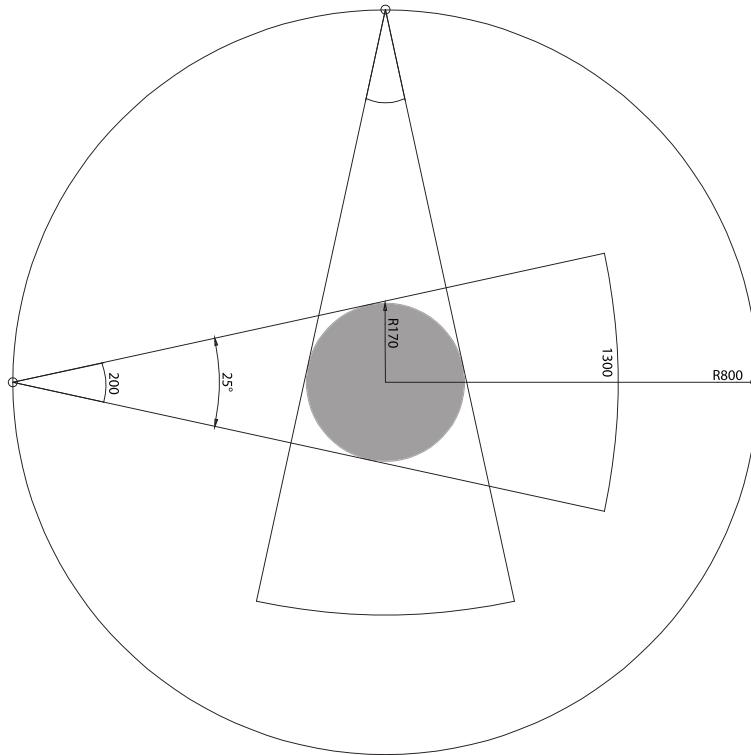


Figure 7.4: Suggestion of Ultrasonic sensor installation

In figure 7.4 an suggestion on how to install the sensor to obtain measurement of the wire with up to 15 degree sway (grey area) by installing it 635mm below the sheave in the boom tip.

7.1.4 Experiment

An experiment is done to test the concept of this sensor. During the experiment the following equipment is used.



(a) Siemens PLC rack

(b) P+F Ultrasonic sensor

(c) Sample of whip hoistline

Figure 7.5: Lab test

Description	Technical Information	Manufacture
Ultrasound distance sensor 20-130cm	3RG6113-3BF00-0XB7 P/N:559734	Pepperl+Fuchs
M12 Connector 5-pin w/2m 5-wire cable	V15-G-YE2M-PVC	Pepperl+Fuchs
PLC CPU	319-3-PN/DP	Siemens
Analog Input Module	331-7HF01-0AB0	Siemens
PLC Logger	v3.3 Beta-1	NOV
LogFileViewer	v3.3-Beta-1	NOV
Simatic Manager	-	Siemens
Profibus PC-Card	CP5512	Siemens
HW - Adapter for CP5512	C79459-A1890-A10	Siemens

Table 7.2: List of equipment used in ultrasound proximity switch test

Results

Figure 7.6 shows the results of the test where a flat bar is placed in front of the sensor and carefully moved throughout the whole range of the sensor (20-130cm) to test the accuracy and resolution of the sensor.

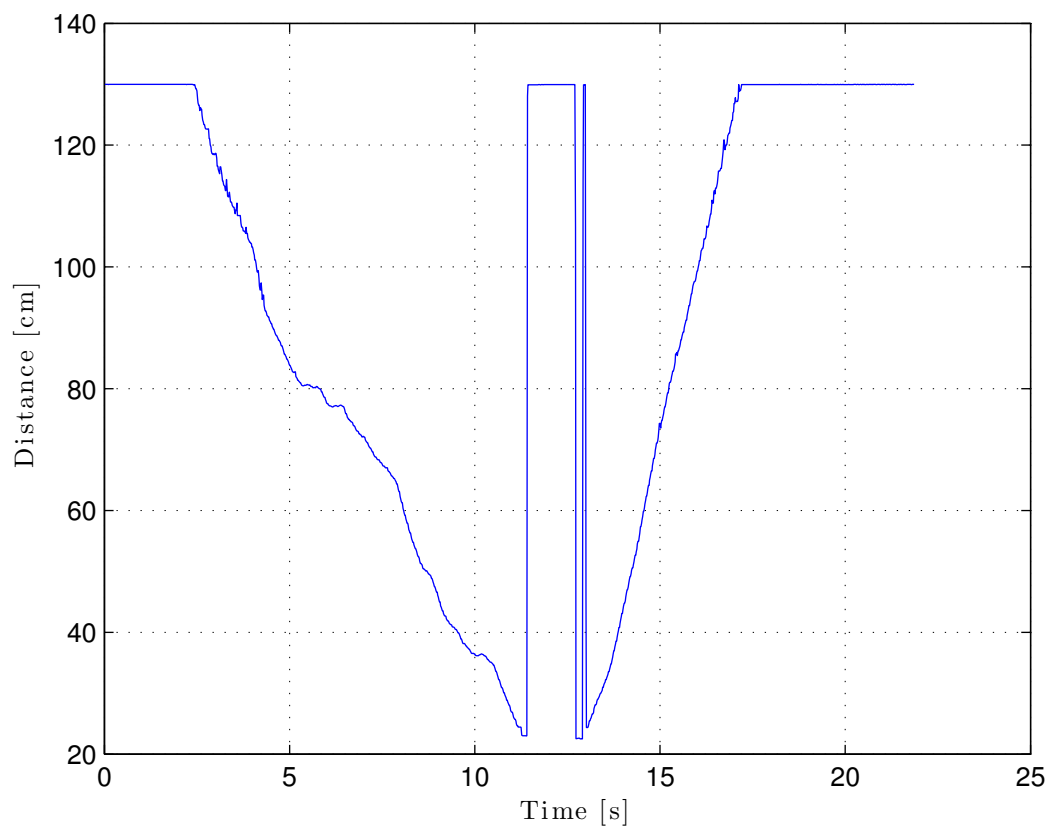


Figure 7.6: Ultrasound resolution and measurement area

As seen in figure 7.6 the results show that the resolution and accuracy of the sensor are good for the experiment where the wire is used at arbitrary positions inside the measurement area. As seen in the figure at time 10 – 15s the sensor give an output equal 20mA(130cm) when an object is closer than minimum measuring distance of 20cm.

Left			Center			Right		
M	A	D	M	A	D	M	A	D
20.1	20	+0.1	20.5	20	+0.5	20.4	20	+0.4
30	30	0	29.7	30	-0.3	29.5	30	-0.5
39.9	40	-0.1	39.7	40	-0.3	40	40	0
50.2	50	+0.2	49.5	50	-0.5	50.3	50	+0.3
59.7	60	-0.3	59.7	60	-0.3	59.5	60	+0.5
70	70	0	69.7	70	-0.3	70.3	70	+0.3
77.7	77.3	+0.4	75	75.4	-0.4	80	79.8	+0.2
84.3	84.5	-0.2	85.2	85	+0.2	86.5	86.7	+0.2
99.5	99.3	+0.2	92	92.2	-0.2	94.5	94.5	0

Table 7.3: Test of Ultrasound Distance Sensor, showing measured(M), actual(A) and deviation(D) distance in [cm]

As seen in Table (7.3) the largest deviation between measured and real distance is $\pm 0.5cm$, which gives an accuracy of

$$Accuracy(\%) = \left(\frac{\pm 0.5cm}{(130cm - 20cm)} \right) * 100 \quad (7.1)$$

$$= \pm 0.45\% \quad (7.2)$$

But according to the data sheet of the sensor (A.3) the accuracy is $\pm 1,5\%$, which gives an maximum deviation of

$$Deviation_{max} = \left(\frac{(130cm - 20cm)}{100} \right) * \pm 1,5 = \pm 1.65cm \quad (7.3)$$

7.1.5 Measure the position of the whip line and main hoist line by use of real-time stereo video measurements

Another approach to be able to measure the side lead/off lead angle of the whip/main hook is to use a stereo video camera solution, similar to the one used by Hornang, S. [5] to track the position of the hook relative to the boom tip to calculate the wanted distance and angles. To be able to use this the solution it will be necessary to install angle measurement on the beam where the two cameras are installed to measure the angle of the cameras, relative to the vertical axis. Also it might be necessary to mark the hook with some circles, which the camera can use as a tracking points.

Chapter 8

Conclusion

Working on this thesis has been a challenging but exciting experience. A lot of different topics is covered, such as modelling, control, simulation, visualization, filtering and instrumentation.

Anti-sway, boom tip positioning and operator-in-the-loop

In this thesis a cascade controller that consist of an anti-sway and boom tip position system with the operator-in-the-loop has been investigated. The simulations shows that by using filtered sensor feedback from the sway angles, the anti-sway system is able to reduce the load sway effectively at various wire length, but since the boom tip position system also is tracking a desired position the sway dynamics is not eliminated completely.

In the definition of the control algorithm improvement can be done, since the described controller swaps between being a cascade controller and a boom tip position controller by the an comparing of the sway angles and a threshold. This means that if the two sway angles oscillate in the same phase and crosses zero at the same time the controller will swap mode, giving a ripple on the output. Despite this the simulation shows that even though the cascade controller is active, the operator still has the superior control of the crane. All the simulations done without environmental disturbances shows that the closed loop system with anti-sway, boom tip positioning and operator-in-the-loop is stable. This conclusion is done, based on the fact that there are no friction terms in the model, which means that no energy dissipates throughout the simulation. Simulation done in this thesis also shows that the controller is not robust in sense of environmental disturbances, this can be improved by using the parameter estimation algorithm to estimate the slowly varying bias on the sway angles caused either by wind, sensor bias or by wave induced forced acting on the rig and compensate for this bias in the desired sway angle.

The simulation of the mathematical model of the rotary crane with spherical pendulum has not been compared to data from real cranes, but the simulation and visualization shows realistic behaviors. This conclusion is based on the authors own experience with offshore cranes, and similar simulation of the model in [20].

Wave following system

The wave following system described in this thesis is simulated on a linear crane model [2]. The results of the wave following system shows that it is possible to predict the future behaviour of the vessel, control the hoist winch to follow the same motion as long as the closed loop system time delay is not too large, since the quality of the predicted signal is reduced with the prediction time. During simulation it has been shown that the deviation between the hoist winch and vessel motion was about $\pm 25\text{cm}$ with an observed wave height of 4m. The contribution to the wave following system in this thesis is the derivation of the online parameter estimation scheme with adaptive Kalman filter which makes it possible to remove bias and filter the measurement signal from the camera during simulation. Even though the winch velocity constraints are implemented in the model, further investigation should be made in order to conclude on the efficiency of the controller on a real crane, also the time delays and step response of the actuator dynamics on a real crane should be investigated further and compared to the model used in this thesis.

Instrumentation

Several different suggestions on how to measure the sway angles of the crane are presented in this thesis. Most work is done with the ultrasonic proximity switch which measures the distance between the sensor and an object using sound waves. The test done on the ultrasound sensor shows that it has good resolution. The ultrasound sensor solution presented in this thesis assumes that several sensors are used to track the wire in the X-Y plane to indirectly measure the sway angles in the crane fixed frame. The sensor was chosen based on a high international protection rating, which makes it durable in a harsh environment. Also since the sensor has an Ex-sone 2 classification, which makes it possible to use over sea on an oil rig. In order to conclude on the proposed sensor application further test should be done, to see how the sensor signal is affected when the sound cone is applied to disturbances like rain, snow and other ultrasound sensors.

The suggestion that is most likely ready to use is the potentiometer application described [28]. Potentiometers or absolute encoders are used to measure boom angle on real crane application today. The drawback of the potentiometer solution is the mechanical interference between the Teflon ring and the wire, which would over time lead to inaccuracy and possible bias on the measurements.

The suggestion to use a camera system to indirectly measure the sway angle by measuring the position of the hook relative to the boom tip, needs further investigation.

Visualization

Three different 3D Visualization models are presented in this thesis. The experience I have achieved after working with these models, makes it quite certain that it is not the last time. These models can be really effective in a hardware-in-the-loop system where the user immediately can see the response on the model in case of a well known

environment instead of looking at several graphs. Also the S-function from the 3D Animation toolbox demo that were modified and presented in this thesis in section 5.2.3 shows how to combine 3D animations with standard plots in order to get more accurate information during , then when only the 3D animation models is used.

Chapter 9

Further work

Power Management System

In this thesis the author has assumed that it is possible to operator all the crane actuators at 100% at the same time. This is not the case in most real life offshore rotary crane where the total available power is less then the demanded power if all actuator is running full speed at the same time. Therefore it would be interesting to implement a power management system into the mathematical models and retest the control system described here.

Real measurement data from the camera system

National Oilwell Varco has a ongoing project involving the prototype testing of the camera solution described in [5]. Real measurement from the camera system should be used to tune the parameter estimation algorithm and Kalman filterm and do new simulations of the WFS system.

Hoist winch dynamics

Further work should be done to derive a mathematical model of the winch machinery, which is tuned to match the response of a real crane.

Hardware in the loop

In this thesis a joystick interface was used to interact with the crane model. Further work should be done to be able to use a real crane PLC which interact with a mathematical model of the crane.

Launch indication

A possibility of the WFS is a launch indicator which can be implemented in the control system HMI. During this thesis the linearised crane model has been used to test the WFS. During testing it has been shown that by using the camera measurement and predict to compensate for the time delays in the camera system and control system, the input given to the system makes the crane follow the vessel motion. By using the predicted measurement it should be possible to give a good estimate of when it is most

desirable to unload cargo from the vessel, which is when the relative velocity between the vessel and the hook is lowest, i.e. when the vessel is rising from the bottom of a wave and before it reaches the top of the wave. By introducing such a system dynamic forces during launching of a load from the vessel to the air would be reduced. This system provide the crane operator an extra tool, and might let the operator perform operations during higher significant wave height than before, since the potential forces acting on the crane would be smaller. This topic should be further investigated.

Weather indication

The camera measurement can be used as an extension to the weather stations in the crane to give real time information about wave height, and it is also possible to give quite exact information about significant wave height which is continuously updated. This information can be implemented in the already existing HMI in the crane or as an stand alone system. Inspiration for this is taken from [7], since they already have developed a system which is approved by the use of radio link. This idea is well worth looking into.

Appendices

Appendix A

Contents of the digital attachment

The following directories is found in the attached zip file and described more in the following sections.

- Literature
- Matlab
- Data sheets
- VRML

A.1 Literature

In this directory some of the publications referenced in the Bibliography G.1 is found.

A.2 Matlab

This directory contains the following folders and sub folders

- Models
 - Kalman filter
 - Parameter_estimator
 - Gantry_Crane_3DOF
 - Rotary_Crane_5DOF
- Data
- Scripts

Under *Scripts* relevant scripts for reproducing figures based on data in the *Data* folder is found.

A.3 Data sheets

In this folder the following data sheets is found:

- Ultrasonic_proximity_switch.pdf
- Inclinator-PF.pdf
- Cable connector V15-G-YE5M-PVC.pdf

A.4 VRML

This folder contains the following 3D animation files

- Gantry_Crane_3DOF
- Rotary_Crane_5DOF
- Rotary_Crane_Inventor_dwg

Appendix B

Mathematical modeling of trolley

In this appendix a an early stage attempt to derive a mathematical model of a trolley with pendant load is described using Euler-Lagrange equations.

B.1 3DOF trolley with pendant load in wire

In this section a mathematical model is derived for the trolley with pendant load using Euler-Lagrange.

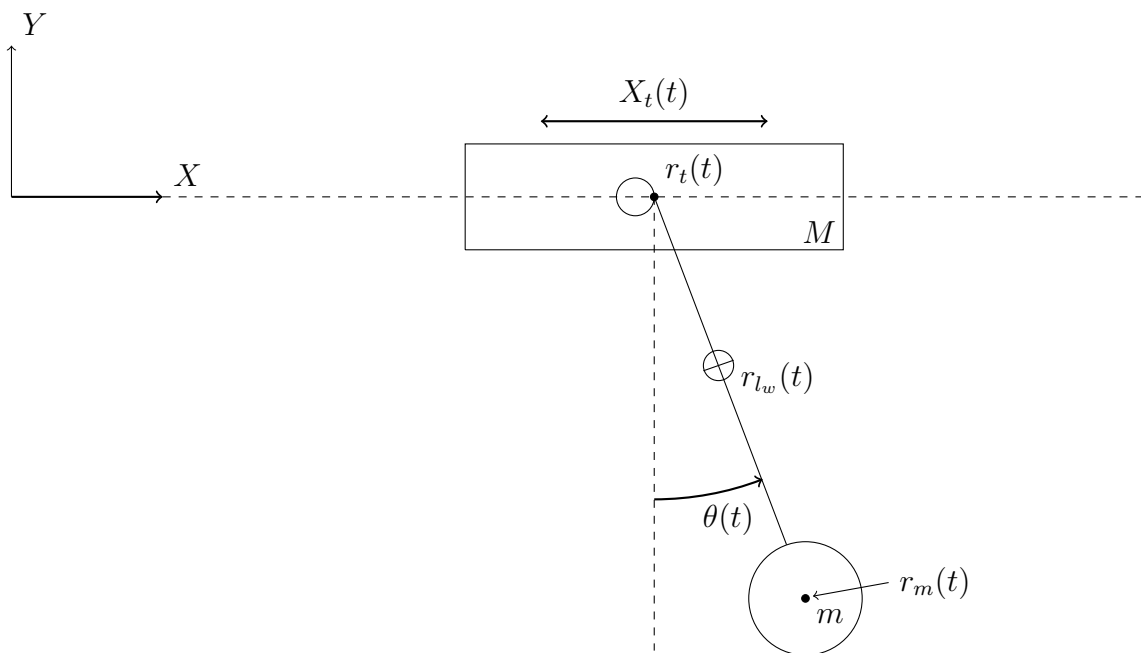


Figure B.1: Sketch of trolley with pendant load in wire

The following assumptions is taken:

- The trolley ride on a frictionless rail.
- The load is pending about a frictionless pivot point on the trolley.

- The length of the wire is varying with time based on the given commanded length τ_3 , but the wire is rigid in the sense that there is no spring or damper effect in the wire. This assumption is valid if the load hanging in the wire has relative much height mass that the wire itself. ($m \gg m_w$).
- The time derivative of m_w is assumed to be equal to zero, that is $\dot{m}_w = 0$.

Notation	Description
X_t	X-position of the trolley relative to the fixed X-axis
Y_t	Y-position of the trolley relative to the fixed Y-axis
X_m	X-position of the load relative to the fixed X-axis
Y_m	Y-position of the load relative to the fixed X-axis
l_w	Length of wire between the trolley and load (varies with time)
θ	Relative angle between the wire and the fixed Y-axis

Table B.1: Notation for 3DOF trolley with pendant load in wire

B.1.1 Position

The position of the trolley relative to the origin of the frame fixed coordinate system is given by equation (B.1).

$$r_t(t) = \begin{bmatrix} X_t(t) \\ 0 \end{bmatrix} \quad (\text{B.1})$$

The position for the COG of the wire relative to the earth fixed coordinate system is

$$r_{l_w}(t) = \begin{bmatrix} X_t(t) + \frac{1}{2}l_w(t) \sin \theta(t) \\ \frac{1}{2}l_w(t) \cos \theta(t) \end{bmatrix} \quad (\text{B.2})$$

The position of the load relative to the earth fixed coordinate system is defined by equation (B.3).

$$r_m(t) = \begin{bmatrix} X_t(t) + l_w(t) \sin \theta(t) \\ l_w(t) \cos \theta(t) \end{bmatrix} \quad (\text{B.3})$$

B.1.2 Velocity

Velocity vector \dot{r}_t is given as the derivative of equation (B.1) with respect to time as

$$\dot{r}_t(t) = \begin{bmatrix} \dot{X}_t(t) \\ 0 \end{bmatrix} \quad (\text{B.4})$$

The time derivative of position vector B.2 gives the velocity vector for the COG of the wire.

$$\dot{r}_{l_w}(t) = \begin{bmatrix} \dot{X}_t(t) + \frac{1}{2}\dot{l}_w(t) \sin \theta(t) + \frac{1}{2}l_w \cos \theta(t)\dot{\theta}(t) \\ \frac{1}{2}\dot{l}_w(t) \cos \theta(t) - \frac{1}{2}l_w(t) \sin \theta(t)\dot{\theta}(t) \end{bmatrix} \quad (\text{B.5})$$

Velocity in x- and y-axis respectively of the load is described by the time differentiate of equation (B.3).

$$\dot{r}_m(t) = \begin{bmatrix} \dot{X}_t(t) + \dot{l}_w(t) \sin \theta(t) + l_w \cos \theta(t)\dot{\theta}(t) \\ \dot{l}_w(t) \cos \theta(t) - l_w(t) \sin \theta(t)\dot{\theta}(t) \end{bmatrix} \quad (\text{B.6})$$

B.1.3 Lagrangian

Define the Lagrangian [23] L , with kinetic energy T and potential energy as U .

$$L = T - U \quad (\text{B.7})$$

$$T = \frac{1}{2}mv^2 \quad (\text{B.8})$$

$$U = mgh \quad (\text{B.9})$$

where v is velocity, g is gravity and h is height. To describe the equations of motion the Euler-Lagrange equations [23] is used.

$$\frac{d}{dt} \frac{\partial L}{\partial \dot{x}} - \frac{\partial L}{\partial x} = \tau \quad (\text{B.10})$$

Lagrangian for the trolley

The following section describe the Euler-Lagrange equation of motion for the trolley. Since the trolley rides on a rail in the horizontal plane, it can be seen that only the kinetic energy is present.

$$T_1 = \frac{1}{2}M\|\dot{r}_t\|^2 \quad (\text{B.11})$$

$$U_1 = 0 \quad (\text{B.12})$$

$$L_1 = T_1 - U_1 \quad (\text{B.13})$$

$$L_1 = \frac{1}{2}M\|\dot{r}_t\|^2 \quad (\text{B.14})$$

$$L_1 = \frac{1}{2}M\dot{X}_t^2 \quad (\text{B.15})$$

Lagrangian for the wire

The second subsystem needed to be analysed is the wire.

$$T_2 = \frac{1}{2}m_w\|\dot{r}_{l_w}\|^2 \quad (\text{B.16})$$

$$\begin{aligned} &= \frac{1}{2}m_w \left[\left(\dot{X}_t(t) + \frac{1}{2}l_w(t) \sin \theta(t) + \frac{1}{2}l_w \cos \theta(t) \dot{\theta}(t) \right)^2 \right. \\ &\quad \left. + \left(\frac{1}{2}l_w(t) \cos \theta(t) - \frac{1}{2}l_w(t) \sin \theta(t) \dot{\theta}(t) \right)^2 \right] \quad (\text{B.17}) \end{aligned}$$

Rewriting $\sin \theta(t) = s_\theta$, $\cos \theta(t) = c_\theta$ and removing the time varying notation (t) for convenience.

$$\begin{aligned} T_2 &= \frac{1}{2}m_w \left(\dot{X}_t^2 + \frac{1}{4} \left(l_w^2 s_\theta^2 + l_w^2 c_\theta^2 \dot{\theta}^2 + l_w^2 c_\theta^2 + l_w^2 s_\theta^2 \dot{\theta}^2 \right) \right) \\ &\quad + 2\dot{X}_t \left(\frac{1}{2}l_w s_\theta + \frac{1}{2}l_w c_\theta \dot{\theta} \right) + 2 \left(\frac{1}{2}l_w s_\theta \right) \left(\frac{1}{2}l_w c_\theta \dot{\theta} \right) \quad (\text{B.18}) \end{aligned}$$

$$+ 2 \left(\frac{1}{2} \dot{l}_w c_\theta \right) \left(-\frac{1}{2} l_w s_\theta \dot{\theta} \right) \quad (\text{B.19})$$

$$= \frac{1}{2} m_w \left[\left(\dot{X}_t^2 + \frac{1}{4} \left(\dot{l}_w^2 + l_w^2 \dot{\theta}^2 \right) \right) + \dot{X}_t \left(\dot{l}_w s_\theta + l_w c_\theta \dot{\theta} \right) \right] \quad (\text{B.20})$$

and the potential energy is

$$U_2 = 0 \quad (\text{B.21})$$

giving the total Lagrangian for the wire as

$$L_2 = T_2 - U_2 \quad (\text{B.22})$$

$$= \frac{1}{2} m_w \left[\left(\dot{X}_t^2 + \frac{1}{4} \left(\dot{l}_w^2 + l_w^2 \dot{\theta}^2 \right) \right) + \frac{1}{2} \dot{X}_t \left(\dot{l}_w s_\theta + l_w c_\theta \dot{\theta} \right) \right] \quad (\text{B.23})$$

Lagrangian for the payload

The third subsystem is the payload, where the kinetic energy is defined as

$$T_3 = \frac{1}{2} m_p \|r_m\|^2 \quad (\text{B.24})$$

$$= \frac{1}{2} m_p \left[\left(\dot{X}_t + \dot{l}_w s_\theta + l_w c_\theta \dot{\theta} \right)^2 + \left(\dot{l}_w c_\theta - l_w s_\theta \dot{\theta} \right)^2 \right] \quad (\text{B.25})$$

$$= \frac{1}{2} m_p \left[\dot{X}_t^2 + \dot{l}_w^2 s_\theta^2 + l_w^2 c_\theta^2 \dot{\theta}^2 + \dot{l}_w^2 c_\theta^2 + l_w^2 s_\theta^2 \dot{\theta}^2 \right. \\ \left. + 2 \dot{X}_t \left(\dot{l}_w s_\theta + l_w c_\theta \dot{\theta} \right) + 2 \left(\dot{l}_w s_\theta \right) \left(l_w c_\theta \dot{\theta} \right) + 2 \left(\dot{l}_w c_\theta \right) \left(-l_w s_\theta \dot{\theta} \right) \right] \quad (\text{B.26})$$

Which finally yields

$$T_3 = \frac{1}{2} m_p \left[\dot{X}_t^2 + \dot{l}_w^2 + l_w^2 \dot{\theta}^2 + 2 \dot{X}_t \left(\dot{l}_w s_\theta + l_w c_\theta \dot{\theta} \right) \right] \quad (\text{B.27})$$

and the potential energy of the payload is

$$U_3 = (m_w + m_p) g l_w (1 - \cos\theta) \quad (\text{B.28})$$

The resulting Lagrangian for the payload is

$$L_3 = T_3 - U_3 \quad (\text{B.29})$$

$$L_3 = \frac{1}{2} m_p \left[\dot{X}_t^2 + \dot{l}_w^2 + l_w^2 \dot{\theta}^2 + 2 \dot{X}_t \left(\dot{l}_w s_\theta + l_w c_\theta \dot{\theta} \right) \right] - (m_w + m_p) g l_w (1 - \cos\theta) \quad (\text{B.30})$$

Total Euler-Lagrange equation for the trolley with pendant load

The total Lagrangian for the system is then defined by

$$L = L_1 + L_2 + L_3 \quad (\text{B.31})$$

where L_1 , L_2 and L_3 is the Euler-Lagrange equations for the subsystems described in equation (B.23), (B.23) and (B.30) respectively.

$$L = \frac{1}{2} M \dot{X}_t^2 + \frac{1}{2} m_w \left[\left(\dot{X}_t^2 + \frac{1}{4} \left(\dot{l}_w^2 + l_w^2 \dot{\theta}^2 \right) \right) + \frac{1}{2} \dot{X}_t \left(\dot{l}_w s_\theta + l_w c_\theta \dot{\theta} \right) \right] \\ + \frac{1}{2} m_p \left[\dot{X}_t^2 + \dot{l}_w^2 + l_w^2 \dot{\theta}^2 + 2 \dot{X}_t \left(\dot{l}_w s_\theta + l_w c_\theta \dot{\theta} \right) \right] - (m_w + m_p) g l_w (1 - \cos\theta) \quad (\text{B.32})$$

B.1.4 Equation of motion

The equation of motion is defined by

$$\frac{d}{dt} \frac{\partial L}{\partial \dot{q}} - \frac{\partial L}{\partial q} = W_q \quad (\text{B.33})$$

where q is the degree of freedom.

Equation of motion for the trolley

The equation of motion for the trolley is defined as

$$\frac{d}{dt} \frac{\partial L}{\partial \dot{x}} - \frac{\partial L}{\partial x} = W_x \quad (\text{B.34})$$

where W_x is the sum of forces working on the trolley

$$W_x = \tau_1 - \beta_1 \dot{x} \quad (\text{B.35})$$

and $\beta_1 \dot{x}$ is the forces generated by friction between the trolley and the rail. To complete the equation of motion for the trolley the following derivatives has to be written out.

$$\frac{\partial L}{\partial x} = 0 \quad (\text{B.36})$$

$$\frac{\partial L}{\partial \dot{x}} = M \dot{X}_t + m_w \dot{X}_t + \frac{1}{4} m_w (\dot{l}_w s_\theta + l_w c_\theta \dot{\theta}) + m_p \dot{X}_t + m_p (\dot{l}_w s_\theta + l_w c_\theta \dot{\theta}) \quad (\text{B.37})$$

$$\begin{aligned} \frac{d}{dt} \frac{\partial L}{\partial \dot{x}} &= M \ddot{X}_t + m_w \ddot{X}_t + \frac{1}{4} m_w (\ddot{l}_w s_\theta + 2\dot{l}_w c_\theta \dot{\theta} - l_w s_\theta \dot{\theta}^2 + l_w c_\theta \ddot{\theta}) \\ &+ m_p \ddot{X}_t + m_p (\ddot{l}_w s_\theta + 2\dot{l}_w c_\theta \dot{\theta} - l_w s_\theta \dot{\theta}^2 + l_w c_\theta \ddot{\theta}) \end{aligned} \quad (\text{B.38})$$

Finally using equation (B.34) and factorize with respect to $\ddot{X}_t, \ddot{\theta}$ and \ddot{l}_w the EOM for the trolley yields

$$\begin{aligned} \tau_1 &= \beta_1 \dot{X}_t + (M + m_w + m_p) \ddot{X}_t + \left(\frac{1}{4} m_w + m_p \right) s_\theta \ddot{l}_w + \left(\frac{1}{4} m_w + m_p \right) l_w c_\theta \ddot{\theta} \\ &+ \left(\frac{1}{2} m_w + 2m_p \right) c_\theta \dot{l}_w \dot{\theta} - \left(\frac{1}{4} m_w + m_p \right) l_w s_\theta \dot{\theta}^2 \end{aligned} \quad (\text{B.39})$$

Equation of motion for the pendulum

The equation of motion for the pendulum is defined as

$$\frac{d}{dt} \frac{\partial L}{\partial \dot{\theta}} - \frac{\partial L}{\partial \theta} = W_\theta \quad (\text{B.40})$$

with

$$W_\theta = -\beta_2 \dot{\theta} \quad (\text{B.41})$$

where $\beta_2\dot{\theta}$ is friction between wire and sheave. To derive the EOM the following partial and time derivatives is necessary

$$\frac{\partial L}{\partial \theta} = \frac{1}{4}m_w\dot{X}_t \left(\dot{l}_w c_\theta - l_w s_\theta \dot{\theta} \right) + m_p \dot{X}_t \left(\dot{l}_w c_\theta - l_w s_\theta \dot{\theta} \right) - (m_w + m_p) g l_w s_\theta \quad (\text{B.42})$$

$$\frac{\partial L}{\partial \dot{\theta}} = \frac{1}{2}m_w \left(\frac{1}{2}l_w^2 \dot{\theta} + \frac{1}{2}\dot{X}_t l_w c_\theta \right) + m_p \left(l_w^2 \dot{\theta} + \dot{X}_t l_w c_\theta \right) \quad (\text{B.43})$$

$$\begin{aligned} \frac{d}{dt} \frac{\partial L}{\partial \dot{\theta}} &= \frac{1}{2}m_w l_w \dot{\theta} \dot{l}_w + \frac{1}{4}m_w l_w^2 \ddot{\theta} + \frac{1}{4}m_w \left(\ddot{X}_t l_w c_\theta + \dot{X}_t \dot{l}_w c_\theta - \dot{X}_t l_w s_\theta \dot{\theta} \right) \\ &\quad + m_p \left(2l_w \dot{l}_w \dot{\theta} + l_w^2 \ddot{\theta} + \ddot{X}_t l_w c_\theta + \dot{X}_t \dot{l}_w c_\theta - \dot{X}_t l_w s_\theta \dot{\theta} \right) \end{aligned} \quad (\text{B.44})$$

Using equation (B.40) and factorize with respect to \ddot{X}_t , $\ddot{\theta}$ and $\dot{\theta}$ yields the equation of motion for the pendulum.

$$\begin{aligned} 0 &= \beta_2 \dot{\theta} + \left(\frac{1}{2}m_w + 2m_p \right) l_w \dot{l}_w \dot{\theta} + \left(\frac{1}{4}m_w + m_p \right) l_w^2 \ddot{\theta} + \left(\frac{1}{4}m_w + m_p \right) l_w c_\theta \ddot{X}_t \\ &\quad + (m_w + m_p) g l_w s_\theta \end{aligned} \quad (\text{B.45})$$

Equation of motion for the wirelength

The equation of motion for the wire is defined as

$$\frac{d}{dt} \frac{\partial L}{\partial \dot{l}_w} - \frac{\partial L}{\partial l_w} = W_{l_w} \quad (\text{B.46})$$

where

$$W_{l_w} = \tau_3 - \beta_3 \dot{l}_w - m_w g \quad (\text{B.47})$$

and $\beta_3 \dot{l}_w$ is the friction of the wire over the sheave. To describe the equation of motion it is necessary to find the partial and time derivative $\frac{\partial L}{\partial l_w}$, $\frac{\partial L}{\partial \dot{l}_w}$ and $\frac{d}{dt} \frac{\partial L}{\partial \dot{l}_w}$ from (B.32).

$$\frac{\partial L}{\partial l_w} = \frac{1}{4}m_w \left(l_w \dot{\theta}^2 + \dot{X}_t c_\theta \dot{\theta} \right) + m_p \left(l_w \dot{\theta}^2 + \dot{X}_t c_\theta \dot{\theta} \right) - (m_w + m_p) g (1 - c_\theta) \quad (\text{B.48})$$

$$\frac{\partial L}{\partial \dot{l}_w} = \frac{1}{4}m_w \left(\dot{l}_w + \dot{X}_t s_\theta \right) + m_p \left(\dot{l}_w + \dot{X}_t s_\theta \right) \quad (\text{B.49})$$

$$\frac{d}{dt} \frac{\partial L}{\partial \dot{l}_w} = \frac{1}{4}m_w \left(\ddot{l}_w + \ddot{X}_t s_\theta + \dot{X}_t c_\theta \dot{\theta} \right) + m_p \left(\ddot{l}_w + \ddot{X}_t s_\theta + \dot{X}_t c_\theta \dot{\theta} \right) \quad (\text{B.50})$$

The equation of motion for the wire length $l_w(t)$ is then described using equation (B.46)

$$\begin{aligned} \tau_3 = & \beta_3 \dot{l}_w + \frac{1}{4} m_w \left(\ddot{l}_w + \ddot{X}_t s_\theta + \dot{X}_t c_\theta \dot{\theta} \right) + m_p \left(\ddot{l}_w + \ddot{X}_t s_\theta + \dot{X}_t c_\theta \dot{\theta} \right) \\ & - \frac{1}{4} m_w \left(l_w \dot{\theta}^2 + \dot{X}_t c_\theta \dot{\theta} \right) - m_p \left(l_w \dot{\theta}^2 + \dot{X}_t c_\theta \dot{\theta} \right) + (m_w + m_p) g(1 - c_\theta) \end{aligned} \quad (\text{B.51})$$

factorize with respect to \ddot{X}_t , $\dot{\theta}$, \dot{l}_w and \ddot{l}_w

$$\begin{aligned} \tau_3 = & \beta_3 \dot{l}_w + \left(\frac{1}{4} m_w + m_p \right) \ddot{l}_w \\ & + \left(\frac{1}{4} m_w + m_p \right) s_\theta \ddot{X}_t - \left(\frac{1}{4} m_w + m_p \right) l_w^2 \dot{\theta}^2 + (m_w + m_p) g(1 - c_\theta) \end{aligned} \quad (\text{B.52})$$

B.1.5 Equation of motion on matrix form

By combining equation (B.39), (B.45) and (B.52), the equations of motion for the trolley with pendant load in wire written on matrix form yields:

$$\mathbf{M}\ddot{z} + \mathbf{C}\dot{z} + \mathbf{g}_0 = \tau \quad (\text{B.53})$$

where $z = [X_t \ \theta \ l_w]^\top$, \mathbf{M} is the rigid body inertia matrix, \mathbf{C} is a matrix of rigid-body Coriolis and centripetal forces and \mathbf{g}_0 is a vector of restoring forces.

$$\begin{bmatrix} m_{11} & m_{12} & m_{13} \\ m_{21} & m_{22} & m_{23} \\ m_{31} & m_{32} & m_{33} \end{bmatrix} \ddot{z} + \begin{bmatrix} c_{11} & c_{12} & c_{13} \\ c_{21} & c_{22} & c_{23} \\ c_{31} & c_{32} & c_{33} \end{bmatrix} \dot{z} + \begin{bmatrix} g_{11} \\ g_{21} \\ g_{31} \end{bmatrix} = \begin{bmatrix} \tau_1 \\ 0 \\ \tau_3 \end{bmatrix} \quad (\text{B.54})$$

where the terms in the \mathbf{M} matrix is

$$m_{11} = (M + m_w + m_p) \quad (\text{B.55})$$

$$m_{12} = \left(\frac{1}{4} m_w + m_p \right) l_w c_\theta \quad (\text{B.56})$$

$$m_{13} = \left(\frac{1}{4} m_w + m_p \right) s_\theta \quad (\text{B.57})$$

$$m_{21} = \left(\frac{1}{4} m_w + m_p \right) l_w c_\theta \quad (\text{B.58})$$

$$m_{22} = \left(\frac{1}{4} m_w + m_p \right) l_w^2 \quad (\text{B.59})$$

$$m_{23} = 0 \quad (\text{B.60})$$

$$m_{31} = \left(\frac{1}{4} m_w + m_p \right) s_\theta \quad (\text{B.61})$$

$$m_{32} = 0 \quad (\text{B.62})$$

$$m_{33} = \left(\frac{1}{4} m_w + m_p \right) \quad (\text{B.63})$$

the terms in the \mathbf{C} matrix is

$$c_{11} = \beta_1 \tag{B.64}$$

$$c_{12} = \left(\frac{1}{2}m_w + 2m_p\right) c_\theta \dot{l}_w - \left(\frac{1}{4}m_w + m_p\right) l_w s_\theta \dot{\theta} \tag{B.65}$$

$$c_{13} = 0 \tag{B.66}$$

$$c_{21} = 0 \tag{B.67}$$

$$c_{22} = \beta_2 + \left(\frac{1}{2}m_w + 2m_p\right) l_w \dot{l}_w \tag{B.68}$$

$$c_{23} = 0 \tag{B.69}$$

$$c_{31} = 0 \tag{B.70}$$

$$c_{32} = \left(\frac{1}{4}m_w + m_p\right) l_w^2 \dot{\theta} \tag{B.71}$$

$$c_{33} = \beta_3 \tag{B.72}$$

$$\tag{B.73}$$

and finally the terms in the \mathbf{g}_0 matrix is

$$g_{11} = 0 \tag{B.74}$$

$$g_{21} = (m_w + m_p) g l_w s_\theta \tag{B.75}$$

$$g_{31} = (m_w + m_p) g(1 - c_\theta) \tag{B.76}$$

Appendix C

Mathematical model of spherical pendulum

In this chapter an mathematical model derived by use of Euler Lagrange equations is derived, this model was used early in the project, but due to singularity issues, a new parametrization was derived. The new model is described in 2.2.2.

C.1 Position and velocity of the load

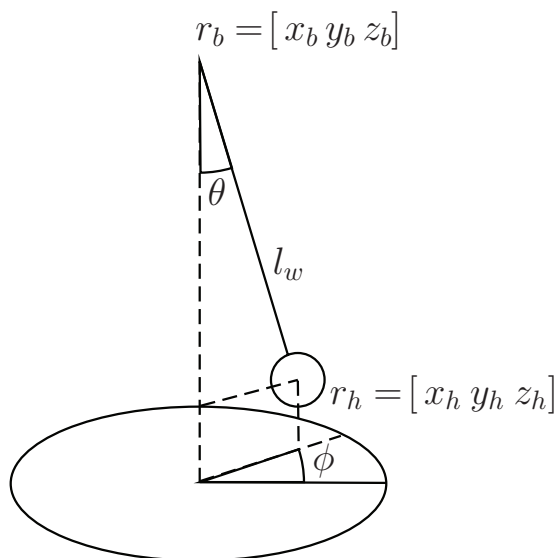


Figure C.1: Sketch of spherical pendulum

It is of interest to be able to describe the position, velocity and acceleration of the load with respect to the position of the earth fixed coordinate system. To do this the following notation are defined.

Notation	Description
x_b	X-axis position of the boom tip relative to the earth fixed coordinate system
y_b	Y-axis position of the boom tip relative to the earth fixed coordinate system
z_b	Z-axis position of the boom tip relative to the earth fixed coordinate system
l_w	Length of wire paid out, measured from boom tip
ϕ	Rotation angle in the hook coordinate system
θ	Offlead angle, measured between the z-axis and the wire.

Table C.1: Hook coordinate system

The position of the load with respect to the boom tip is described by the following equations and the direct measurement of ϕ and θ .

$$r_h(x_b, y_b, z_b, l_w, \theta, \phi) = \begin{bmatrix} x_b + l_w \sin \theta \cos \phi \\ y_b + l_w \sin \theta \sin \phi \\ z_b - l_w \cos \theta \end{bmatrix} \quad (\text{C.1})$$

To describe the velocity of the hook it is necessary to differentiate (C.1) with respect to time, which yields

$$\dot{r}_h = \begin{bmatrix} \dot{x}_b + \dot{l}_w \sin \theta \cos \phi + l_w \cos \theta \cos \phi \dot{\theta} - l_w \sin \theta \sin \phi \dot{\phi} \\ \dot{y}_b + \dot{l}_w \sin \theta \sin \phi + l_w \cos \theta \sin \phi \dot{\theta} + l_w \sin \theta \cos \phi \dot{\phi} \\ \dot{z}_b - \dot{l}_w \cos \theta + l_w \sin \theta \dot{\theta} \end{bmatrix} \quad (\text{C.2})$$

By the assumption that the hook is a concentrated mass connected to the end of a massless rod the Lagrangian is defined as

$$L_p = T_p - U_p \quad (\text{C.3})$$

$$T_p = \frac{1}{2} m_p \|\dot{r}_h\|^2 \quad (\text{C.4})$$

$$U_p = m_p g h \quad (\text{C.5})$$

where L_p is the kinetic energy and U_p is the potential energy caused by gravity and h is potential above the resting point of the "pendulum".

$$\begin{aligned} T_p &= \frac{1}{2} m_p \left[\dot{x}_b^2 + (\dot{l}_w \sin \theta \cos \phi)^2 + (l_w \cos \theta \cos \phi \dot{\theta})^2 + (-l_w \sin \theta \sin \phi \dot{\phi})^2 \right. \\ &\quad + 2\dot{x}_b \left(\dot{l}_w \sin \theta \cos \phi + l_w \cos \theta \cos \phi \dot{\theta} - l_w \sin \theta \sin \phi \dot{\phi} \right) \\ &\quad + 2(\dot{l}_w \sin \theta \cos \phi)(l_w \cos \theta \cos \phi \dot{\theta}) \\ &\quad + 2(\dot{l}_w \sin \theta \cos \phi)(-l_w \sin \theta \sin \phi \dot{\phi}) \\ &\quad + 2(l_w \cos \theta \cos \phi \dot{\theta})(-l_w \sin \theta \sin \phi \dot{\phi}) \\ &\quad + \dot{y}_b^2 + (\dot{l}_w \sin \theta \sin \phi)^2 + (l_w \cos \theta \sin \phi \dot{\theta})^2 + (l_w \sin \theta \cos \phi \dot{\phi})^2 \\ &\quad + 2\dot{y}_b \left(\dot{l}_w \sin \theta \sin \phi + l_w \cos \theta \sin \phi \dot{\theta} + l_w \sin \theta \cos \phi \dot{\phi} \right) \\ &\quad \left. + 2(\dot{l}_w \sin \theta \sin \phi)(l_w \cos \theta \sin \phi \dot{\theta}) \right] \end{aligned}$$

$$\begin{aligned}
& + 2(\dot{l}_w \sin \theta \sin \phi)(l_w \sin \theta \cos \phi \dot{\phi}) \\
& + 2(l_w \cos \theta \sin \phi \dot{\theta})(l_w \sin \theta \cos \phi \dot{\phi}) \\
& + \dot{z}_b^2 + (-\dot{l}_w \cos \theta)^2 + (l_w \sin \theta \dot{\theta})^2 \\
& + 2\dot{z}_b \left(-\dot{l}_w \cos \theta + l_w \sin \theta \dot{\theta} \right) \\
& + 2(-\dot{l}_w \cos \theta)(l_w \sin \theta \dot{\theta}) \Big] \tag{C.6}
\end{aligned}$$

The kinetic energy for the load finally yields

$$\begin{aligned}
T_p = \frac{1}{2} m_p \Big[& \dot{x}_b^2 + \dot{y}_b^2 + \dot{z}_b^2 + \dot{l}_w^2 + l_w^2 \dot{\theta}^2 + l_w^2 \sin^2 \theta \dot{\phi}^2 \\
& + 2\dot{x}_b \left(\dot{l}_w \sin \theta \cos \phi + l_w \cos \theta \cos \phi \dot{\theta} - l_w \sin \theta \sin \phi \dot{\phi} \right) \\
& + 2\dot{y}_b \left(\dot{l}_w \sin \theta \sin \phi + l_w \cos \theta \sin \phi \dot{\theta} + l_w \sin \theta \cos \phi \dot{\phi} \right) \\
& + 2\dot{z}_b \left(-\dot{l}_w \cos \theta + l_w \sin \theta \dot{\theta} \right) \Big] \tag{C.7}
\end{aligned}$$

The potential energy for the load is then simply

$$U_p = m_p g l_w \cos \theta \tag{C.8}$$

giving the total Lagrangian for the load described in (C.3) as

$$\begin{aligned}
L_p = \frac{1}{2} m_p \Big[& \dot{x}_b^2 + \dot{y}_b^2 + \dot{z}_b^2 + \dot{l}_w^2 + l_w^2 \dot{\theta}^2 + l_w^2 \sin^2 \theta \dot{\phi}^2 \\
& + 2\dot{x}_b \left(\dot{l}_w \sin \theta \cos \phi + l_w \cos \theta \cos \phi \dot{\theta} - l_w \sin \theta \sin \phi \dot{\phi} \right) \\
& + 2\dot{y}_b \left(\dot{l}_w \sin \theta \sin \phi + l_w \cos \theta \sin \phi \dot{\theta} + l_w \sin \theta \cos \phi \dot{\phi} \right) \\
& + 2\dot{z}_b \left(-\dot{l}_w \cos \theta + l_w \sin \theta \dot{\theta} \right) \Big] \\
& - m_p g l_w \cos \theta \tag{C.9}
\end{aligned}$$

C.1.1 Equation of motion for the load

The equation of motion of the pendulum is given by

$$\frac{d}{dt} \frac{\partial L}{\partial \dot{q}} - \frac{\partial L}{\partial q} = \tau \tag{C.10}$$

where L is the total Lagrangian, q is the degrees of freedom here represented by $q = \{\theta, l_w, \phi\}^\top$ and $\tau = \{0, \tau_w, 0\}^\top$.

$$\begin{aligned}
\frac{\partial L_p}{\partial \theta} = \frac{1}{2} m_p \Big[& l_w^2 s_{(2\theta)} \dot{\phi}^2 + 2\dot{x}_b \left(\dot{l}_w c_\theta c_\phi - l_w s_\theta c_\phi \dot{\theta} - l_w c_\theta s_\phi \dot{\phi} \right) \\
& + 2\dot{y}_b \left(\dot{l}_w c_\theta s_\phi - l_w s_\theta s_\phi \dot{\theta} + l_w c_\theta c_\phi \dot{\phi} \right) + 2\dot{z}_b \left(\dot{l}_w s_\theta + l_w c_\theta \dot{\theta} \right) \Big] + m_p g l_w s_\theta \tag{C.11}
\end{aligned}$$

$$\frac{\partial L_p}{\partial \dot{\theta}} = \frac{1}{2} m_p \left[2l_w^2 \dot{\theta} + 2\dot{x}_b l_w c_\theta c_\phi + 2\dot{y}_b l_w c_\theta s_\phi + 2\dot{z}_b l_w s_\theta \right] \quad (\text{C.12})$$

$$\begin{aligned} \frac{d}{dt} \frac{\partial L_p}{\partial \dot{\theta}} &= m_p \left[2l_w \dot{l}_w \dot{\theta} + l_w^2 \ddot{\theta} + \ddot{x}_b l_w c_\theta c_\phi + \dot{x}_b \dot{l}_w c_\theta c_\phi - \dot{x}_b l_w s_\theta c_\phi \dot{\theta} - \dot{x}_b l_w c_\theta s_\phi \dot{\phi} \right. \\ &\quad \left. + \ddot{y}_b l_w c_\theta s_\phi + \dot{y}_b \dot{l}_w c_\theta s_\phi - \dot{y}_b l_w s_\theta s_\phi \dot{\theta} + \dot{y}_b l_w c_\theta c_\phi \dot{\phi} + \ddot{z}_b l_w s_\theta + \dot{z}_b \dot{l}_w s_\theta \right. \\ &\quad \left. + \dot{z}_b l_w c_\theta \dot{\theta} \right] \end{aligned} \quad (\text{C.13})$$

$$\frac{\partial L_p}{\partial l_w} = m_p \left[l_w \dot{\theta}^2 + l_w s_\theta^2 \dot{\phi}^2 + \dot{x}_b c_\theta c_\phi \dot{\theta} - \dot{x}_b s_\theta s_\phi \dot{\phi} + \dot{y}_b c_\theta s_\phi \dot{\theta} + \dot{y}_b s_\theta c_\phi \dot{\phi} + \dot{z}_b s_\theta \dot{\theta} - g c_\theta \right] \quad (\text{C.14})$$

$$\frac{\partial L_p}{\partial \dot{l}_w} = m_p \left[\dot{l}_w + \dot{x}_b s_\theta c_\phi + \dot{y}_b s_\theta s_\phi - \dot{z}_b c_\theta \right] \quad (\text{C.15})$$

$$\begin{aligned} \frac{d}{dt} \frac{\partial L_p}{\partial \dot{l}_w} &= m_p \left[\ddot{l}_w + \ddot{x}_b s_\theta c_\phi + \dot{x}_b c_\theta c_\phi \dot{\theta} - \dot{x}_b c_\theta s_\phi \dot{\phi} + \ddot{y}_b s_\theta s_\phi + \dot{y}_b c_\theta s_\phi \dot{\theta} + \dot{y}_b s_\theta c_\phi \dot{\phi} \right. \\ &\quad \left. - \ddot{z}_b c_\theta + \dot{z}_b s_\theta \dot{\theta} \right] \end{aligned} \quad (\text{C.16})$$

$$\frac{\partial L_p}{\partial \phi} = m_p \left[\dot{x}_b \left(-\dot{l}_w s_\theta s_\phi - l_w c_\theta s_\phi \dot{\theta} - l_w s_\theta c_\phi \dot{\phi} \right) + \dot{y}_b \left(\dot{l}_w s_\theta c_\phi + l_w c_\theta c_\phi \dot{\theta} - l_w s_\theta s_\phi \dot{\phi} \right) \right] \quad (\text{C.17})$$

$$\frac{\partial L_p}{\partial \dot{\phi}} = m_p \left[l_w^2 s_\theta^2 \dot{\phi} - \dot{x}_b l_w s_\theta s_\phi + \dot{y}_b l_w s_\theta c_\phi \right] \quad (\text{C.18})$$

$$\begin{aligned} \frac{d}{dt} \frac{\partial L_p}{\partial \dot{\phi}} &= m_p \left[2l_w \dot{l}_w s_\theta^2 \dot{\phi} + l_w^2 s_{(2\theta)} \dot{\theta} \dot{\phi} + l_w^2 s_\theta^2 \ddot{\phi} - \ddot{x}_b l_w s_\theta s_\phi - \dot{x}_b \dot{l}_w s_\theta s_\phi - \dot{x}_b l_w c_\theta s_\phi \dot{\theta} \right. \\ &\quad \left. - \dot{x}_b l_w s_\theta c_\phi \dot{\phi} + \ddot{y}_b l_w s_\theta c_\phi + \dot{y}_b \dot{l}_w s_\theta c_\phi + \dot{y}_b l_w c_\theta c_\phi \dot{\theta} - \dot{y}_b l_w s_\theta s_\phi \dot{\phi} \right] \end{aligned} \quad (\text{C.19})$$

The equation of motion for the pendulum is defined by equation (C.10), and yields

$$m_p \begin{bmatrix} 2l_w \dot{l}_w \dot{\theta} + l_w^2 \ddot{\theta} + \ddot{x}_b l_w c_\theta c_\phi + \ddot{y}_b l_w c_\theta s_\phi + \ddot{z}_b l_w s_\theta - \frac{1}{2} l_w^2 s_{(2\theta)} \dot{\phi}^2 + g l_w s_\theta \\ \dot{l}_w + \ddot{x}_b s_\theta c_\phi + \dot{y}_b s_\theta s_\phi - \ddot{z}_b c_\theta - l_w \dot{\theta}^2 - l_w s_\theta^2 \dot{\phi}^2 + g c_\theta \\ 2l_w \dot{l}_w s_\theta^2 \dot{\phi} + l_w^2 s_{(2\theta)} \dot{\theta} \dot{\phi} + l_w^2 s_\theta^2 \ddot{\phi} - \ddot{x}_b l_w s_\theta s_\phi + \ddot{y}_b l_w s_\theta c_\phi \end{bmatrix} = \begin{bmatrix} 0 \\ \tau_{l_w} \\ 0 \end{bmatrix} \quad (\text{C.20})$$

As seen in equation (C.20), only the dynamics of l_w is dependent of the payload m_p .

$$\begin{aligned} &\begin{bmatrix} l_w^2 & 0 & 0 \\ 0 & 1 & 0 \\ 0 & 0 & l_w^2 s_\theta^2 \end{bmatrix} \begin{bmatrix} \ddot{\theta} \\ \ddot{l}_w \\ \ddot{\phi} \end{bmatrix} + \begin{bmatrix} l_w c_\theta c_\phi & l_w s_\theta & l_w c_\theta c_\phi \\ s_\theta c_\phi & s_\theta s_\phi & l_w s_\theta s_\phi \\ l_w s_\theta s_\phi & l_w s_\theta c_\phi & 0 \end{bmatrix} \begin{bmatrix} \ddot{x}_b \\ \ddot{y}_b \\ \ddot{z}_b \end{bmatrix} + \dots \\ &+ \begin{bmatrix} 2l_w \dot{l}_w \dot{\theta} + \frac{1}{2} l_w^2 s_{(2\theta)} \dot{\phi}^2 \\ -l_w \dot{\theta}^2 - l_w s_\theta^2 \dot{\phi}^2 \\ 2l_w \dot{l}_w s_\theta^2 \dot{\phi} + l_w^2 s_{(2\theta)} \dot{\theta} \dot{\phi} \end{bmatrix} + \begin{bmatrix} l_w s_\theta \\ c_\theta \\ 0 \end{bmatrix} g = \frac{1}{m_p} \begin{bmatrix} 0 \\ \tau_{l_w} \\ 0 \end{bmatrix} \end{aligned} \quad (\text{C.21})$$

C.2 Model problems

C.2.1 $\ddot{\phi} \rightarrow \infty$

As seen in equation (C.21) the differential equation of $\ddot{\phi}$ tends to infinity when θ is near 0, since $\ddot{\phi} = \frac{1}{l_w^2 s_\theta^2}(\dots)$. That makes this parametrization inferior, from a mathematical point of view [20].

Appendix D

Derivation of the Equations of Motion for a Pendulum

In this appendix the equation of motion for a spherical pendulum with two degree of freedom is presented. Lagrangian is used to describe the dynamics of the pendulum, while Euler-Lagrange equation is used to derive the equations of motion. This derivation is made by use of the program Mathematica [24]. This method is the same as in [20].

D.1 Crane-Fixed Coordinate System

To derive the equation of motion the following step is made. First the coordinates of the boomtip is defined as in (2.11).

$$r_b = \begin{bmatrix} -(r_p + l_b \cos q_2) \sin q_1 \\ (r_p + l_b \cos q_2) \cos q_1 \\ l_p + l_b \sin q_2 \end{bmatrix} \quad (D.1)$$

where r_p is the radius of the pedestal, l_b is the length of the boom, l_p is the height of the pedestal, q_1 is the slew angle and q_2 is the boom angle respectively. The next step is to find the coordinates of the hook. This is done by substituting equation (2.37) in to equation (2.14).

$$r_h^i = r_b^i + l_w R_c^i \Omega_v \quad (D.2)$$

$$= \begin{bmatrix} -(r_p + l_b c_{q_2}) s_{q_1} \\ (r_p + l_b c_{q_2}) c_{q_1} \\ l_p + l_b s_{q_2} \end{bmatrix} + l_w \begin{bmatrix} c_{q_1} & -s_{q_1} & 0 \\ s_{q_1} & c_{q_1} & 0 \\ 0 & 0 & 1 \end{bmatrix} \begin{bmatrix} -s_{\alpha_v} \\ c_{\alpha_v} s_{\beta_v} \\ -c_{\alpha_v} c_{\beta_v} \end{bmatrix} \quad (D.3)$$

$$= \begin{bmatrix} -r_p s_{q_1} - l_b c_{q_2} s_{q_1} - l_w c_{q_1} s_{\alpha_v} - l_w s_{q_1} c_{\alpha_v} s_{\beta_v} \\ r_p c_{q_1} + l_b c_{q_2} c_{q_1} - l_w s_{q_1} s_{\alpha_v} + l_w c_{q_1} c_{\alpha_v} s_{\beta_v} \\ l_p + l_b s_{q_2} - l_w c_{\alpha_v} c_{\beta_v} \end{bmatrix} \quad (D.4)$$

The Lagrangian is defined as

$$L_p = T_p - U_p \quad (D.5)$$

where

$$T_p = \frac{1}{2} m_p |\dot{r}_h|^2 \quad (\text{D.6})$$

$$U_p = m_p g z_h \quad (\text{D.7})$$

Using Mathematica [24] to define the Lagrangian.

```

1 %Define the boom tip position  $r_b^i$ 
2 xb[t] := -(rp + lb Cos[q2[t]]) Sin[q1[t]] // Expand;
3 yb[t] := (rp + lb Cos[q2[t]]) Cos[q1[t]] // Expand;
4 zb[t] := lp + lb Sin[q2[t]];
5 % Define hook position in the inertial coordinate system  $r_h^i$ 
6 xh[t] := xb[t] +
7     lw[t] (-Cos[q1[t]] Sin[av[t]] - Sin[q1[t]] Cos[av[t]] Sin[bv[t]]);
8 yh[t] := yb[t] +
9     lw[t] (-Sin[q1[t]] Sin[av[t]] + Cos[q1[t]] Cos[av[t]] Sin[bv[t]]);
10 zh[t] := zb[t] + lw[t] (-Cos[av[t]] Cos[bv[t]]);
11 %Defining the Lagrangian as L=T-U
12 L=(1/2 (D[xh[t],t]^2+D[yh[t],t]^2+D[zh[t],t]^2)-g zh[t]) //Expand;

```

Then calculating the Euler-Lagrange equations for $\ddot{\beta}_v$ and $\ddot{\alpha}_v$

```

1 %Calculate the Euler-Lagrange equation for  $\beta_v$  and  $\alpha_v$ :
2 L1 = (D[D[L, D[bv[t], t]], t] - D[L, bv[t]]) == 0;
3 L2 = (D[D[L, D[av[t], t]], t] - D[L, av[t]]) == 0;
4 dynamics = Solve[{L1, L2}, {bv''[t], av''[t]}];

```

Solving the $L1$ Euler-Lagrange equation with respect to $c_{\alpha_v} l_w \ddot{\beta}_v$

```

1 %Calculate the EOM for  $c_{\alpha_v} l_w \ddot{\beta}_v$ 
2 Cos[av[t]] lw[t] bv''[t] /. dynamics // Simplify

```

with the resulting output from Mathematica

$$\begin{aligned}
& \{-g \sin[bv[t]] - 2 \cos[av[t]] bv'[t] lw'[t] + 2 \cos[bv[t]] \sin[av[t]] lw'[t] q1'[t] + \\
& rp \cos[bv[t]] q1'[t]^2 + lb \cos[bv[t]] \cos[q2[t]] q1'[t]^2 + \\
& lb \cos[bv[t]] \cos[q2[t]] q2'[t]^2 + lb \sin[bv[t]] \sin[q2[t]] q2'[t]^2 + \\
& lw[t] (2 av'[t] (\sin[av[t]] bv'[t] + \cos[av[t]] \cos[bv[t]] q1'[t]) + \\
& \cos[bv[t]] (\cos[av[t]] \sin[bv[t]] q1'[t]^2 + \sin[av[t]] q1''[t])) - \\
& lb \cos[q2[t]] \sin[bv[t]] q2''[t] + lb \cos[bv[t]] \sin[q2[t]] q2''[t] \}
\end{aligned}$$

Figure D.1: Mathematica output of the EOM for $c_{\alpha_v} l_w \ddot{\beta}_v$

Again using Mathematica to solve the $L2$ Euler-Lagrange equation with respect to $2l_w \ddot{\alpha}_v$

```

1 %Calculate the EOM for  $2l_w \ddot{\alpha}_v$ 
2 2 lw[t] av''[t] /. dynamics // Simplify

```

with the resulting output from Mathematica

$$\begin{aligned}
& \{-l_w[t] (\sin[2 \text{av}[t]] \text{bv}'[t]^2 + 4 \cos[\text{av}[t]]^2 \cos[\text{bv}[t]] \text{bv}'[t] \text{q1}'[t] - \\
& \quad \cos[\text{bv}[t]]^2 \sin[2 \text{av}[t]] \text{q1}'[t]^2 + 2 \sin[\text{bv}[t]] \text{q1}''[t]) - \\
& \quad 2 (g \cos[\text{bv}[t]] \sin[\text{av}[t]] + 2 \text{av}'[t] l_w'[t] + 2 \sin[\text{bv}[t]] l_w'[t] \text{q1}'[t] + \\
& \quad \text{rp} \sin[\text{av}[t]] \sin[\text{bv}[t]] \text{q1}'[t]^2 + l_b \cos[\text{q2}[t]] \sin[\text{av}[t]] \sin[\text{bv}[t]] \text{q1}'[t]^2 - \\
& \quad 2 l_b \cos[\text{av}[t]] \sin[\text{q2}[t]] \text{q1}'[t] \text{q2}'[t] + l_b \cos[\text{q2}[t]] \sin[\text{av}[t]] \sin[\text{bv}[t]] \text{q2}'[t]^2 - \\
& \quad l_b \cos[\text{bv}[t]] \sin[\text{av}[t]] \sin[\text{q2}[t]] \text{q2}'[t]^2 + \text{rp} \cos[\text{av}[t]] \text{q1}''[t] + \\
& \quad l_b \cos[\text{av}[t]] \cos[\text{q2}[t]] \text{q1}''[t] + l_b \cos[\text{bv}[t]] \cos[\text{q2}[t]] \sin[\text{av}[t]] \text{q2}''[t] + \\
& \quad l_b \sin[\text{av}[t]] \sin[\text{bv}[t]] \sin[\text{q2}[t]] \text{q2}''[t]) \}
\end{aligned}$$

Figure D.2: Mathematica output of the EOM for $2l_w\ddot{\alpha}_v$

Rewriting the equation of motion to a more readable form yields

$$\begin{aligned}
\ddot{\beta}_v = \frac{1}{c_{\alpha_v} l_w} & \left[-g s_{\beta_v} - 2c_{\alpha_v} \dot{\beta}_v \dot{l}_w + 2c_{\beta_v} s_{\alpha_v} \dot{l}_w \dot{q}_1 + r_p c_{\beta_v} \dot{q}_1^2 + l_b c_{\beta_v} c_{q_2} (\dot{q}_1^2 + \dot{q}_2^2) \right. \\
& + l_b s_{\beta_v} s_{q_2} \dot{q}_2^2 + l_w \left(2\dot{\alpha}_v (s_{\alpha_v} \dot{\beta}_v + c_{\alpha_v} c_{\beta_v} \dot{q}_1) + c_{\beta_v} (c_{\alpha_v} s_{\beta_v} \dot{q}_1^2 + s_{\alpha_v} \ddot{q}_1) \right) \\
& \left. - l_b c_{q_2} s_{\beta_v} \ddot{q}_2 + l_b c_{\beta_v} s_{q_2} \ddot{q}_2 \right] \tag{D.8}
\end{aligned}$$

$$\begin{aligned}
\ddot{\alpha}_v = \frac{1}{2l_w} & \left[-l_w \left(s_{2\alpha_v} \dot{\beta}_v^2 + 4c_{\alpha_v}^2 c_{\beta_v} \dot{\beta}_v \dot{q}_1 - c_{\beta_v}^2 s_{2\alpha_v} \dot{q}_1^2 + 2s_{\beta_v} \ddot{q}_1 \right) \right. \\
& - 2 \left(g c_{\beta_v} s_{\alpha_v} + 2\dot{\alpha}_v \dot{l}_w + 2s_{\beta_v} \dot{l}_w \dot{q}_1 + r_p s_{\alpha_v} s_{\beta_v} \dot{q}_1^2 + l_b c_{q_2} s_{\alpha_v} s_{\beta_v} \dot{q}_1^2 \right. \\
& \left. - 2l_b c_{\alpha_v} s_{q_2} \dot{q}_1 \dot{q}_2 + l_b c_{q_2} s_{\alpha_v} s_{\beta_v} \dot{q}_2^2 - l_b c_{\beta_v} s_{\alpha_v} s_{q_2} \dot{q}_2^2 + r_p c_{\alpha_v} \ddot{q}_1 + l_b c_{\alpha_v} c_{q_2} \ddot{q}_1 \right. \\
& \left. + l_b c_{\beta_v} c_{q_2} s_{\alpha_v} \ddot{q}_2 + l_b s_{\alpha_v} s_{\beta_v} s_{q_2} \ddot{q}_2 \right) \left. \right] \tag{D.9}
\end{aligned}$$

Appendix E

Plots

E.1 Parameter estimation and Kalman filtering

Parameter estimation and Kalman Filtering

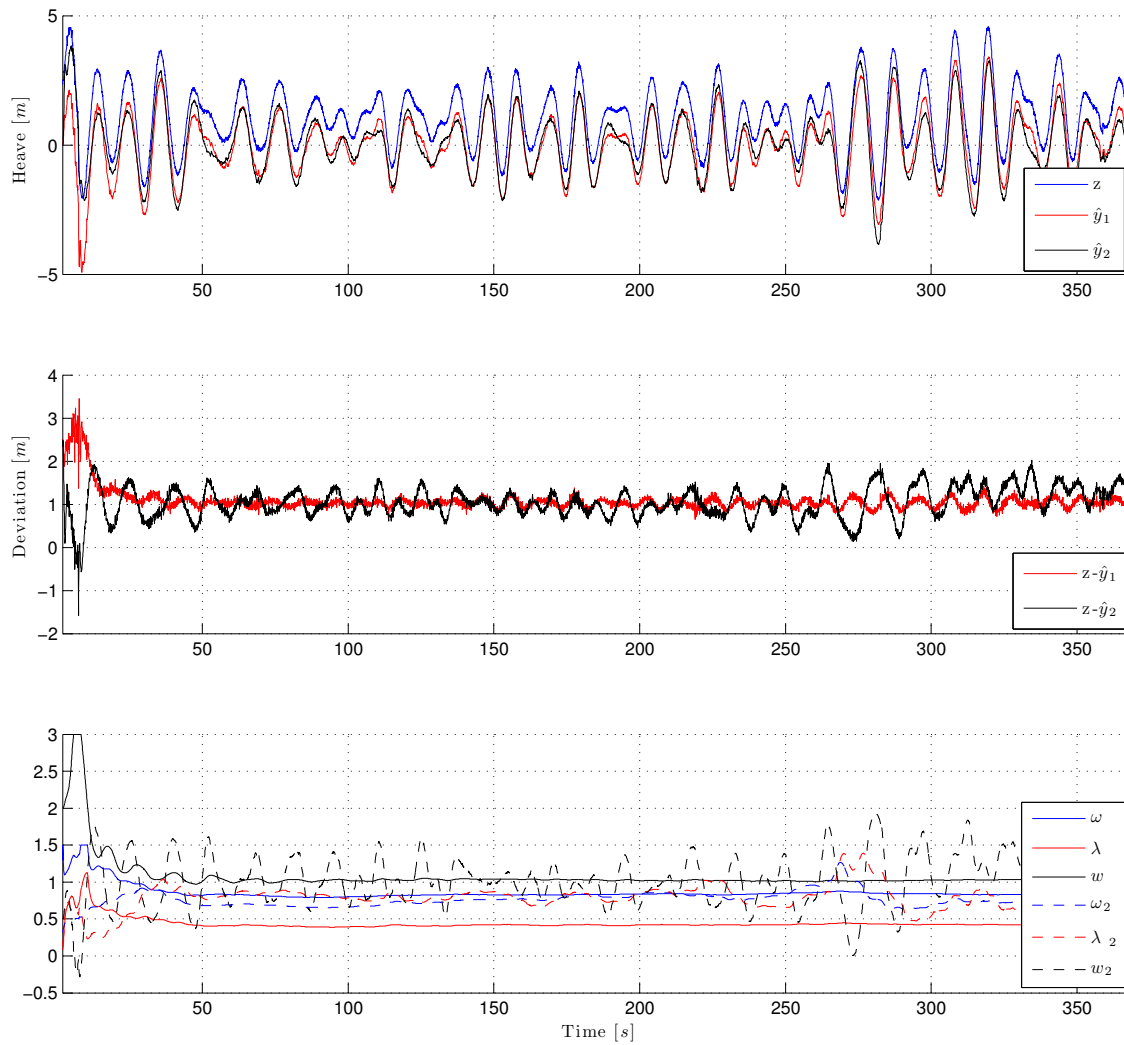


Figure E.1: Comparison between two parameter estimation algorithms as input to the Kalman filter

Appendix F

Simulink models

Appendix G

Matlab files

In this appendix the initialization file for the Simulink model of the Rotary Crane described in section 2.2 is presented.

G.1 Initialization file for Rotary Crane Model

```
1 %% Init file for pendulum_matrix_form_final_win
2 % Initialization file to used to configure setup of the
3 % simulink model of the rotary crane with spherical pendulum
4 %
5 % Attachment to M.sc Thesis 2012, NTNU
6 % Author: Oddvar Gjelstenli
7 % Version: final
8 % Version date: 2012-08-06
9
10 % Define simulation time and sample rate
11 simstart=0;      %Simulation start time
12 simstop=120;    %Simulation stop time
13 Ts=0.01;        %Sample time
14 % Operator input
15   operator_activated=0; %Joystick input enabled 1=true 0=false
16 % Test signal ramp
17   slope=0.5;      %Rise time of 1/slope
18   start_time_ramp=10; %ramp start time
19   stop_time_ramp=40; %ramp stop time
20   percent=1;      %percentage [0 1] where 1 is 100%
21   wind=0;
22 % Test signal generator hoist
23   %ramp
24   hoisting_lowering=1; %-1=hoisting 1=lowering
25   %camera measurement
26   load heave_test_signal %test signal for the hoist winch
27   %sine wave
28   amplitude=1;
29   frequency=1/5;
30   %hoist signal type selector
31   selector=2; %1=ramp 2=camera measurement 3=sine
32 % Test regulator activation deactivation time
33   test_reg_on_time=50; %simtime when regulator is activated
```

```

34     test_reg_off_time=100;%simtime when regulator is deactivated
35 % Test signal on/off
36     test_signal_slew=-1;
37     test_signal_boom=1;
38     test_signal_hoist=0.5;
39 % Regulator parameters
40 Kp_alpha=-10;
41 Kp_beta=20;
42 Kp_pos=120;
43 Ki_pos=60;
44 Kd_pos=0;%0.6*T;
45 %Regulator test selector
46 %regulator = 'beta' to test beta regulator
47 %regulator = 'alpha' to test alpha regulator
48 %regulator = 'sway' to test alpha+beta regulator
49 %regulator = 'pos' to test boom tip pos reg
50 %regulator = 'all' to anti-sway and boom tip position regulator
51 %regulator = 'off' to turn off all regulators
52 regulator_test = 'all';
53 switch regulator_test
54     %alpha controller on=1 off=0
55     %alpha controller on=1 off=0
56     %boomtip positioning controller on=1 off=0
57     %regulator activated at test_reg_on/off time
58     case 'beta'
59         alpha_control_activated=0;
60         beta_control_activated=1;
61         pos_reg_activated=0;
62         test_reg_on =1;
63     case 'alpha'
64         alpha_control_activated=1;
65         beta_control_activated=0;
66         pos_reg_activated=0;
67         test_reg_on =1;
68     case 'sway'
69         alpha_control_activated=1;
70         beta_control_activated=1;
71         pos_reg_activated=0;
72         test_reg_on =1;
73     case 'pos'
74         alpha_control_activated=0;
75         beta_control_activated=0;
76         pos_reg_activated=1;
77         test_reg_on =1;
78     case 'all'
79         alpha_control_activated=1;
80         beta_control_activated=1;
81         pos_reg_activated=1;
82         test_reg_on =1;
83     case 'off'
84         alpha_control_activated=0;
85         beta_control_activated=0;
86         pos_reg_activated=0;
87         test_reg_on =0;
88 end
89 %% Joystick interface block

```

```

90
91 %Define joystick axis deadband (All joystick axis has the range [-1 1])
92 db_slew=0.3;           %Deadband slew axis on joystick
93 db_luffing=0.3;       %Deadband luffing axis on joystick
94 db_hoist=0.5;         %Deadband hoist axis on joystick
95 button_number=11;     %Button number for the button used to activate
96                       %the antisway and boom tip positioning regulator
97 %Define actuator limitatons
98 max_hoist_velocity=2.2; %Max hoising speed in [m/s]
99 %% Saturation and time delay
100 %filter constants in the 'lorder exp filter' block
101 T=2;                 %Response time for crane machinery dynamics
102 %% Model
103 % 'ddot_r_p->dot_r_p' integrator inital values
104 beta_angle_vel_init=0;%initial angular velocity for beta [rad/s]
105 alpha_angle_vel_init=0;%initial angular velocity for alpha [rad/s]
106 % 'dot_r_p->r_p' integrator initial values
107 beta_angle_init=0;    % initial angle for beta [deg]
108 alpha_angle_init=0;   % initial angle for alpha [deg]
109 % 'Crane' block
110     %Define actuator limitations
111     max_slew_velocity=0.1;
112     max_boom_velocity=0.02;
113     %Define initial conditions
114     slew_angle_init=270; %Initial slew angle (q-1) [deg]
115     boom_angle_init=14; %Initial boom angle (q-2) [deg]
116     % 'luffing angle saturation' block and 'dot_q-2->q-2' integrator
117     upper_limit_boom=84.2; %Upper boom limit angle [deg]
118     lower_limit_boom=14; %Lower boom limit angle [deg]
119     % 'ddot_r_b_block' constants
120     rad_pedestal=1.75; % radius of pedestal [m]
121     l_b=50; % length of boom [m]
122     l_p=10; % length of pedestal [m]
123     % 'Hoist winch' block
124     wire_length_init=80; %initial wire length [m]
125     upper_limit_wirelength=99;%max wire length below boom tip [m]
126     lower_limit_wirelength=10;%min wire length below boom tip [m]
127     % 'Pendulum' block
128     g=9.81; %gravity constant
129     delta=0; %friction coefficient for the pendulum
130 %% VR Visualization with Graphs
131     %Parameters
132     % ylim for beta plot in visu figure [deg]
133     beta_plot_y_lim=[-15 15];
134     % ylim for alpha plot in visu figure [deg]
135     alpha_plot_y_lim=[-15 15];
136     % ylim for slew angle (q-1) plot [deg]
137     q1_plot_y_lim=[0 360];
138     % ylim for boom angle (q-2) plot [deg]
139     q2_plot_y_lim=[13 85];
140     % ylim for boom and slew angle velocity (actuator input) [rad/s]
141     tau_range=[-0.1 0.1];
142     %Run simulation
143     sim('pendulum_matrix_form_final_crane_fixed')

```


Bibliography

- [1] International Journal of Control, Automation, and Systems, vol. 5, no. 4, pp. 379-387, August 2007
- [2] Kyllingstad, A. National Oilwell Varco, Damping of crane oscillations, 2007
- [3] Chen, Chi-Tsong. Linear System Theory and Design, 1998.
- [4] Khalil, H.K. Nonlinear Systems, 2001.
- [5] Hornang, S., Determination of Real-Time Positions of a Seagoing Vessel Based on Real-Time Video, 2010
- [6] DNV. Recommended practice, DNV-RP-H103. Modelling and analysis of marine operations, 2010
- [7] Shore Connection
<http://www.shoreconnection.no/products/deck-motion-monitoring>
Accessed 2011-12-07.
- [8] Fossen, T. I., Handbook of Marine Craft Hydrodynamics and Motion Control, 2011.
- [9] Brown, R. G. and Hwang P. Y. C., Introduction to Random Signals and Applied Kalman Filtering, 1997.
- [10] Ching-Yaw Tzeng and Ju-Fen Chen, Fundamental Properties of Linear Ship Steering Dynamic Models, 1999
- [11] Fossen, T.I. and Perez T., Kalman Filtering for Positioning and Heading Control of Ships and Offshore Rigs, 1999
- [12] Anti-windup
http://www.20sim.com/webhelp/library/signal/control/pid_control/antiwindup.htm
Accessed 2012-06-05.

- [13] MSS. Marine Systems Simulator (2010).
<http://www.marinecontrol.org>
 Accessed 2012-03-14.
- [14] Ioannou, P. A and Sun J.
Robust Adaptive Control, 2003
- [15] Johansen, T.A. and Fossen, T.I.
Modelling and identification of offshore crane-rig system., Technical report,
 Department of Engineering Cybernetics, Norwegian University of Science and
 Technology, 2002.
- [16] H. Park, D.Chwa and K. Hong
A Feedback Linearization Control of Container Cranes: Varying Rope Length,
 International Journal of Control, Automation, and Systems, vol. 5, no. 4, pp.
 379-387, August 2007.
- [17] Ho-Hoon Lee
A new approach for the anti-swing control of overhead cranes with high-speed
 load hoisting, International Journal of Control, 76:15, 1493-1499, 2003.
- [18] H.-H. Lee
Motion planning for three-dimensional overhead cranes with high-speed load
 hoisting, International Journal of Control, 78:12, 875-886, 2005.
<http://dx.doi.org/10.1080/00207170500197571>
 Accessed 2012-04-20
- [19] NORSOK-R-CR-002 Lifting equipment rev. 1, January 1995
- [20] Gustafsson, T.
Modelling and Control of Rotary Crane Systems, Doctoral thesis, Tekniska
 högskolan i Luleå, ISSN 0348-8373, 1993:120D.
- [21] Ioannou, P and Sun, J.
Robust Adaptive Control, 1995.
- [22] ISO/IEC 14772-1:1997 and ISO/IEC 14772-2:2004 - Virtual Reality Modeling
 Language (VRML)
<http://www.web3d.org/x3d/specifications/vrml/>
 Accessed 2012-06-20
- [23] Egeland, O. and Gravdahl, T.
Modeling and Simulation for Automatic Control, 2003.
- [24] Mathematica for Students, trial version
<http://www.wolfram.com/solutions/education/students/>
 Accessed 2012-07-15
- [25] Gjelstenli, O.
 Project work TTK4550, NTNU.
Wave Following System for Offshore Rig Crane, 2011.

- [26] Autodesk Inventor
<http://usa.autodesk.com/autodesk-inventor/>
- [27] Okino Computer Graphics
PolyTrans Software Package
<http://www.okino.com/conv/conv.htm/>
Accessed 2012-04-20
- [28] Journal of System Design and Dynamics, vol. 5, no. 4, pp. 535-546, 2011.
Suppression of Two-Dimensional Load-Sway in Rotary Crane Control Using Only Horizontal Boom Motion
- [29] Dønnestad,K.
Simulation, Control and Visualization of UAS, M.sc Thesis, NTNU, 2011.